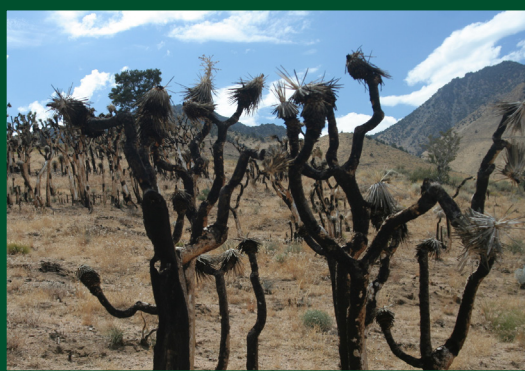


Development of a Severe Fire Potential Map for the Contiguous United States

Gregory K. Dillon, Matthew H. Panunto, Brett Davis, Penelope Morgan, Donovan S. Birch, William M. Jolly



Dillon, Gregory K.; Panunto, Matthew H.; Davis, Brett; Morgan, Penelope; Birch, Donovan S.; Jolly, William M. 2020. Development of a Severe Fire Potential map for the contiguous United States. Gen. Tech. Rep. RMRS-GTR-415. Fort Collins, CO: U.S. Department of Agriculture, Forest Service, Rocky Mountain Research Station. 107 p.

Abstract

Burn severity is the ecological change resulting from wildland fires. It is often mapped by using prefire and postfire satellite imagery and classified as low, moderate, or high. Areas burned with high severity are of particular concern to land managers and others because postfire vegetation, soil, and other important ecosystem components can be highly altered. In this study, we developed Random Forest statistical models describing the occurrence of high burn severity across the contiguous United States. We divided our work into 17 regions in the western United States and 8 regions in the eastern United States, and further subdivided them by forest and nonforest vegetation settings, resulting in 50 separate models. Our predictor variables represented prefire vegetation, topography, and fuel moisture, and our response variable was satellite-derived burn severity from the U.S. interagency Monitoring Trends in Burn Severity program. We created statistical models from 6,663 fires in the western United States (1984–2007) and 5,295 fires in the eastern United States (2000–2013). We then mapped our model predictions as a Severe Fire Potential (SFP) index ranging from 0 to 100. Our Random Forest models performed reasonably well (area under the receiver operating characteristic curve [AUC] = 0.71–0.93), though independent validation of our spatial predictions was less promising (AUC = 0.50–0.79). We analyzed spatial distributions of our SFP predictions, as well as satellite-based burn severity observations, across mapping regions and broad landform classes. We present observations about the spatial distribution of high severity fire, the variables influencing burn severity, and suggestions for applications of our SFP data that we believe managers and scientists interested in burn severity will find useful. This is the first national effort to understand where and why fires burn severely. Our consistent set of burn severity maps, field observations, and predictor variables together move us toward a better understanding of the “ecological footprint” of fires in forests and rangelands across the contiguous United States.

Keywords: burn severity, fire severity, fire ecology, landscape, remote sensing, RdNBR, dNBR, Composite Burn Index

Cover: Main photo: Burned area from the 2009 Kootenai Creek fire on the Bitterroot National Forest in western Montana, showing a mosaic of high, moderate, and low burn severity. Credit: Greg Dillon, USDA Forest Service. Small photos: Left - Burned Joshua trees (*Yucca brevifolia*) in the 2010 Indian fire on Bureau of Land Management land in Kern County, California. Credit: Chris Bernau and Tim Moran, University of Idaho. Middle-Composite Burn Index field plot from the 2001 Green Mountain fire in Great Smoky Mountains National Park, Tennessee, showing burned trees and resprouting vegetation one year after fire. Credit: Carl Key, Nate Benson, and Suzanna Soileau; U.S. Geological Survey and National Park Service. Right- Lodgepole pine (*Pinus contorta*) seedlings germinating one year after fire in a high severity area of the 2009 Kootenai Creek Fire, Bitterroot National Forest, Montana. Credit: Greg Dillon, USDA Forest Service.

All Rocky Mountain Research Station publications are published by U.S. Forest Service employees and are in the public domain and available at no cost. Even though U.S. Forest Service publications are not copyrighted, they are formatted according to U.S. Department of Agriculture standards and research findings and formatting cannot be altered in reprints. Altering content or formatting, including the cover and title page, is strictly prohibited.

Authors

Gregory K. Dillon is a Spatial Fire Analyst with the Rocky Mountain Research Station at the Missoula Fire Sciences Lab in Missoula, Montana. He has a B.S. in geography from James Madison University, and an M.A. in geography from the University of Wyoming.

Matthew H. Panunto is currently a Geographic Information System Specialist with the Bureau of Land Management in West Valley City, Utah. He was previously an ecologist with the Rocky Mountain Research Station at the Missoula Fire Sciences Lab in Missoula, Montana. He has a B.S. in environmental science from Wesley College, and an M.S. in geography and environmental systems from the University of Maryland, Baltimore County.

Brett Davis is currently a Biological Science Information Specialist with the Pacific Northwest Research Station with the Resource Monitoring and Assessment program in Portland, Oregon. He was previously an ecologist with the Rocky Mountain Research Station at the Missoula Fire Sciences Lab in Missoula, Montana. He has a B.A. in environmental, population and organismic biology from the University of Colorado Boulder and an M.S. in forestry from Colorado State University.

Penelope Morgan is an Emeritus Professor in the Department of Forest, Rangeland, and Fire Sciences at the University of Idaho. She is certified as a Senior Fire Ecologist by the Association for Fire Ecology. She has a B.S. in applied biology from Utah State University, an M.S. in forest resources from Utah State University, and a Ph.D. in fire ecology from the University of Idaho.

Donovan S. Birch is a Fire Management Specialist in Prescribed Fire and Fuels for the Bureau of Land Management in Miles City, Montana, as well as a previous Fire Severity Mapping Research Specialist in the Department of Forest, Rangeland, and Fire Sciences at the University of Idaho. He has a B.S. in forestry with a minor in geographic information systems and remote sensing from Utah State University, and an M.S. in natural resources from the University of Idaho.

William M. Jolly is a Research Ecologist with the Fire, Fuel, and Smoke Science program of the Rocky Mountain Research Station at the Missoula Fire Sciences Lab in Missoula, Montana. He has a B.A. in environmental science from the University of Virginia and a Ph.D. in forestry from the University of Montana.

Acknowledgements

Funding came from the Joint Fire Sciences Program (JFSP project # 09-1-07-4), the Wildland Fire Management Research Development and Applications program and the Fire Modeling Institute of the USDA Forest Service, Rocky Mountain Research Station, and the University of Idaho. Work was facilitated through Research Joint Venture Agreements 09-JV-1221637-270 and 14-JV-11221637-122 between the University of Idaho and the Rocky Mountain Research Station. Jory Shelton provided information technology support for the University of Idaho. Zack Holden was instrumental in conceiving the project and guiding initial development. Jason Herynk and Robin Silverstein conducted spatial analysis work for much of the western study area. Fieldwork was conducted by Greg Cohn, Sarah Flanary, Violet Holley, Brian Izbicki, Signe Leirfallom, Christy Lowney, Amy Olson, and Aaron Sparks from the Missoula Fire Sciences Laboratory and Chris Bernau and Tim Moran from the University of Idaho. Additional Composite Burn Index data were contributed by Jay Miller, Eric Gdula, Susan Prichard, Mike McClellan, Mike Wimberly, Zack Holden, Marti Witter, Karen Kopper, Joel Silverman, Bob Keane, Eva Karau, Alina Cansler, Tony Guay, Steve Bunting, Allison Snyder, Josh Picotte, and others in the eastern United States. Chris Stalling helped to acquire and assemble CBI data for the eastern US. Bob Keane, Arjan Meddens, and Josh Picotte provided reviews that greatly improved the final manuscript. Cynthia Moser and Frances Smith provided careful editorial review and layout of the final publication.

Table of Contents

1. Introduction	1
2. Methods	4
2.1 Phase 1: Acquire and Process Input Data for Modeling	5
2.1.1 Study Area, Mapping Regions, and Data Organization	5
2.1.2 Forest and Nonforest Masks	7
2.1.3 Response Variable: Burn Severity Data	9
2.1.3.1 Burn Severity Data: Western Study Area	11
2.1.3.2 Burn Severity Data: Eastern Study Area	14
2.1.4 Predictor Variables: Topographic Data	19
2.1.5 Predictor Variables: Vegetation Data	21
2.1.5.1 Vegetation Data: Western Study Area	21
2.1.5.2 Vegetation Data: Eastern Study Area	21
2.1.6 Predictor Variables: 1,000-Hour Fuel Moisture at the Time of Burning	22
2.2 Phase 2: Develop Random Forest Statistical Models	23
2.2.1 Sample Selection and Data Preparation	25
2.2.2 Random Forest Model Development	25
2.2.3 Random Forest Model Performance	26
2.3 Phase 3: Create the Severe Fire Potential Map	26
2.3.1 Normalized Difference Vegetation Index	26
2.3.1.1 Western Study Area	27
2.3.1.2 Eastern Study Area	29
2.3.2 1,000-hour Fuel Moisture	29
2.3.3 Making Spatial Predictions	29
2.3.4 Creating the Severe Fire Potential Deliverables	30
2.4 Phase 4: Evaluate the Severe Fire Potential Map	30
2.4.1 Evaluating the Severe Fire Potential Map at the Pixel Scale	30
2.4.2 Evaluating the Severe Fire Potential Map at the Landscape Scale	32
2.4.3 Defining Landform Classes	33
3. Results	34
3.1 Random Forest Statistical Models	34
3.1.1 Data Availability and Sample Sizes	34
3.1.2 Relative Importance of Variables	37
3.1.3 Random Forest Model Performance	40
3.2 Severe Fire Potential Map	40
3.3 Severe Fire Potential Map Validation	48
3.3.1 Comparisons of Predicted and Observed Binary Severity	48
3.3.2 Relationship Between Predicted and Observed Continuous Severity Metrics	51
3.3.3 Assessing Variations in Observed Severity at the Landscape Scale	51

4. Discussion	55
4.1 Limitations	59
4.2 Management Implications	61
5. Conclusions	63
6. References	64
Appendix A: Solar Radiation Modeling	75
Appendix B: Prefire NDVI Pixel Reliability for The Eastern Study Area	78
Appendix C: Defining Fire Season for Each Mapping Region	81
Appendix D: Landsat and MODIS NDVI Normalization— Western Study Area	84

1. Introduction

Burn severity is the degree of ecological change resulting from wildland fire (Keeley 2009; Lentile et al. 2006; Morgan et al. 2014). When large, contiguous areas experience relatively high burn severity, policymakers, land managers, and scientists often become concerned because ecosystems in these areas can be highly altered from prefire conditions. Within higher severity patches, less vegetation survives, vegetation regrowth can be slower than in otherwise similar but less severely burned areas (Morgan et al. 2014, 2015), postfire tree regeneration may be lacking or delayed (Stevens-Rumann and Morgan 2019; Stevens-Rumann et al. 2018), soil erosion potential is often increased (Parsons et al. 2010; Robichaud et al. 2013), and wildlife habitat is altered (Keeley et al. 2008; Lentile et al. 2007; Romme et al. 2011; Turner et al. 1997). But in many ecosystems, areas that experience high severity—or a mixture of high, moderate, and low severity—can see ecological benefits (DellaSala and Hanson 2015; Hutto et al. 2016). In all ecosystems, areas of high burn severity will have different vegetation trajectories than less severely burned or unburned areas, and the differences can vary from pronounced to subtle (Lewis et al. 2017; Morgan et al. 2015). Whether the ecological consequences of high burn severity are positive or negative, it is important to be able to map areas where burn severity was, is, or could be high to support informed land management decisions. Mapping burn severity promotes understanding of the ecological effects of fires.

In recent decades, large fires have burned extensive areas (Dennison et al. 2014), threatened people and property, and cost millions of dollars to suppress and rehabilitate post-fire. The full costs of fire management often amount to 2 to 30 times suppression costs (Western Forestry Leadership Coalition 2010). More large fires are likely in the future in many locations due to both changing climate and changes in fuel loadings and distributions (Abatzoglou and Williams 2016; Littell et al. 2009; Westerling et al. 2006). Yet not all fires burn with high severity, and most large fires include unburned areas and areas burned with low to moderate severity (Birch et al. 2015; Kolden et al. 2012; Meddens et al. 2018b). The proportion of burned area mapped with high severity in large fires in the United States since 1984 is less than one-third of total area burned in those fires (Finco et al. 2012; Picotte et al. 2016). Even under conditions where large areas burn in a single day with extreme weather, most high severity occurs on a minority of burned area, except in the most extreme cases (Birch et al. 2014, 2015). Spatial variability in fire intensity, weather, and vegetation—influenced by many factors—results in spatial variability in fire effects and long-term ecological benefits or detriments from fire.

Accurate, consistent, and timely burn severity maps are needed in all phases of fire management, including planning, managing, and rehabilitating. As it is typically used, however, burn severity is measured and mapped based on postfire observations, making it mostly a tool for postfire rehabilitation and postfire natural resource management. Soil burn severity is often mapped by Burned Area Emergency Response (BAER) teams using observations from both field and remotely sensed imagery in an effort to assess where treatments may reduce the potential of soil erosion to affect values at risk (Parsons et al. 2010). The process for creating burn severity maps from a combination of prefire and postfire satellite imagery is well documented and has been widely applied (Key and Benson 2006; Miller and Thode 2007; Morgan et al. 2014; Parks et al. 2014a). Because burn severity from one fire can alter fire behavior, and therefore severity, of a subsequent fire (Parks et al. 2014b; Prichard et al. 2017; Stevens-Rumann et al. 2016), satellite-derived postfire burn severity

maps can be useful in planning for and managing subsequent fires in the same location (Pabst 2010). Similarly, anticipating burn severity and what determines it can be useful in planning prescribed burns or managing wildfires in areas not recently burned.

Because burn severity often varies with physical landscape characteristics that can be mapped (Birch et al. 2015; Parks et al. 2014c; Picotte and Robertson 2011b; Picotte et al. 2016), maps of potential burn severity can be created from statistical relationships between observed burn severity and factors such as topography, vegetation, climate, and weather (Dillon et al. 2011; Parks et al. 2018). Maps produced based on these statistical relationships provide an inherently different type of information than satellite-derived postfire severity maps and fill a knowledge gap around understanding the potential for high severity fires before they occur. This type of information could inform decisionmaking, including fuels treatment planning and strategic management of active wildfires.

Fire managers currently use a variety of models and information to support their decisions. These include the Interagency Fuel Treatment Decision Support System (IFTDSS; <https://iftdss.firenet.gov>) for fuels treatment planning, and fire behavior modeling tools available through the Wildland Fire Decision Support System (WFDSS; <https://wfdss.usgs.gov>), as well as climatological and fire danger indices available through the Wildland Fire Assessment System (WFAS; <https://m.wfas.net/>), for active wildfire management. Unfortunately, these models are less useful for predicting the effects of those fires on vegetation response, soil erosion potential, and many other short- and long-term fire effects related to the duration of soil heating and fuel consumption.

The Severe Fire Potential map (SFP map) is intended to complement these tools. We developed this tool to help managers with landscape-level planning. In particular, the SFP map could help identify areas where fire may play beneficial rather than detrimental roles, and thus support the consideration of the ecological role that fire plays in different vegetation communities. With this knowledge, decisionmakers may be better able to meet land and vegetation management objectives when working with fire. The SFP map estimates the potential for any location within our study area to experience high severity fire, based on past observations. This static product can be downloaded from the web (<https://www.frames.gov/firesev>) for advance planning and also provides an initial estimate of where fire is likely to be severe that could be checked or modified at the time of a fire with more process-based tools such as the WFDSS.

Our specific objectives in creating the SFP map included: (1) developing a comprehensive map of the potential for high burn severity for all areas in the contiguous United States (CONUS) using empirical observations and statistical modeling and (2) evaluating the quality of the SFP map to provide managers with guidance on its interpretation and use. The creation of the SFP map was a part of a larger project called FIRESEV (FIRE SEVERITY Mapping Tools) in which we approached the topic of burn severity from several angles, creating a suite of digital maps, simulation models, analysis tools, study results, and synthesis papers to inform wide-ranging fire management applications, including wildfire rehabilitation efforts and long-term planning (Dillon et al. 2011; Karau et al. 2014; Keane et al. 2014; Morgan et al. 2014; Sikkink et al. 2013). As part of the FIRESEV project, Morgan et al. (2014) provided a thorough background on methods used to measure, interpret, and apply burn severity

in fire management, and offered suggestions for best practices. FIRESEV products expand upon the suite of burn severity products currently used by fire management in the United States, including those provided by BAER (<https://www.fs.fed.us/eng/rsac/baer/>), Rapid Assessment of Vegetation Condition (RAVG; <https://www.fs.fed.us/postfirevegcondition/index.shtml>), and Monitoring Trends in Burn Severity (MTBS; <https://www.mtbs.gov/>) programs. The combination of these existing burn severity resources with the new information and resources produced by the FIRESEV project provides fire managers—and land managers in general—a complementary set of tools for assessing fire effects on their landscapes based on their objectives and available time, funding, and resources. This is the first national effort to understand where and why fires burn severely, and thus to understand the “ecological footprint” of fires in forests and rangelands in the contiguous United States.

2. Methods

Our methods for creating the SFP map consisted of four distinct phases: (1) acquiring and processing input spatial data, (2) developing statistical models, (3) applying statistical models spatially to produce maps of severe fire potential, and (4) assessing the accuracy of the SFP map (fig. 1). Each phase is described in detail in the next sections.

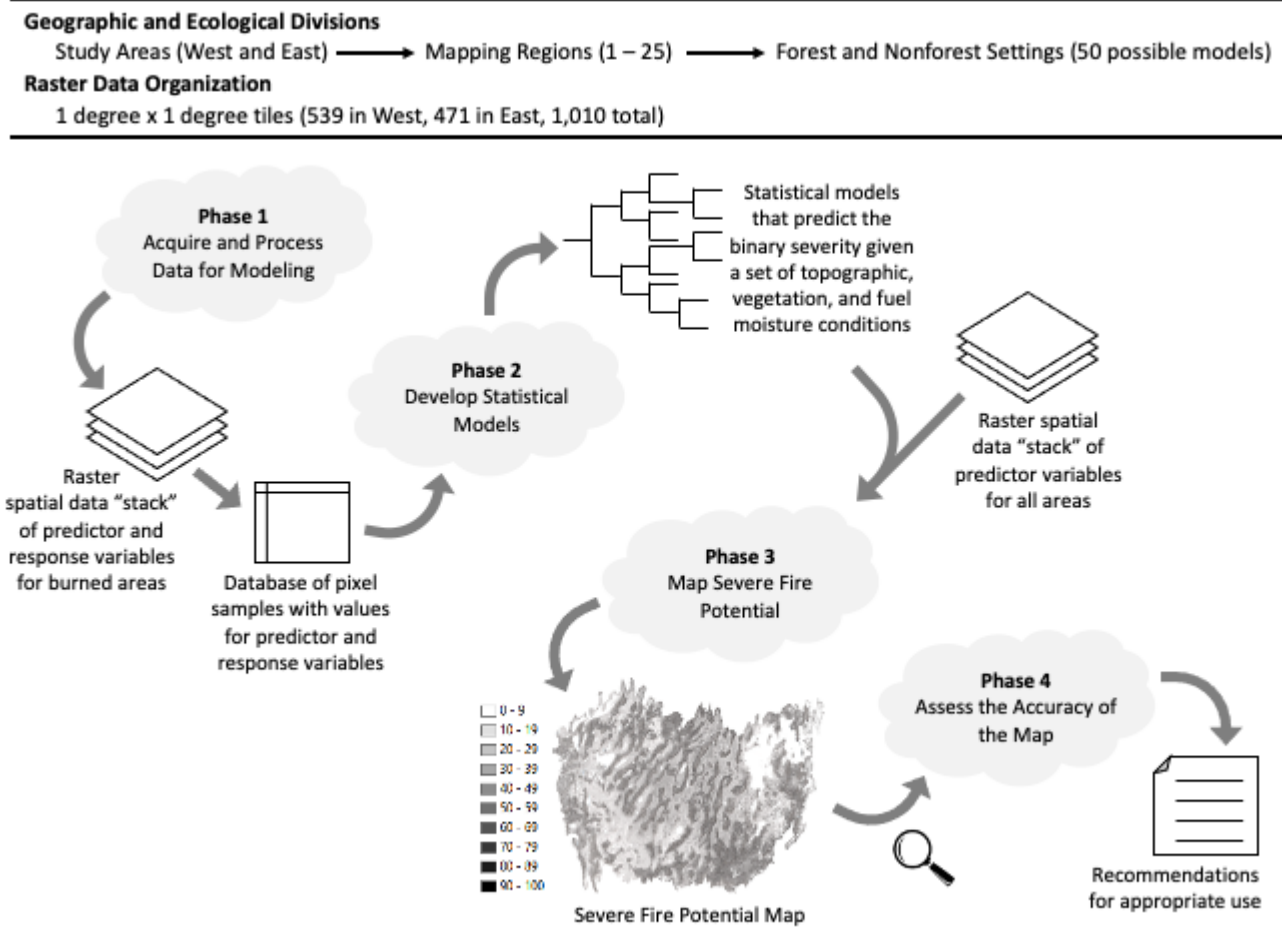


Figure 1—Flowchart of the general methods involved in creating the Severe Fire Potential map. Each of the four phases depicted here is described in detail in the *Methods* section.

2.1 Phase 1: Acquire and Process Input Data for Modeling

2.1.1 Study Area, Mapping Regions, and Data Organization

The study area for this project was the entire contiguous United States, divided into two stages for the western and eastern United States. We completed the western SFP map in 2012 and the eastern SFP map in 2016. The western study area included California, Oregon, Washington, Idaho, Nevada, Montana, Wyoming, Utah, Colorado, Arizona, New Mexico, and western portions of North Dakota, South Dakota, Nebraska, Kansas, Oklahoma, and Texas (fig. 2). The eastern study area consisted of the remainder of CONUS. While we strove for consistency across all of CONUS, we had to use some different input data sources and methods between the western and eastern study areas because of differences in underlying ecology, data availability, and timing of imagery acquisition (fig. 3). We explain these differences in applicable subsections.

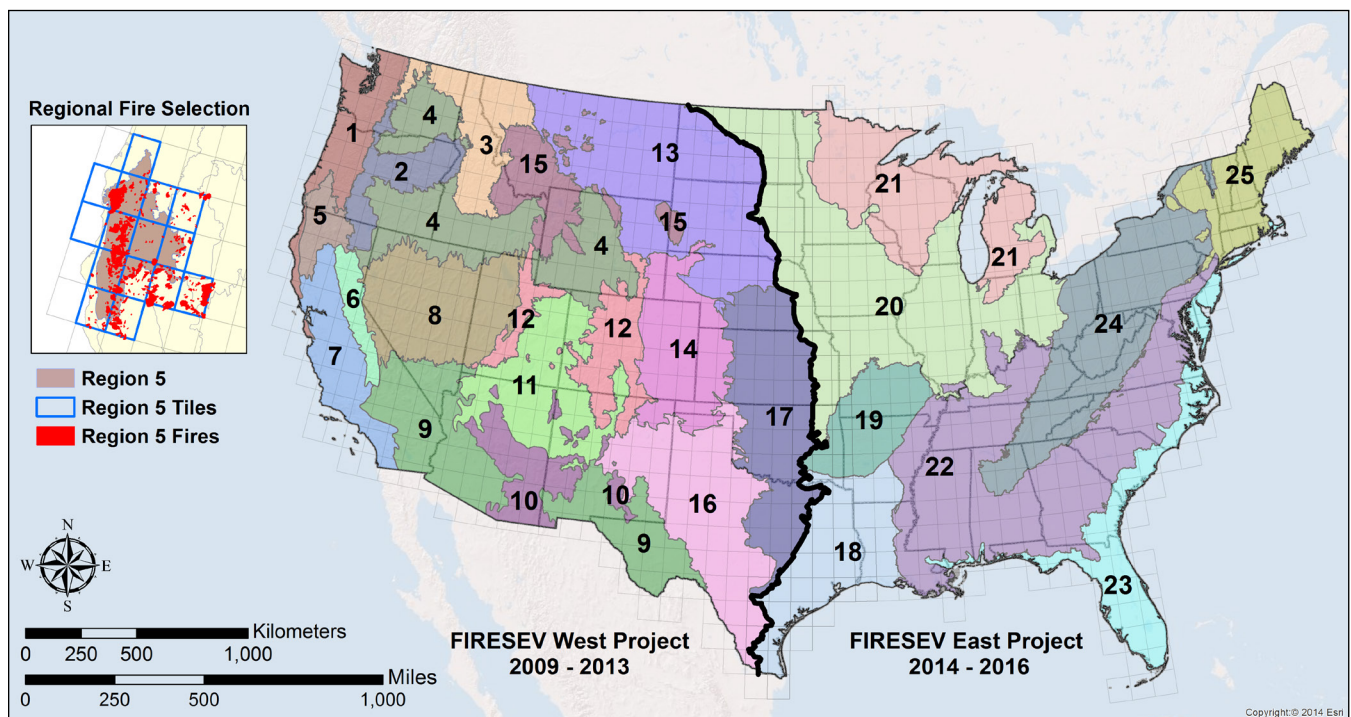


Figure 2—Study areas, mapping regions, and 1-degree tiles used for data organization. The bold north-south line depicts the division between the western and eastern study areas. Individual mapping regions are shown as colored polygons and labeled by region numbers. The 1-degree tiles are visible as thin gray outlines. The inset map illustrates how any tiles touching a region’s boundary were included in selecting the fires for model development in that region.

	Burn Severity Data	Topographic Data	Vegetation Data	Fuel Moisture Data
Acquire	West: RdNBR ¹ from MTBS ² for 1984 to 2007. East: dNBR ³ or NBR ⁴ from MTBS for 2000 to 2013. CONUS: Field CBI ⁵ data.	CONUS: National Elevation Dataset (NED) 3 arc second (approximately 30 m) digital elevation model (DEM). Acquired in 2009 (West) and 2014 (East).	West: prefire Landsat scenes from MTBS. East: prefire MODIS ⁶ NDVI ⁷ images.	CONUS: daily 4-km gridded weather data for 1980 to 2010 (West) and 1980 to 2013 (East).
Process	West: Calculate thresholds to classify severity from statistical relationship between RdNBR and CBI. East: Calculate thresholds to classify severity from statistical distribution of MTBS thematic classifications.	West: Calculate potential solar radiation with SOLPET6 ⁸ model. East: Calculate relative potential solar radiation with ArcGIS Area Solar Radiation tool. CONUS: Calculate 11 topographic indices from NED DEM.	West: Calculate NDVI from 30-m Landsat scenes. East: Select prefire 250-m MODIS NDVI with highest quality.	CONUS: Calculate sea-level potential temperature and subsequently 1,000-hour fuel moisture for every grid cell every day in the time series. Calculate the lowest site-specific fuel moisture percentile for each fire in the study, within a 10-day window of each fire's start date.
Data Product	West: 30-m binary severity raster for burned areas. Classified to high severity vs. other. East: 30-m binary severity raster for burned areas. Classified to high or moderate ("higher") severity vs. other.	West: six 30-m solar radiation rasters for all lands. East: one 30-m solar radiation raster for all lands. CONUS: elevation and 11 30-m topographic index rasters for all lands.	West: 30-m prefire NDVI raster for burned areas. East: 250-m prefire NDVI raster for burned areas.	CONUS: Database of minimum 1,000-hour fuel moisture percentiles at the time of each fire in the study.

¹ RdNBR = Relative differenced normalized burn ratio, ² MTBS = Monitoring Trends in Burn Severity, ³ dNBR = differenced normalized burn ratio, ⁴ NBR = normalized burn ratio, ⁵ CBI = Composite Burn Index, ⁶ MODIS = Moderate-Resolution Imaging Spectroradiometer, ⁷ NDVI = normalized differenced vegetation index, ⁸ SOLPET6 = Flint and Childs (1987) solar radiation model.

Figure 3—Overview of the main categories of response variable (burn severity) and predictor variable (topography, vegetation, and fuel moisture) data used in phase 1 of creating the Severe Fire Potential map: Acquire and process input data for modeling. Specific differences between western and eastern study areas with respect to datasets acquired, processing steps, and model-ready data products are shown.

We subdivided our modeling and mapping work in both the western and eastern study areas into smaller regions with similar ecological characteristics. Fire behaves differently under disparate biophysical and climatic conditions (Pyne et al. 1996), so we expected the relative influence of biophysical, climatic, and weather conditions on burn severity to differ by region. We created these “mapping regions” based on an existing classification of North American terrestrial ecoregions (CEC 2007; Wiken et al. 2011). While the source ecoregions had four nested hierarchical levels, no one level fit our ideal characteristics of size (large enough to have a sufficient sample of fires) and similarity of ecological and fire regime characteristics. Therefore, we drew upon boundary lines forming existing level II, III, and IV ecoregion polygons (Omernik and Griffith 2014), but consolidated or subdivided them (or a combination thereof) to arrive at our mapping region polygons. This process resulted in 25 mapping regions across CONUS (fig. 2) that range in size from 5.3 million to 87 million hectares (13 million–215 million acres). The western study area has 17 mapping regions and the eastern study area has 8.

To organize the large sets of raster spatial data required for a project of this size, we used both the mapping regions and a system of spatial tiles. Raster data are arranged in a grid of rectangular pixels, or cells, with attribute information associated to each cell to represent geographic information. Most of the data we used in this project have a spatial resolution (i.e., pixel size) of 30 meters (approximately 98 feet). Raster data at this resolution across an area as large as CONUS represent a substantial volume of data that can be cumbersome to process. Our solution to this challenge was to store and process data in smaller subsets, or tiles, each 1 degree of latitude by 1 degree of longitude (fig. 2). Our entire study area consisted of 1,010 of these tiles, with 539 tiles for the western study area and 471 for the eastern study area.

We used the North American datum of 1983 (NAD83) with an Albers equal-area conic projection as the standard projection for our geographic data. Unless otherwise noted, all geographic data were modeled and mapped in this projection. We used digital elevation models (DEMs) acquired from the U.S. Geological Survey (USGS) National Elevation Dataset (Gesch 2007) as our reference geographic dataset and aligned all other datasets to them.

We defined the modeling area for each mapping region using the outer footprint of all the tiles associated with each mapping region (fig. 2, inset map). This created overlap in the analysis areas between adjacent mapping regions, increased the quantity of burn severity data used in each regional analysis, and reduced seam lines in the final product. In addition, we created outer tile footprints for the entire western study area and eastern study area for use in extracting geographic input data.

2.1.2 Forest and Nonforest Masks

Burn severity measurement and interpretation are very different in forest versus nonforest environments (Key and Benson 2006; Meddens et al. 2016; Morgan et al. 2014; Parsons et al. 2010). Therefore, we performed all modeling and mapping separately for these two broad vegetation categories. We created two sets of forest and nonforest masks: one set representing prefire conditions that we used in the modeling phase of the project, and the other representing current conditions that we used in the mapping phase of the project. In both cases, the “forest” masks represent ecosystems with generally more than 10% tree cover (i.e., forests, woodlands, and savannas) and the nonforest masks represent grass-, forb-, and shrub-dominated vegetation without trees.

We primarily used data from the LANDFIRE project (Rollins 2009) to create our forest and nonforest masks. LANDFIRE produces a suite of spatial data representing vegetation, wildland fuels, and fire regimes on all lands across the United States. In both the western and eastern study areas, we used the most current LANDFIRE data available at the time of our analysis. In general, we used LANDFIRE 2008 (version 1.1.0) for the western United States and LANDFIRE 2012 (version 1.3.0) for the eastern United States.

To represent current conditions we used LANDFIRE’s Existing Vegetation Cover (EVC; <https://www.landfire.gov/NationalProductDescriptions23.php>), which represents the live canopy layer of tree, shrub, and herbaceous vegetation measured in percent cover. The EVC

raster layer was used to create the current forest mask by extracting those areas that represent tree canopy cover of 10% or more. We took the inverse of the forest mask to create the current nonforest mask.

We developed the prefire masks (fig. 4) using the current conditions masks just described and two other national geospatial vegetation products, LANDFIRE’s Environmental Site Potential (ESP; <https://www.landfire.gov/NationalProductDescriptions19.php>) and the Landsat Time Series Stacks—Vegetation Change Tracker (LTSS-VCT; Huang et al. 2010). The Environmental Site Potential represents the vegetation that could be supported on a site given the site’s biophysical characteristics; LTSS-VCT was developed to differentiate between disturbed forests, persistent forest, and persistent nonforest using a time series of Landsat

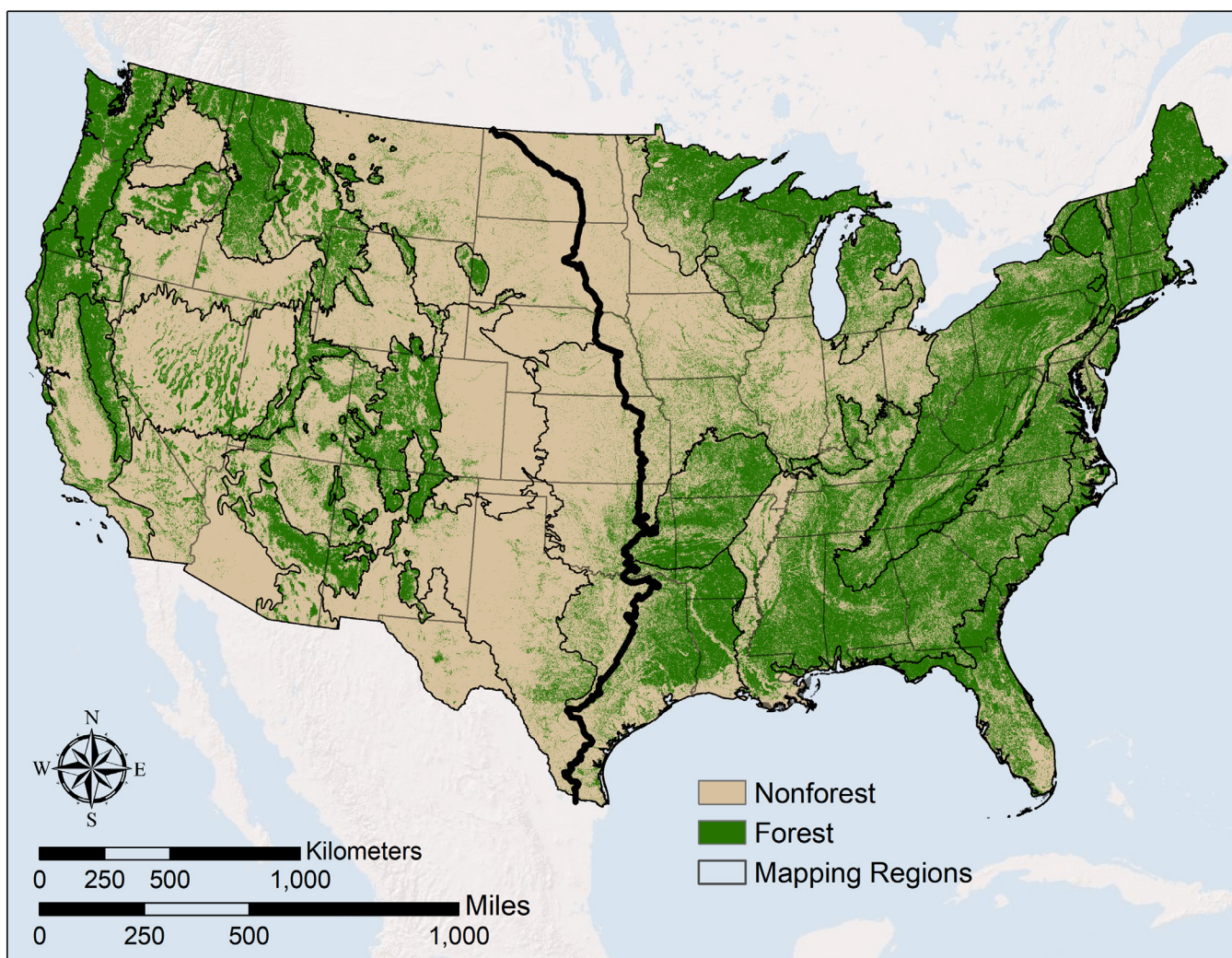


Figure 4—Prefire forest mask used to identify forest, woodland, and savanna settings in the modeling phase of the project. Pixels identified as forest in this mask are likely to have been tree dominated (>10% cover of trees) before burning, as indicated by LANDFIRE Existing Vegetation Cover and Environmental Site Potential as well as a Landsat Time Series Stack dataset (Huang et al. 2010).

images spanning 1984 through 2006 (Huang et al. 2010; Thomas et al. 2011). Our process for identifying sites likely to have been tree dominated pre-fire was to include any pixels identified as forest in the current conditions mask and any pixels with a tree-dominated ESP that are identified as persistent or disturbed forest in the LTSS-VCT data. All other pixels were assumed to have been nonforest pre-fire.

2.1.3 Response Variable: Burn Severity Data

We acquired burn severity data for 11,958 fires that occurred from 1984 through 2013 from the Monitoring Trends in Burn Severity (MTBS) project (<http://www.mtbs.gov/>). Analysts with the MTBS project map the burn severity of all fires greater than 405 hectares (1,000 acres) in the western United States (west of the 97th meridian) and greater than 202 hectares (500 acres) in the eastern United States that have occurred since 1984 (Eidenshink et al. 2007). They produce maps of burn severity using the near- and mid-infrared bands from Landsat satellite imagery. Depending on data availability and quality, MTBS uses either Landsat 5 Thematic Mapper (TM), Landsat 7 Enhanced Thematic Mapper plus (ETM+), or Landsat 8 Operational Land Imager (OLI) sensor data. They offer several satellite-derived burn severity products, including continuous measures of burn severity based on the normalized burn ratio (NBR) algorithm (Key and Benson 2006) (eqn. 1), packaged in individual, fire-level datasets.

$$NBR = \frac{NIR - MIR}{NIR + MIR} \quad (1)$$

where NIR is reflectance in the near-infrared band (TM, ETM+: 0.77–0.90 μm ; OLI: 0.851–0.879 μm) and MIR is reflectance in the mid-infrared band, or shortwave infrared (SWIR) band (TM, ETM+: 2.09–2.35 μm ; OLI: 2.107–2.294 μm).

The burn severity products available for an individual fire vary based on image availability and ecological setting. In cases when both prefire and postfire scenes are used (i.e., multiscene fires), MTBS produces both the differenced NBR (dNBR; Key and Benson 2006) (eqn. 2) and the relative dNBR (RdNBR; Miller and Thode 2007) (eqn. 3). Both measure the degree of change in vegetation and litter-plus-substrate conditions; the dNBR measures absolute change and the RdNBR measures change relative to prefire conditions. In cases where paired prefire and postfire imagery is not available or ecologically appropriate (e.g., wetlands), MTBS produces only a postfire NBR to differentiate healthy and burned vegetation (i.e., single-scene fires) (Eidenshink et al. 2007).

$$dNBR = NBR_{prefire} - NBR_{postfire} \quad (2)$$

$$RdNBR = \frac{dNBR}{\sqrt{\frac{NBR_{prefire}}{1,000}}} \quad (3)$$

Multiscene burn severity analyses can be divided into initial and extended assessment types based on when the postfire imagery was captured. Initial assessments characterize severity based on imagery captured as soon after a fire as possible (within the same growing season). Initial assessments are most often used in ecosystems that exhibit rapid postfire vegetation recovery (e.g., grasslands and some shrublands) (Eidenshink et al. 2007). Extended assessments characterize severity based on postfire imagery captured in a subsequent growing season (preferably as close to the fire anniversary date as possible). Extended assessments are generally used in areas where vegetative fire impacts may not be readily apparent for one or two growing seasons (e.g., forests) (Eidenshink et al. 2007).

In addition to measures of continuous burn severity, MTBS provides thematic classified burn severity (e.g., fig. 5), original Landsat imagery used for each fire, vector-based polygon fire perimeters, and national point-based fire occurrence data. We used each of these products at different stages in our analysis.

Our goal in creating the SFP map was to predict the potential for high severity fire in an area if it should burn. Therefore, we needed to reclassify the continuous satellite-based measures of severity into binary categories of high severity versus not high severity. Our methods for doing this varied between the western and eastern study areas and the three different burn severity indices, as described next (fig. 5).

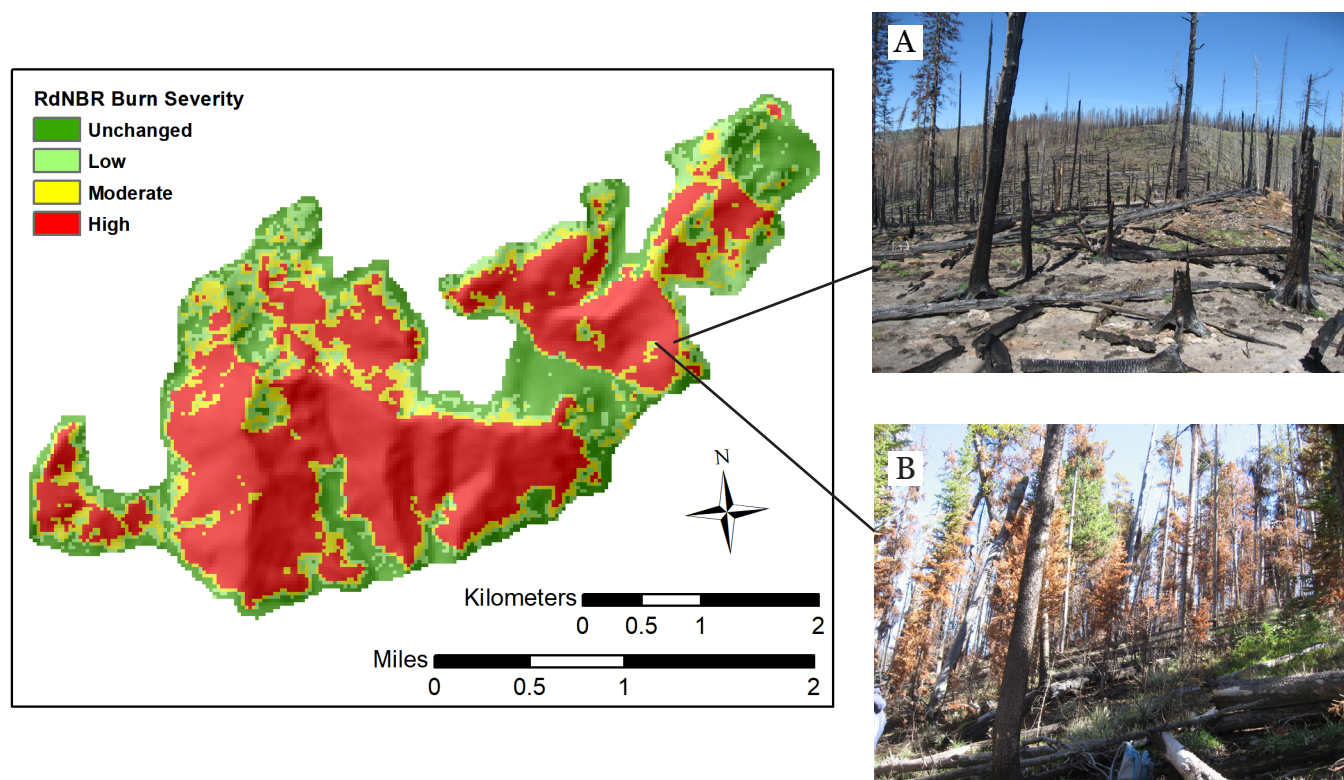


Figure 5—An example map of burn severity for a single fire, derived from the relative differenced normalized burn ratio (RdNBR) satellite index. The site in photo A is located on a ridge and illustrates high severity fire effects, with complete overstory mortality, consumption of most surface fuels, and moderate to high soil heating (Composite Burn Index [CBI] = 3.0). The site in photo B is located below the photo A site, mid-slope on a west aspect, and illustrates low to moderate severity fire effects, with needle scorch on some trees and only partial consumption of surface fuels (CBI = 1.6) (Photos: Greg Dillon, USDA Forest Service).

2.1.3.1 Burn Severity Data: Western Study Area

We used RdNBR as our continuous burn severity metric in the western study area. We chose RdNBR because it is provided by MTBS, and studies from the western United States have shown that relativized measures of severity that incorporate a “phenology offset” from unburned areas are the most appropriate for comparing fires in different vegetation types (Miller et al. 2009b; Parks et al. 2014a). The phenology offset minimizes the effect of background changes to vegetation when satellite imagery is compared from two dates, and is applied by subtracting an average dNBR value from an unburned area outside the burn perimeter with similar vegetation (Miller et al. 2009b) before calculating RdNBR.

We acquired MTBS data for the western study area in March 2011. We selected fires with RdNBR data available that occurred from 1984 through 2007 and fell within the western study area tile footprint (fig. 2). Using these criteria, we selected, downloaded, and processed data for 6,663 fires (fig. 6).

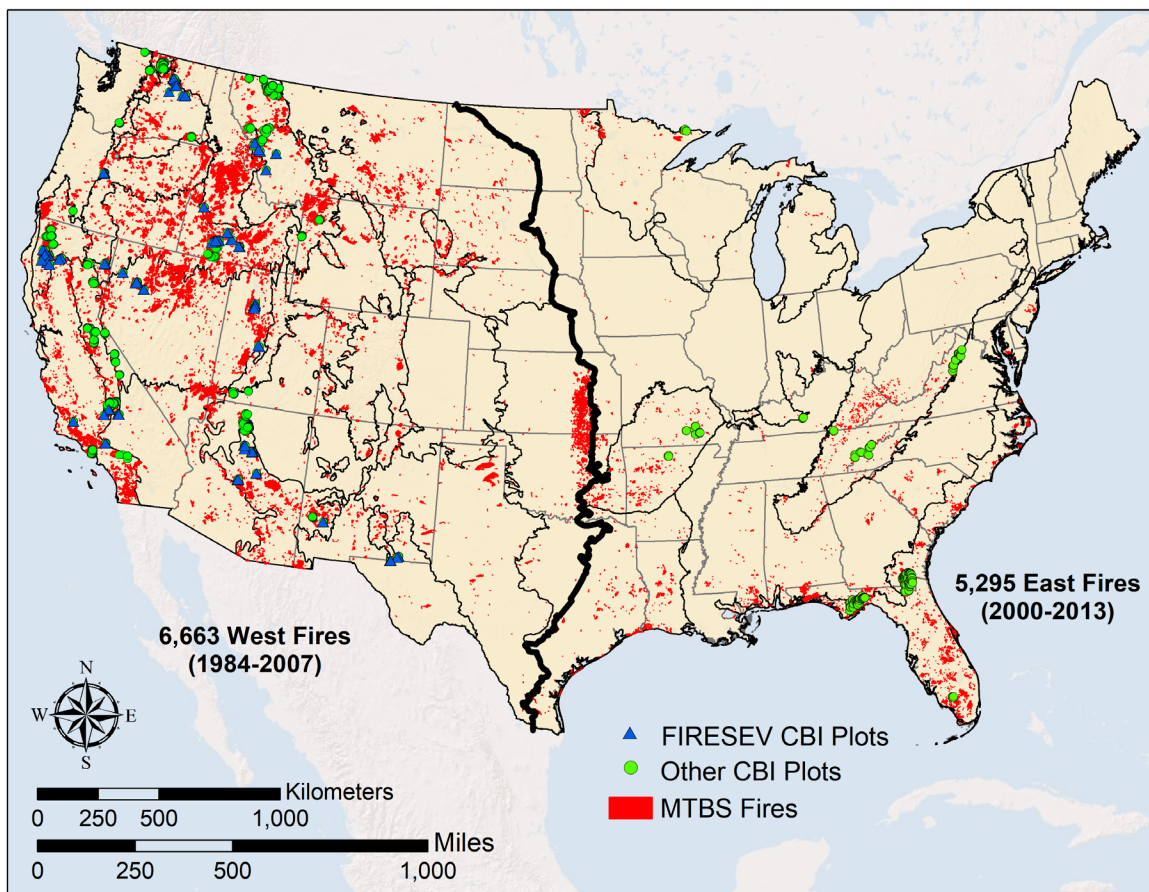


Figure 6—Location of Monitoring Trends in Burn Severity (MTBS) fires and Composite Burn Index (CBI) field plots used in this study. Data were acquired from MTBS in 2011 for western fires, and in 2015 for eastern fires. Data were collected at 542 CBI plots in the western United States specifically for this study, and the remainder were acquired from other sources.

After downloading the MTBS data, we did some initial geospatial processing to prepare the data for our analysis. This step involved converting the data to our preferred format (ESRI Grid format), projecting them to our standard projection, and eliminating all unburned pixels in the RdNBR data that fell outside the fire perimeter. We divided the fires into two groups based on whether their burn severity assessments were initial or extended. Using fire detection and imagery dates from the metadata included with each MTBS fire, we divided the fires as follows: Postfire imagery 180 days or less after the fire was considered an initial assessment, and postfire imagery more than 180 days after the fire was considered an extended assessment. With the seasonal timing of fires in the western United States, we found this approach to reliably categorize assessments where postfire imagery was in the subsequent growing season as extended assessments, while initial assessments tended to be clustered in the months immediately post-fire. The separation of fires by assessment type was necessary because the amount of time for vegetation recovery greatly affects RdNBR values (Lydersen et al. 2016). The final step in the initial processing of the burn severity data was to mosaic the processed RdNBR raster layers by mapping region, year, and assessment type. The result of this process was a set of RdNBR raster layers representing each unique combination of year, region, and assessment type.

While MTBS does not provide a classified version of the RdNBR, several studies have used regressions between a field measure of severity called the Composite Burn Index (CBI; Key and Benson 2006) and RdNBR to determine thresholds for classifying RdNBR into discrete classes of burn severity (Cansler and McKenzie 2012; Dillon et al. 2011; Holden et al. 2009; Miller et al. 2009b; Miller and Thode 2007; Pabst 2010). This index is based on visual estimations in the field of postfire changes in several vertical strata from the soil up to the upper tree canopy (if present) and represents a composite, point-based measure of burn severity ranging from 0.0 (unchanged) to 3.0 (highest severity possible) (see figure 5 for examples). A value of 2.25 is commonly used as the breakpoint between moderate and high on the CBI burn severity scale (Dillon et al. 2011; Key and Benson 2006; Miller and Thode 2007). The corresponding threshold RdNBR value between high severity and lower severity classes is somewhat consistent among studies, ranging from 641 to 703 (table 1), but these results represent a relatively small subset of forest ecosystems in the western study area. Because we needed thresholds applicable across all forest and nonforest ecosystems, and fine-tuned to initial versus extended assessments, we chose to develop our own set of thresholds.

To acquire field severity data, we requested and acquired CBI data from many different sources and also collected some of our own. For our data collection efforts, we focused on geographic locations and vegetation types not well represented in previously collected data (many nonforest). We collected data at 542 plots in 10 western States (Sikkink et al. 2013). In total, we gathered CBI data from 3,609 plots located across the western United States (fig. 6). To associate an RdNBR value to each CBI plot location, we intersected each plot with the appropriate RdNBR mosaic (year, mapping region, assessment type). To account for possible alignment errors, we used the average RdNBR value from a 3 pixel × 3 pixel window centered on each plot location. We then identified whether plots were considered forest or nonforest based on the prefire masks described earlier. Plots with extreme values of RdNBR (greater than 2,000 [n = 33] or less than -500 [n = 10]) were deleted from the dataset before regressions were run.

Table 1—Calculated high severity thresholds for the relative differenced normalized burn ratio (RdNBR) from previous studies.

Study	Location	High severity threshold ^a	Regression model
Miller and Thode (2007)	Sierra Nevada conifer forests, woodlands, and some shrublands	641	$RdNBR = a + b \times EXP(CBI \times c)$
Miller et al. (2009b)	Sierra Nevada conifer forests, woodlands, and some shrublands	657	$RdNBR = a + b \times EXP(CBI \times c)$
Holden et al. (2009)	Gila Wilderness, New Mexico	677	$CBI = a \times RdNBR + b$
Cansler and McKenzie (2012)	North Cascades conifer forest	703	$RdNBR = a + [b \times (CBI \wedge c)]$
Pabst (2010)	Grand Canyon National Park conifer forests and woodlands	698	$RdNBR = a + b \times EXP(CBI \times c)$
Dillon et al. (2011)	Grand Canyon National Park conifer forests and woodlands	695	$RdNBR = b \times EXP(CBI \times c)$

^a Thresholds represent the RdNBR value that corresponds to a field Composite Burn Index (CBI) of 2.25.

Using the paired CBI and RdNBR data points, we tested four different regression equations on different spatial groupings of the data: individual mapping regions, groups of regions, and the western study area as a whole. We attempted to build separate models for four scenarios: initial and extended assessment for forest and nonforest settings. The models we tested were a simple linear regression and three forms of nonlinear regression reported in previous studies (Cansler and McKenzie 2012; Dillon et al. 2011; Holden et al. 2009; Miller and Thode 2007). Using a CBI of 2.25, we calculated the RdNBR high severity threshold for each regression model.

We evaluated model performance using the regression R^2 and the binary classification accuracy (high severity vs. other) compared to the CBI values. Ultimately, we chose to use thresholds calculated from the largest possible dataset in each scenario. This meant using the regression models built with all plots across the western study area, rather than geographic (regional) subsets. Both field and remotely sensed data are inherently noisy, and we felt that including as many plots as possibly might help mitigate some of this noise and allow for more complete sampling of the possible burn severity spectrum present both on the ground and in the imagery. For each scenario, we chose the best performing model according to R^2 and classification accuracy: a nonlinear regression model for the forest extended assessment and nonforest initial assessment scenarios, and a linear regression for the nonforest extended assessment scenario (table 2). We had by far the most plots in the forest extended assessment group, resulting in much stronger model performance than the other scenarios. The high severity threshold of 640 for this group is in line with previous studies (table 1). Model performance for our forest initial assessment plots was too poor to calculate reliable thresholds, so we eliminated the 108 fires in this category from our analysis. The regression models for both assessment types in nonforest had relatively poor performance. However, lacking any better thresholds for nonforest, we did proceed with these thresholds for this analysis.

Table 2—Results of regression analyses between the relative differenced normalized burn ratio (RdNBR) and field Composite Burn Index (CBI) data in the western study area.

Setting	Assessment type	n	Regression model	High severity threshold ^a	R ²	Accuracy
Forest	Extended	2,553	RdNBR = b × EXP(CBI × c)	640	0.61	84.6%
Forest	Initial	108	--	--	--	--
Nonforest	Extended	310	RdNBR = a × CBI + b	612	0.36	76.1%
Nonforest	Initial	79	RdNBR = b × EXP(CBI × c)	891	0.29	75.9%

^a Thresholds represent the RdNBR value that corresponds to a field CBI of 2.25.

Using our threshold values (table 2), we reclassified the continuous RdNBR datasets to create binary severity grids (high vs. other) by year (1984–2007), mapping region (1–17), and setting (forest vs. nonforest). Finally, we created binary severity mosaics across all years, still keeping outputs separate by mapping region and setting, and giving precedence to high severity values in those areas that burned in multiple years.

2.1.3.2 Burn Severity Data: Eastern Study Area

Data from MTBS were much more limited in the eastern United States, which led to some different considerations in data acquisition. We acquired MTBS data for the eastern study area in December 2015. Due to the weather patterns, vegetation, and disturbance dynamics in much of the eastern study area, we found single-scene NBR severity data to be more common than in the western study area. Single-scene assessments were particularly common in the southeastern United States, due to persistent cloud cover and the prevalence of woody and herbaceous wetlands whose hydrology can complicate selecting a suitable prefire image (MTBS 2016). We also found that for multiscene assessments, dNBR is more commonly used as the preferred severity metric, rather than RdNBR (Picotte and Robertson 2011b). Therefore, to maximize our pool of burn severity observations we acquired data for both single-scene (postfire NBR) and multiscene (dNBR) fires. Due to considerations involved in developing prefire vegetation data (see section 2.1.5.2), we selected only fires from 2000 through 2013. For about 500 of those fires, we found logical inconsistencies between the fire occurrence date and the postfire image date (e.g., postfire image date occurring before fire occurrence date, possibly due to data entry errors), so we eliminated them from the analysis. Ultimately, after applying all selection criteria, we acquired and processed data from 5,295 fires to use in model development in the eastern study area (fig. 6).

The initial geospatial processing for the eastern MTBS data differed from the western methods in several important ways. The first steps of converting data from GeoTIFF to ESRI Grid format, projecting them to our standard projection, and eliminating unburned pixels outside the fire perimeter in NBR and dNBR datasets were consistent with processing for the western study area. However, unlike the western analysis, we did not separate fires by assessment type (initial vs. extended) or by mapping region at this point due to different methods for calculating severity thresholds (see following paragraphs). For those fires with dNBR data, we chose to apply a “phenology offset” value to the raw raster layer. The offset value is derived from a homogeneous area of unburned vegetation outside the burned area but

similar to the vegetation that burned (Key 2006; Miller and Thode 2007). The MTBS program calculates a phenology offset value but does not apply it, except in the RdNBR calculation. We applied the offset value to dNBR data to facilitate the comparison of fires occurring in different vegetation types and at different points in time (Miller et al. 2009b; Parks et al. 2014a). Finally, we mosaicked the eastern severity data by metric (NBR or dNBR) and year, resulting in 28 mosaicked raster layers.

Thresholding methods also differed considerably between the western and eastern study areas. As in the western study area, we attempted to acquire all available CBI plot data for the eastern study area. While we were able to acquire data from 1,208 plots in 9 States (fig. 6), we still had insufficient field data to model the relationship between field severity and satellite-derived severity in most eastern mapping regions. Therefore, we used the distribution of historical MTBS thematic classified burn severity data to determine thresholds.

The MTBS program classifies continuous NBR or dNBR (depending on availability) data into thematic categories including areas of low, moderate, and high severity as well as areas within the fire perimeter that appeared unburned or showed increased greenness. For our study we focused on the low, moderate, and high severity categories. The MTBS program mosaics these data to create yearly, nationwide burn severity raster layers. To create our binary severity rasters we could have simply reclassified these thematic datasets from MTBS into high versus other severity, but we chose not to for two primary reasons. First, thresholds used by MTBS project analysts to break continuous severity data into classes are adjusted subjectively on a fire-by-fire basis. While this approach works well when severity is mapped for a single fire, it introduces an element of inconsistency and potential but unknown bias when many fires are compared across space and time (Kolden et al. 2015). Second, MTBS thresholds are determined for continuous severity without the integration of a phenology offset, and we applied an offset value to all dNBR data to facilitate comparisons among fires.

Instead of using the MTBS-classified severity data directly, we evaluated the statistical distributions of their mosaicked yearly classified data that fell within the eastern study area, for the years 2000 through 2013 divided by mapping region, setting (forest vs. nonforest), and severity metric (NBR vs. dNBR). We identified the proportion of burned area in low, moderate, and high severity classes across this 14-year timespan (fig. 7). This analysis revealed that very little burned area was categorized by MTBS into the high severity class in most eastern mapping regions.

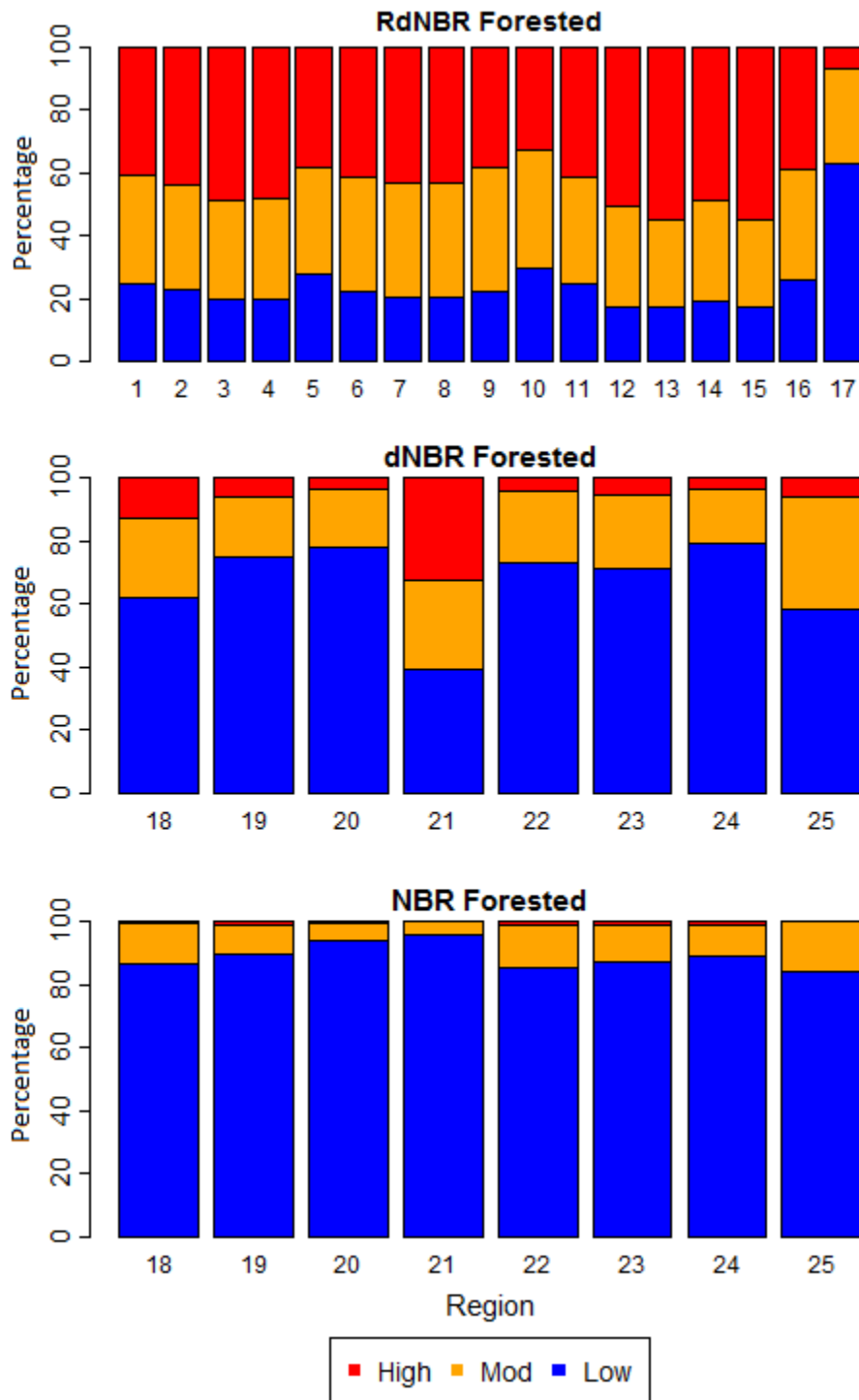


Figure 7—Proportion of forested burned area mapped as low, moderate (mod), or high severity based on satellite indices. The top graph summarizes the relative differenced normalized burn ratio (RdNBR) for western mapping regions, classified using thresholds that we calculated. The bottom two graphs summarize the Monitoring Trends in Burn Severity classified severity product, mapped with dNBR and single-scene NBR, in eastern mapping regions. Note the relatively small proportion mapped as high severity in most eastern regions, particularly with the single-scene NBR.

Due to the small area burned with high severity across all fires in the eastern United States, we made a substantial change from the methods we used in the western study area. Rather than model the potential for “high severity” fire in the eastern mapping regions, we chose to combine high and moderate severity and instead model the potential for “higher severity” fire. Following this logic, we identified percentile thresholds that marked the percentage of burned area above which MTBS mapped moderate to high severity. We subsequently found the continuous NBR or dNBR value corresponding to the percentile threshold (fig. 8). For example, if the MTBS thematic severity data in a particular mapping region and setting classified 80 percent of burned area as low severity and 20% as higher severity, we would sort all continuous dNBR values in that data subset, identify the 80th-percentile value, and classify everything above it as higher severity. The direction of sorting continuous severity metrics was important; for dNBR higher values represent higher severity, while for single-scene NBR data lower values represent higher severity. We calculated thresholds for each mapping region in the eastern study area this way, separately by setting (forest vs. nonforest) and severity metric (NBR vs. dNBR) (table 3).

Using our threshold values (table 3) we reclassified the continuous NBR and dNBR datasets to create binary severity grids (higher vs. other) by year (2000–2013), mapping region (18–25), and setting (forest vs. nonforest). As in the western United States, we consolidated binary severity mosaics across all years, keeping outputs separate by mapping region and setting, and giving precedence to high or moderate severity values in those areas that burned in multiple years.

Table 3—Calculated normalized burn ratio (NBR) and differenced normalized burn ratio (dNBR) thresholds for the eastern study area.

Region	-----NBR -----				-----dNBR -----			
	----Forest ----		----Nonforest ----		----Forest ----		----Nonforest ----	
	Percentile	Threshold	Percentile	Threshold	Percentile	Threshold	Percentile	Threshold
18	87	0	94	-247	62	327	80	399
19	90	-125	95	-253	75	256	78	369
20	94	-169	97	-284	78	345	95	474
21	96	-226	98	-328	40	360	79	453
22	85	-31	87	-85	73	320	80	339
23	87	-101	95	-231	71	354	87	434
24	89	-75	82	-57	79	264	83	316
25	84	-14	76	-15	58	358	92	416

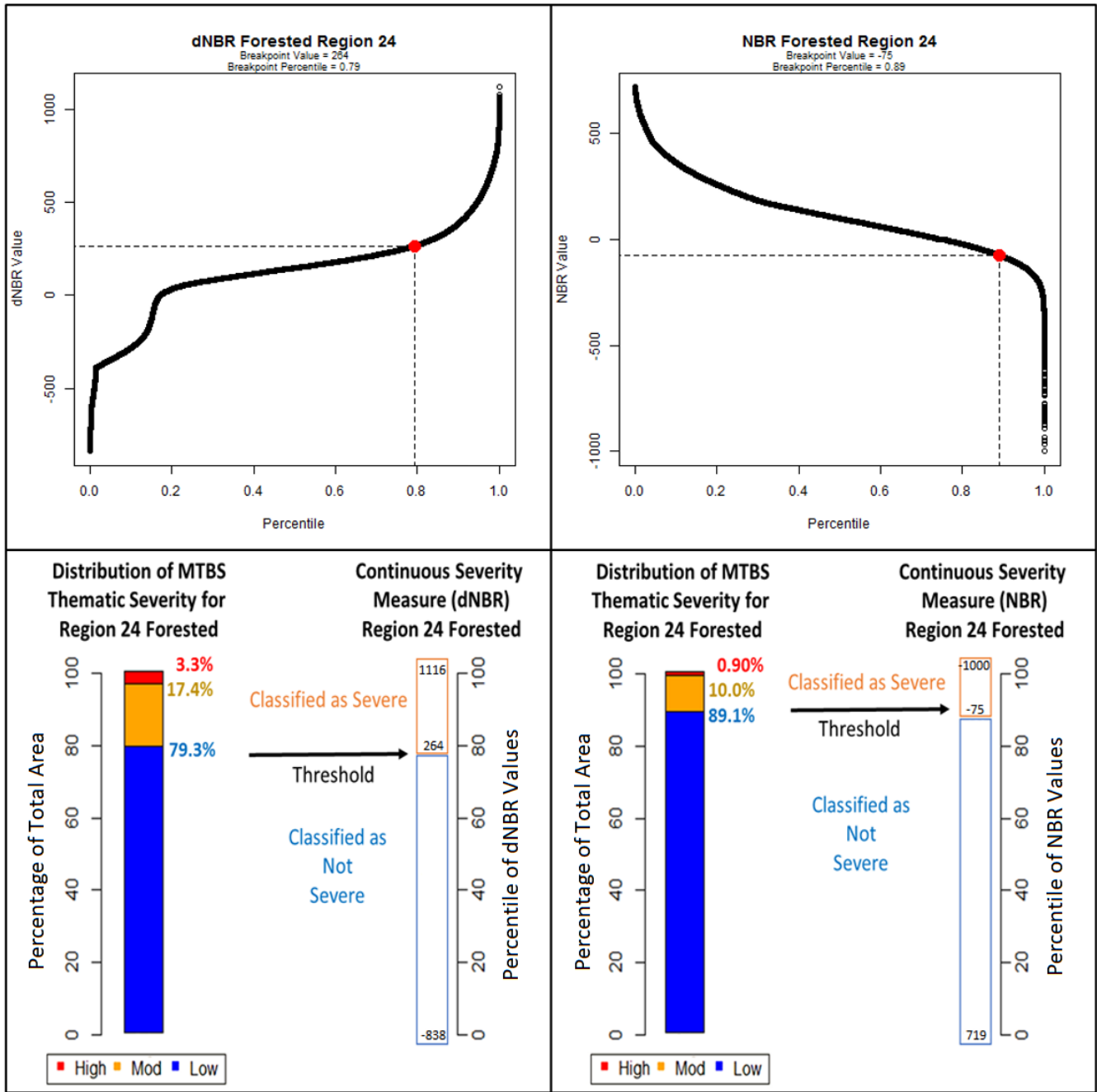


Figure 8—Illustration of the thresholding logic used to classify continuous severity data from Monitoring Trends in Burn Severity for eastern mapping regions. In each region, and separately for differenced normalized burn ratio (dNBR) and NBR, we first identified the percentile breakpoint between low and moderate (mod) severity (the percentile value between blue and orange bars in figure 7). We then found the corresponding dNBR or NBR index value (upper graphs) and classified values above that breakpoint for dNBR, or below the breakpoint for NBR, as higher severity (lower graphs).

2.1.4 Predictor Variables: Topographic Data

We derived a series of topographic indices from DEMs acquired from the USGS National Elevation Dataset (Gesch 2007). Topography describes the physical features of a geographical area and can influence temperature, moisture (Holden and Jolly 2011), vegetation (Whittaker 1970), and fire behavior (Pyne et al. 1996). For the western study area, we acquired the full set of 1-degree tiles of 1 arc second (approximately 30-meter pixel size) DEM data for CONUS in February 2009. For the eastern study area, we acquired updated DEM tiles in November 2014. All tiles were converted to our Albers projection with 30-meter resolution and with elevation units in feet, rounded to the nearest integer. We then derived 11 topographic indices for each tile. Calculations of slope aspect (i.e., the compass direction that a slope faces) using the CONUS Albers projection can be up to 21 degrees off for locations farthest from the projection's central meridian of 96 degrees West (i.e., the coasts). We adjusted our aspect calculations accordingly for any topographic indices using aspect. We accomplished this by adding a correction factor that realigned each tile not falling along the central meridian to true north.

The calculation of topographic indices occurs at each cell of the DEM and is dependent on the values of the surrounding cells. An "edge effect" will occur when a surrounding cell is missing. Therefore, we buffered each of the 1,010 DEM tiles covering the eastern and western study areas by 5 kilometers (approximately 3.1 miles) to facilitate the calculation of the following topographic indices:

- Elevation relief ratio (ERR): The elevation relief ratio describes the complexity or ruggedness of an elevation surface (Pike and Wilson 1971) and is defined as $(\text{mean elevation} - \text{minimum elevation}) \div (\text{maximum elevation} - \text{minimum elevation})$. We calculated ERR at three different scales with circular search areas with a radius of 3 cells, 15 cells, and 27 cells, resulting in three predictor variables. We refer to these as ERR3, ERR15, and ERR27.
- Heat load index (HLI): The heat load index is a transformation of aspect that accounts for the differences in the heating of slopes in the afternoon compared to the morning (McCune and Keon 2002: eqn. 3). A southwest-facing slope will reach a higher temperature than an equivalent southeast-facing slope at the same elevation. The magnitude of the slope also influences the amount of solar radiation (shortwave radiation) absorbed and reflected as heat (longwave radiation). The heat load index rescales aspect so that northeastern slopes receive the lowest values and southwestern slopes receive the highest while incorporating the effects of slope and latitude.
- Hierarchical slope position (HSP): Hierarchical slope position identifies landforms (e.g., ridges, valleys, slopes) based on their slope position relative to their surroundings (Murphy et al. 2010). The HSP algorithm accomplishes this by comparing surrounding elevations to a central elevation at multiple scales.
- Martonne's modified dissection coefficient (DISS): Dissection is a measure of topographic complexity and is defined as the ratio between relative relief and absolute relief, specifically $(\text{cell elevation} - \text{minimum elevation}) \div (\text{maximum elevation} - \text{minimum elevation})$ (Evans 1972). Minimum and maximum elevation are drawn from

a search area surrounding the central cell's elevation. We calculated two spatial scales of DISS using rectangular search areas of 3×3 cells and 27×27 cells, resulting in three predictor variables. We refer to these as DISS₃ and DISS₂₇.

- Slope (SLOPE): Slope steepness in percent.
- Topographic position index (TPI): The topographic position index calculates relative position on a slope as compared to its neighbors (Weiss 2001). This is accomplished by comparing a central cell's elevation to the average elevation of cells in a predefined search area surrounding it. The size of the search area determines the scale of the TPI. We calculated two TPI predictor variables using two different scales with an annular (doughnut-shaped) search area. To represent finer-scale topographic features, we used an interior radius of two cells and an exterior radius of five cells. For broader features, we used interior and exterior radii of 62 cells and 67 cells, respectively. We refer to each by their approximate outer radius in meters (i.e., TPI₁₅₀ and TPI₂₀₀₀).

We scaled the values of all topographic indices to integers and removed their 5-kilometer buffers to save storage space and reduce subsequent processing time. Including elevation, this process resulted in 12 topographic predictor variables.

In addition, we calculated variables representing potential solar radiation as part of our suite of topographic predictors. Solar radiation plays a variety of roles in determining the potential severity of wildfire, and is a function of aspect, sun angle, and shading. It affects the type and quantity of vegetation, minimum and maximum ambient temperature, the level and flux of fuel moisture (Holden and Jolly 2011), and a host of other environmental variables (Waring and Schlesinger 1985). Surface insolation is the amount of solar radiation that reaches the Earth's surface over a particular area (e.g., Watts per square meter). It is complex and varies by day of the year, latitude, topographic shading, and atmospheric interference (Iqbal 2012). While actual insolation will also vary over time based on cloud cover, potential insolation (i.e., clear-sky conditions) can be modeled for every day of the year at each pixel. We modeled potential surface insolation and calculated various measures to use as predictor variables in our statistical models. The particular measures and the solar radiation modeling tools that we used differed between the western and eastern study areas and are described in Appendix A.

Although the tools used to calculate solar radiation differed between East and West, much of the preprocessing and postprocessing was the same for the two study areas. All tiles were processed individually, 539 for the western study area and 471 for the eastern study area. We added a 5-kilometer buffer to each tile as we did with the other topographic indices and projected the DEM to a custom Lambert conformal conic projection to align grid north and true north. We customized the standard Lambert conformal conic projection by defining unique central meridians and standard parallels for each tile such that they cross the horizontal center and vertical upper and lower thirds of the tile, respectively. This step was necessary to reduce distortion and facilitate solar radiation modeling. For each tile, we then reprojected output solar radiation rasters back to our CONUS Albers projection. In the western study area we produced four predictor variables: annual and growing season versions of total solar radiation and potential evapotranspiration (PET) (see Appendix A for details). In the

eastern study area we produced a single solar radiation index representing the average global insolation across the winter solstice, summer solstice, and equinoxes.

2.1.5 Predictor Variables: Vegetation Data

The amount and condition of the vegetation present at the time a fire occurs can potentially have a large impact on the resultant burn severity (Arkle et al. 2012; Birch et al. 2015; Parks et al. 2014b,c). To account for these effects in our analysis, we selected the normalized difference vegetation index (NDVI; Rouse et al. 1974) to represent prefire vegetation conditions. This index is a remotely sensed measure of the amount of live green vegetation present in an area. It is calculated from the red and near-infrared (NIR) bands of spectral reflectance (eqn. 4), and can be derived from any imagery which collects these spectral bands.

$$NDVI = \frac{(NIR - Red)}{(NIR + Red)} \quad (4)$$

where NIR is reflectance in the near-infrared band (0.77–0.90 μm) and Red is reflectance in the red band (0.63–0.69 μm).

2.1.5.1 Vegetation Data: Western Study Area

For the western study area we derived NDVI from the prefire Landsat imagery provided by MTBS with each multiscene fire. Depending on the fire date and availability of imagery, the imagery was from one of three sources: the TM sensor on Landsat 5, the ETM+ on Landsat 7, or the OLI on Landsat 8. Other than projecting the Landsat data to our common Albers projection, we used the imagery as delivered by MTBS; we did not do any further image processing or corrections. We calculated NDVI for each fire (eqn. 4), resulting in a 30-meter-resolution raster of prefire vegetation for all burned areas in the western study area.

2.1.5.2 Vegetation Data: Eastern Study Area

Our choice to include single-scene fires in the eastern study area necessitated a different approach to generating prefire NDVI data. The MTBS program does not deliver a prefire Landsat scene for fires examined using a single-scene NBR image. We concluded that acquiring and processing clear prefire Landsat data for the approximately 2,750 single-scene fires used in the eastern modeling process would be impractical. Therefore, we decided to use precalculated NDVI datasets from the Moderate-Resolution Imaging Spectroradiometer (MODIS) instead.

Using MODIS data for prefire NDVI was a compromise that came with some tradeoffs in resolution and temporal depth. Because MODIS imagery became available only in 2000, we would not be able to use MTBS fire data from 1984 through 1999. The 250-meter (approximately 820 feet) resolution of MODIS NDVI data would also mean lower spatial resolution compared to our western NDVI. However, we concluded that using MTBS data from

2000 through 2013, with consistent, readily available prefire MODIS imagery would yield better modeling results than trying to produce and piece together Landsat-based NDVI for fires prior to 2000.

We acquired MODIS NDVI data (MOD13Q1 V006) for the eastern study area from the National Aeronautics and Space Administration Land Process Distributed Active Archive Center (Didan 2015). We downloaded 3,190 MODIS Terra vegetation index datasets to cover the eastern study area from 2000 through 2013. Each scene covers a 1,200-kilometer × 1,200-kilometer (746 mile × 746 mile) area with a resolution of 250 meters and is available at 16-day intervals. We used the MODIS Reprojection Tool (Dwyer and Schmidt 2006) to process each NDVI dataset into the standard Albers projection used for our analysis.

Vegetation index data from MODIS contains many layers of information, including NDVI and a measure of pixel reliability. The pixel reliability layer indicates whether NDVI for each pixel is good or has been affected by clouds, cloud shadows, and other atmospheric interference such as smoke. To ensure that we were using only the most accurate prefire vegetation data, we decided to use only those pixels with a reliability rank of 0—“Good Data—Use with confidence” as described in the MODIS Vegetation Index User’s Guide (Didan et al. 2015).

Through a careful analysis of the pixel reliability data and prefire imagery dates for MTBS multiscene fires, we evaluated which MODIS NDVI dataset to use for each fire in the eastern study area. We considered only MODIS data captured in the window of 0 to 32 days before a fire, which, given the 16-day repeat cycle of MODIS, gave us two options for each fire. We selected NDVI from the first scene before a fire (0–16 days) for 4,516 fires, and the second scene before a fire (17–32 days) for 779 fires. We eliminated 117 fires from the eastern study area due to a lack of reliable prefire NDVI pixels anywhere in the burned area. Additional details about this MODIS reliability analysis can be found in Appendix B.

2.1.6 Predictor Variables: 1,000-Hour Fuel Moisture at the Time of Burning

In addition to topography and vegetation, weather and climate have an important influence on wildfire behavior and resultant severity (Bessie and Johnson 1995; Birch et al. 2015; Dillon et al. 2011; Parks et al. 2018). Indices that track the combined effect of temperature and drought on the moisture levels in dead woody vegetation are particularly useful indicators of fire potential (Jolly and Freeborn 2017). Energy Release Component (ERC) is one such index that is commonly used by fire managers in the United States to monitor fire danger throughout the year (Andrews et al. 2003; Schlobohm and Brian 2002). The primary driver of ERC is the modeled moisture content in dead woody fuels 3 to 8 inches (8–20 centimeters) in diameter, known as 1,000-hour timelag fuels (Schlobohm and Brian 2002). We chose to use 1,000-hour fuel moisture as our sole climatic predictor because it integrates the effect of temperature, relative humidity, and precipitation (or lack of precipitation) over a period of about 40 days (1,000 hours divided by 24 hours per day). When large fuels and duff become dry enough to burn, the long-duration burning that often results can contribute to high severity fire effects (Morgan et al. 2014).

We derived a 1,000-hour fuel moisture index from a set of daily gridded weather variables at 4-kilometer (approximately 2.5 miles) resolution (from Abatzoglou 2013). Our index is on

a scale of 0 to 100, where higher values represent drier conditions. We removed the effect of elevation on fuel moisture because elevation and elevation-derived indices were included independently as predictor variables. We did that by adjusting gridded weather data to produce sea-level potential temperature and then calculated daily 1,000-hour fuel moisture rasters for each year in the study. We extracted the full daily series (1980 through 2010 for the western study area; 1980 through 2013 for the eastern study area) at each of our sample pixel locations (section 2.2.1), then identified the lowest fuel moisture that occurred during the approximate time each fire was burning (within 10 days after the fire detection date). From these numbers, we calculated the 1,000-hour fuel moisture percentile at the time of burning, specific to each sample location and relative to the fuel moistures found during a defined fire season within each mapping region (see Appendix C for details on how we determined fire seasons for each mapping region). For our index, we inverted the 1,000-hour fuel moisture percentiles, so that higher percentiles reflect drier conditions, to be consistent with other fire weather indices (e.g., ERC) that express higher fire potential with higher numbers. We recognize that using only the 10 days after detection is a weakness of our study, but we did not have a consistent approach for integrating the local weather and drought indices on the specific day of burning for each pixel.

2.2 Phase 2: Develop Random Forest Statistical Models

After acquiring and processing all input data, we developed statistical models relating our satellite observations of severe fire (high severity in the western study area, and moderate to high severity in the eastern study area) to our suite of predictor variables representing topographic, vegetation, and fuel moisture conditions at the time of each fire (table 4). We used the Random Forest machine learning algorithm (Breiman 2001) to develop our models, as implemented in the randomForest package (Liaw and Wiener 2002) for the R statistical software (R Development Core Team 2015). Random Forest is a nonparametric technique that is well suited to complex ecological modeling involving interactions between many predictor variables (Cutler et al. 2007; Dillon et al. 2011; Prasad et al. 2006). In general, our modeling methods follow the Random Forest procedures described by Dillon et al. (2011).

Table 4—Spatial datasets used for response and predictor variables in Random Forest statistical models for predicting severe fire potential in the western and eastern study areas.

Variable name	Abbreviation	Spatial resolution (m)	Response	Predictor
Burn severity				
Relative differenced normalized burn ratio	RdNBR	30	West	
Differenced normalized burn ratio	dNBR	30	East	
Normalized burn ratio	NBR	30	East	
Topography				
Elevation	DEM	30		West and East
Slope	SLOPE	30		West and East
Annual solar radiation ^a	RAD	30		West and East
Growing season solar radiation	GSRAD	30		West
Annual potential evapotranspiration	APET	30		West
Growing season potential evapotranspiration	GSPET	30		West
Heat load index	HLI	30		West and East
Topographic position index—150-meter radius	TPI150	30		West and East
Topographic position index—2,000-meter radius	TPI2000	30		West and East
Hierarchical slope position	HSP	30		West and East
Dissection coefficient—3 × 3 cell	DISS3	30		West and East
Dissection coefficient—27 × 27 cell	DISS27	30		West and East
Elevation relief ratio—3-cell radius	ERR3	30		West and East
Elevation relief ratio—15-cell radius	ERR15	30		West and East
Elevation relief ratio—27-cell radius	ERR27	30		West and East
Vegetation				
Normalized difference vegetation index	NDVI	30 (West); 250 (East)		West and East
Fuel moisture				
1,000-hour fuel moisture index	FM1000	4,000		West and East

^a Annual solar radiation was calculated differently in the western and eastern study areas. See Appendix A for details.

2.2.1 Sample Selection and Data Preparation

The first step in developing our statistical models was to extract values of response and predictor variables at a set of sample locations. Within each mapping region, and separately for forest versus nonforest settings, we generated a spatially balanced random sample of pixels from our MTBS binary severity mosaics. The intent of doing this was to minimize the effects of spatial autocorrelation, thereby increasing the likelihood that each sampled pixel is an independent observation (Theobald et al. 2007). Within each region and setting subset we determined the total number of pixels in each binary severity class. Setting the target sample size as 1% of the smaller of the two binary severity pixel counts, we then drew random pixel samples using the Create Spatially Balanced Points tool in ArcGIS. After drawing samples for each of the two severity classes, we appended them into a single dataset and verified that the sample was balanced both spatially and relative to the two values of our response variable. Using these methods, we generated a set of sample pixels for each combination of mapping region and setting (forest vs. nonforest).

At each sample pixel, we extracted the value for each of our static predictor variables, the daily time series of 1,000-hour fuel moisture, prefire NDVI, and binary severity (table 4). If a sample location burned more than once during our MTBS time series, each fire at that location was recorded in our dataset as a separate record. From the sample pixels in each combination of region and setting, we used 90% of them as training data for developing Random Forest models, and held out a 10% subset for model validation (see section 2.4.2). Before modeling, we performed a correlation analysis on all potential predictor variables for each modeling subset. We identified variables that were highly correlated with others (Spearman's $\rho > 0.75$) as being possibly redundant, and eliminated them from the dataset in an effort to use predictor variables that were relatively independent of one another.

2.2.2 Random Forest Model Development

Random Forest is a powerful tool for elucidating relationships between a response variable and a set of predictor variables. It is an extension of classification and regression trees, and uses a large number of trees (i.e., a “forest”) with random permutations to classify each sample observation into a response category (here, higher severity vs. other severity) based on the values of the predictors. It also provides statistics on the importance of each predictor, and results in a predictive model that can be used to classify new observations into one of the response categories. The process we used to create Random Forest models followed the general workflow described by Dillon et al. (2011), including three main steps: (1) run multiple replicate models with all the predictors that remained after the correlation analysis to determine stable importance rankings for the predictors; (2) use an iterative model selection routine to determine the subset of variables that results in the lowest overall model error; and (3) use the optimal set of predictor variables to run a final model.

We developed Random Forest models separately for forest and nonforest settings in each of our 25 mapping regions, resulting in 50 separate models. These models gave us both binary severity predictions and rankings of the most important predictor variables. Due to significant random permutations each time Random Forest is run, the importance of specific variables can vary from one run to the next. Therefore, we followed the advice of Svetnik et al. (2004) and used five replications of fivefold cross-validation at each step in an iterative model selection routine to identify the best predictor variables. For each of our 50 models, we first determined stable importance rankings of the predictor variables with 5 cross-validated replications of full Random Forest models (i.e., all predictors; tables 4, 8, and 9), each with 1,500 classification trees. Next we iteratively reduced the number of predictor variables by dropping the variable with the lowest importance rank, then running another five cross-validated model replications. During model selection, we used 1,000 classification trees per model. Through this process, we identified the optimal set of predictor variables that produced the lowest overall classification error. In each of the 50 modeling scenarios, we used the set of predictors determined in this way to run the final Random Forest model with 1,500 classification trees.

2.2.3 Random Forest Model Performance

We assessed the performance of our models using two measures of accuracy, each averaged across the cross-validated replicates of the optimal models. These performance measures are overall percentage correctly classified (PCC) and area under the receiver operating characteristic curve (AUC). Due to our efforts to ensure balanced samples with respect to our binary response categories, we expected values of PCC to range between 0.5 (random) and 1.0 (perfect accuracy). We interpreted AUC to indicate whether the overall model accuracy was fair (>0.7), good (>0.8), or excellent (>0.9) (Swets 1988).

2.3 Phase 3: Create the Severe Fire Potential Map

Once the Random Forest models were developed, we used them to make spatial predictions of severe fire potential across the entire study area. While our models were built using samples from burned areas, we were able to apply the predictions across all lands because the spatial data for our static predictor variables are comprehensive across our entire study area. The two temporally specific variables—vegetation (NDVI) and 1,000-hour fuel moisture index—needed special considerations, which are described next.

2.3.1 Normalized Difference Vegetation Index

To predict SFP on all lands in our study area, we needed comprehensive NDVI mosaics representing current vegetation conditions. The best and most readily available source for this was the precalculated NDVI product from MODIS (Didan 2015). Despite a relatively coarse spatial resolution (250 meters) compared to Landsat (30 meters), the MODIS NDVI products are available as relatively cloud-free 16-day composites for all areas of the United States. The relatively cloud-free nature of this product is achieved by choosing the best available pixel

value from all MODIS acquisitions in a 16-day period (Didan et al. 2015). For both the western and eastern study areas, we acquired the MODIS NDVI for the most current full year available at the time of our predictions (2011 for the western study area, 2014 for the eastern study area). In both cases, we used the MODIS Reprojection Tool (Dwyer and Schmidt 2006) to prepare each NDVI dataset for analysis. Within each month, we chose the NDVI mosaic for the first 16-day period available to represent the month. Additional processing required for the MODIS NDVI data differed greatly between the western and eastern study areas.

2.3.1.1 Western Study Area

For the western study area, we acquired and processed MODIS NDVI products for each month in 2011. While the MODIS NDVI is conceptually similar to the Landsat NDVI used in Random Forest model development, some important differences in both spatial resolution and distribution of values between the two products required attention. To adjust the spatial resolution, we resampled the 250-meter MODIS pixels down to 30-meter pixels using bilinear interpolation. This step resulted in MODIS NDVI data that matched the resolution of our other raster data, including the prefire Landsat NDVI data, and also smoothed out the blocky 250-meter pixel footprints so they would not be prominent in our predicted outputs. To adjust the values in the MODIS NDVI data, we performed two types of relative normalization, a major axis (MA) regression and histogram matching. In each mapping region, we chose the method that resulted in the better alignment of MODIS NDVI values with the distribution of values in the prefire Landsat NDVI data (see Appendix D for more details).

The intent of NDVI data for the current landscape is to represent probable vegetation conditions at the time of a new fire. Therefore, we needed to identify the most likely month of fire occurrence for different locations across our study area to choose the most appropriate monthly NDVI raster for prediction. As our spatial predictions would be done individually for each 1-degree tile, we chose to assign the most likely burning month for each tile. To do this, we analyzed the national database of fire occurrence points provided by MTBS (<https://www.mtbs.gov/direct-download>). Based on the detection date recorded for each point, we used kriging to generate a continuous surface of most common burning month. We then used a zonal majority calculation, with tiles as the zones, to assign a month to each tile (fig. 9).

The result of this processing was a 30-meter-resolution “current NDVI” raster for each of the 539 tiles in the western study area.

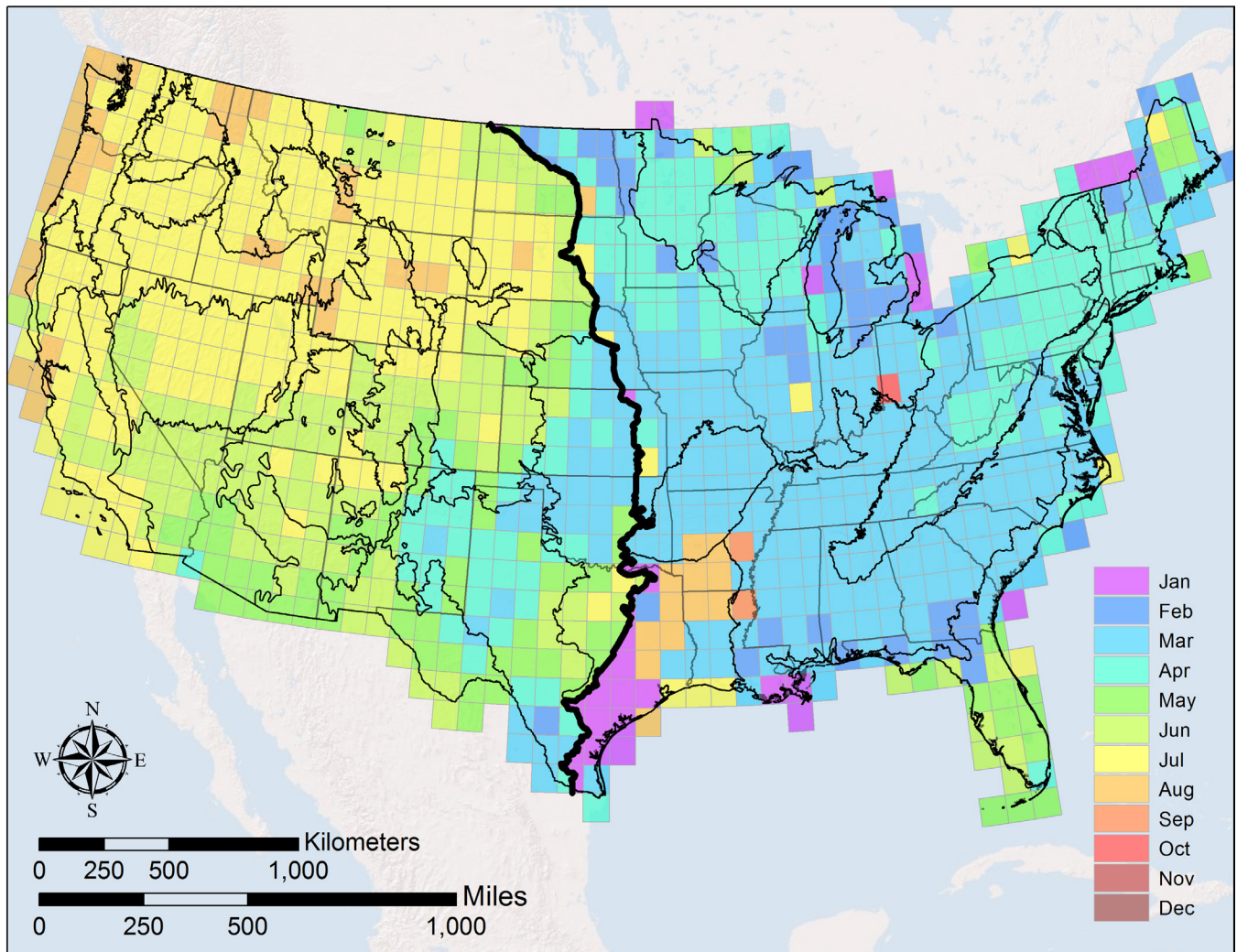


Figure 9—Map showing the month selected for each 1-degree tile for creating the current normalized difference vegetation index (NDVI) raster used in predictions. The intent was to capture the most likely month of fire occurrence in each tile, based on MTBS point fire occurrence data. Methods for selecting the most likely month of fire occurrence differed between the eastern and western study areas. See the text for an explanation of the methods.

2.3.1.2 Eastern Study Area

For the eastern study area, we downloaded and processed MODIS NDVI images for the year 2014. Because we also used MODIS NDVI to depict prefire NDVI in our model development, the value adjustments we did for the western study area were not necessary for this study area. As in the western study area, we used bilinear interpolation to downscale the 250-meter MODIS data to 30-meter pixels. To select the month for each tile in the eastern United States, we simply identified the month in each tile with the most points in the MTBS fire occurrence points dataset (fig. 9). We did not use kriging as we did in the western study area because of the multimodal nature of fire seasons in the eastern study area mapping regions (see Appendix C). We also extracted the NDVI data by tile to create a 30-meter-resolution “current NDVI” raster for each of the 471 tiles in the eastern study area.

2.3.2 1,000-hour Fuel Moisture

Ideally, one could use a current or predicted surface of 1,000-hour fuel moisture as input to our Random Forest models that would be accurate for a specific point in time. However, our SFP map is intended to be a static, predetermined reference layer available for managers to access online. It is not intended to be a prediction for a specific point in time; rather, it needs to reflect the relative potential for higher severity across landscapes based on current vegetation and typical burning conditions. Because our Random Forest models require the 1,000-hour fuel moisture index as an input to make predictions, we chose to set the index to a constant value across all pixels. We selected the 90th percentile as our 1,000-hour fuel moisture index value for predictions.

We recognized that fuel moisture varies across different topographic settings (Holden and Jolly 2011), but we assume that these influences are captured by our specific topographic variables. We also recognized that inherent relationships exist between fuel moisture and elevation-driven biophysical changes (e.g., temperature and other meteorological and topographic factors affecting site-specific water balance). Our decision to use sea-level potential temperature in calculating our 1,000-hour fuel moisture index was specifically intended to decouple these relationships (Jolly et al. 2005). Last, we recognized that percentile thresholds for fire danger indices vary across the country, but chose the 90th percentile because it is recommended as one of two critical percentiles in determining fire business thresholds and climatological breakpoints for fire danger rating (the other being 97th percentile for extreme conditions) (NIFC 2018).

2.3.3 Making Spatial Predictions

We used our Random Forest models to predict severe fire potential for every 30-meter pixel across CONUS. Our final Random Forest models consisted of 1,500 classification trees, so each pixel received 1,500 different binary predictions of whether it would experience higher or lower burn severity. The value assigned to each pixel was the percentage of those 1,500 predictions where the outcome was higher severity. We interpreted this percentage as the probability of high severity (or moderate to high severity in the East), and this number is our SFP index.

Using the spatial framework of our 1-degree tiles, we ran SFP predictions one tile at a time. Within each mapping region, we ran predictions for each tile with the forest and nonforest Random Forest models, using the current condition forest and nonforest masks. We executed all of our spatial predictions in R, using the randomForest (Liaw and Wiener 2002) and raster (Hijmans et al. 2016) packages.

Because the outer tile footprint for each region overlaps neighboring regions (fig. 2, inset map), tiles within these overlap areas ended up with more than one prediction output. To minimize regional edge effects in our final map, we smoothed the modeled outputs within these overlapping tiles (separately for forest vs. nonforest) using a distance-weighted algorithm across a 120-meter-wide (approximately 390 feet) area along the regional boundaries.

2.3.4 Creating the Severe Fire Potential Deliverables

We finalized the SFP data for each tile by masking out nonburnable pixels as defined by the Scott and Burgan (2005) Fire Behavior Fuel Model layer (FBFM40) from LANDFIRE (<https://www.landfire.gov/fbfm40.php>). Nonburnable pixels are those defined as urban, snow or ice, agriculture, water, and barren. With each tile finalized, we created separate forest and nonforest mosaics of the SFP map for each mapping region and made them available for download online via the Fire Research and Management Exchange System (FRAMES; <https://www.frames.gov/partner-sites/firesev/firesev-home/> and <https://www.frames.gov/partner-sites/firesev/firesev-east/>). These regional forest and nonforest SFP map mosaics can be merged within a region, or across multiple regions to create mosaics covering a larger extent (e.g., the full western or eastern study area).

2.4 Phase 4: Evaluate the Severe Fire Potential Map

To provide information to prospective users about the accuracy and interpretation of the SFP map, we evaluated the quality of our predicted SFP map products. The model performance statistics described earlier indicate the strength of statistical relationships within our burned area samples, but given the unprecedented accomplishment of a wall-to-wall map of probability of high severity fires for all lands in the contiguous United States, we wanted a broader assessment of map accuracy in all areas covered by the map. We examined the predictive ability of the SFP map at the pixel scale, and also explored landscape-scale patterns in the SFP predictions and satellite-based severity observations.

2.4.1 Evaluating the Severe Fire Potential Map at the Pixel Scale

A major challenge in evaluating the SFP map is that SFP depicts a likelihood, on a scale of 0 to 100, of a binary outcome (higher severity or not). To test our predictions against observed binary severity inferred from satellite data at the pixel scale, we needed to convert our predictions into the same binary choices (e.g., SFP > 50 is high severity). We did this by trying a range of possible breakpoints to divide the continuous SFP values into a binary depiction of higher severity versus lower severity. We tested 11 breakpoints ranging from 25 to 75 in 5-point

increments. For each breakpoint, we classified SFP values above the breakpoint as higher severity.

As described in section 2.2.1, we withheld a 10% subset of all sample pixels for model validation. To facilitate even comparisons of predicted and observed data, we further limited these validation data to fires that burned under roughly the same conditions as our SFP predictions. Because we set the 1,000-hour fuel moisture index to the 90th percentile for making predictions, we selected validation data only from fires that burned between the 85th and 95th percentile of the 1,000-hour fuel moisture index. This selection process left us with 32,424 sample points originating from 3,094 fires in the forest setting and 57,302 sample points originating from 3,772 fires in the nonforest setting (table 5).

Table 5—The number of individual fires and sample pixels used for validation of the Severe Fire Potential map, by mapping region and forest versus nonforest settings. The horizontal line divides western from eastern mapping regions.

Region	----- Forest -----		----- Nonforest -----	
	Fires	Samples	Fires	Samples
1	125	2,250	97	959
2	119	1,959	244	3,986
3	277	6,052	312	4,947
4	243	3,990	771	18,593
5	98	1,539	68	436
6	82	1,243	106	934
7	161	1,834	258	2,989
8	126	916	473	9,110
9	93	1,061	323	4,867
10	66	981	127	1,044
11	87	1,035	116	1,215
12	54	625	129	1,528
13	57	1,150	148	1,871
14	6	144	28	274
15	184	3,151	205	3,403
16	13	301	38	226
17	2	4	7	15
18	105	279	45	161
19	127	328	13	23
20	83	197	115	431
21	36	401	24	71
22	413	1,352	48	65
23	490	1,549	73	149
24	47	83	4	5
25	0	0	0	0
Totals	3,094	32,424	3,772	57,302

Within each mapping region, and separately for forest and nonforest settings, we tested the agreement between the binary SFP map created from each of the 11 breakpoints and observed binary severity data in our validation dataset, then calculated the receiver operating characteristic (ROC) curve and the associated AUC statistic (Swets 1988). In each case, we selected the breakpoint with the highest AUC statistic as the best break for validating our higher severity predictions.

We also anticipated that users of the SFP map may be inclined to interpret pixel-scale SFP values as a continuous scale of potential severity, much like satellite-derived severity indices (e.g., NBR, dNBR, and RdNBR). To address this possibility and to explore the relationship between our index and the satellite-derived severity indices, we additionally tested the relationship between our predicted SFP values and these severity indices using linear regression analyses. If regressions show strong relationships, then lower values of SFP could be useful for understanding the likelihood of low to moderate severity fire; if the relationships are weak, then interpretation of SFP is limited to its intended purpose of predicting severe fire potential. We performed linear regressions comparing SFP values to the observed continuous severity index values (RdNBR for the western study area and NBR or dNBR for the eastern study area). Regressions were run for each combination of mapping region and forest and nonforest settings.

2.4.2 Evaluating the Severe Fire Potential Map at the Landscape Scale

Zooming out from individual pixels, we expected high severity to be both observed and predicted more often in some landscape settings than others. To examine patterns at the landscape scale, we performed spatial summaries of the observed MTBS data and our SFP predictions. We included all fires acquired from MTBS in these summaries: 6,663 fires in the western study area (1984–2007), and 5,295 fires in the eastern study area (2000–2013) (fig. 6). Within each mapping region, and by forest and nonforest, we summarized both types of severity data by broad landform classes (see following section). For the SFP data, we calculated descriptive statistics of the continuous SFP values. For the satellite-derived MTBS severity data, we used the thematic classifications of MTBS created from our calculated thresholds (section 2.1.3) to summarize the proportion of burned area mapped as high severity in the western study area, or as high or moderate severity in the eastern study area. By providing descriptive information about places on the landscape where high severity fire tends to be more frequently observed or predicted, we hope to provide managers with a broader conceptual understanding of where to anticipate high severity outcomes.

2.4.3 Defining Landform Classes

The distribution of vegetation patterns, moisture regimes, and other biophysical processes varies with topographic setting. Variables depicting the relative degree of sunlight or shading, such as solar radiation or aspect indices, or relative topographic position, such as TPI (Weiss 2001), can substantially affect burn severity (Dillon et al. 2011). We included these types of predictor variables in our models to account for their potential influence at the pixel level.

However, we were also interested in understanding whether higher burn severity is more common on certain broad landform classes in a more general sense.

Weiss (2001) suggested a method for defining landform classes using two scales of TPI; we used the TPI150 and TPI2000 data already generated for model development and prediction. Within each mapping region, we standardized the TPI rasters into units of standard deviations (Weiss 2001) and combined them to create discrete landform classes. For simplicity, we grouped these classes into three broad categories of flats, slopes, and ridges.

To create our final four-class landform classification, we subdivided the slope category into “warm” or “cool” aspects. We determined this by using a combination of HLI (section 2.1.4) (McCune and Keon 2002) and a slope Cosine Aspect Transformation (CAT) (Stage 1976). The CAT converts aspect to values ranging from -1 (steep, south-facing) to 1 (steep, north facing) and accounts for differences in exposure due to slope angle. We considered “warm” slopes as those with HLI above the regional mode of HLI values and CAT values below zero. Conversely, we considered “cool” slopes to be those with HLI below the mode HLI and CAT values above zero. Using the combination of HLI and CAT ensured that we were identifying clear examples of warm and cool aspects. We considered locations with conflicting HLI and CAT values (e.g., a warm HLI value above the mode, but a cool CAT value above zero) to be ambiguous for our purposes and removed them from our landform analysis. With our landform classes defined, we were able to summarize the distribution of observed and predicted severity across flats, ridges, warm slopes, and cool slopes.

3. Results

3.1 Random Forest Statistical Models

3.1.1 Data Availability and Sample Sizes

Fires were more prevalent in some vegetation types and regions, and this strongly influenced our ability to develop robust statistical models in some cases. We were able to develop Random Forest models in 49 of the 50 possible modeling scenarios (forest and nonforest models in each of 25 mapping regions), but the number of MTBS fires available to sample, and subsequently the number of sample points for model development, varied widely among scenarios (tables 6, 7). For forests in the western study area, the number of MTBS fires available to sample varied from 305 in region 17 (Southern Great Plains) to 2,465 in region 4 (Intermountain Basins). Correspondingly, pixels sampled for model development ranged from 2,779 in region 17 to the maximum sample size of 100,000 in regions 3, 4, and 15. For forests in the eastern study area, there were fewer MTBS fires available, ranging from only 7 in region 25 (New England) to 2,938 in region 23 (Southeast Coastal Plain). Sample sizes were also smaller in the eastern regions, ranging from just 122 pixels in region 25 to 66,527 pixels in region 23. In general, sample points for forest models were well distributed across the mountainous areas of the western study area, but highly concentrated in the eastern study area within a few areas in Florida, east Texas, the Ozark Mountains, the central Appalachians, and northern Minnesota (can be inferred from fire location in figure 6).

The data available for nonforest model development also varied widely among mapping regions (table 7, fig. 6). We sampled from the same set of fires used for forest models, but the number of pixels sampled for nonforest model development was very different due to differences in the distribution of forest versus nonforest vegetation within these fires. In the western study area, nonforest sample sizes ranged from 2,743 in region 17 to the maximum sample size of 100,000 in regions 2, 3, 4, 7, 8, 9, and 15. In one eastern mapping region, region 25, there were no nonforest burned areas to sample and we were unable to build a nonforest model. In the remaining eastern regions, nonforest sample sizes ranged from 262 in region 24 (Appalachians) to 64,733 in region 22 (Southern Piedmont and Lower Mississippi Basin). It is important to consider such uneven sample sizes when evaluating the reliability of each model.

Table 6—Number of individual fires and sample pixels used in Random Forest statistical models for forest settings in each mapping region, along with the number of predictor variables (total and in the reduced, optimal model) and Random Forest model performance statistics. The horizontal line divides western from eastern mapping regions.

Region	MTBS fires ^a	Sample points	Number of predictors		Random Forest model performance	
			Full model	Optimal model	PCC ^b	AUC ^c
1	467	73,087	13	9	0.71	0.78
2	830	58,321	12	6	0.72	0.80
3	988	100,000	12	10	0.65	0.71
4	2,465	100,000	12	8	0.68	0.75
5	383	50,301	12	9	0.70	0.77
6	543	39,094	13	5	0.74	0.82
7	1,069	73,253	13	4	0.72	0.80
8	1,611	39,566	14	7	0.71	0.79
9	1,216	39,750	14	6	0.73	0.80
10	789	41,282	13	6	0.77	0.85
11	817	65,235	13	9	0.75	0.83
12	592	37,024	13	9	0.72	0.79
13	690	54,970	12	9	0.72	0.79
14	348	12,872	13	9	0.73	0.80
15	860	100,000	12	8	0.66	0.72
16	467	8,368	12	5	0.74	0.82
17	305	2,779	13	9	0.83	0.91
18	609	17,162	13	5	0.84	0.91
19	482	12,479	13	4	0.77	0.84
20	717	8,941	13	5	0.75	0.82
21	197	9,417	12	5	0.87	0.93
22	2,246	64,733	12	5	0.80	0.88
23	2,938	66,527	11	5	0.80	0.88
24	539	7,642	12	6	0.75	0.83
25	7	122	12	4	0.70	0.73

^a Many fires in the Monitoring Trends in Burn Severity (MTBS) database were used in more than one region. The total number of MTBS fires used across all regions was 11,958 (6,663 in the western United States, 5,295 in the eastern United States).

^b PCC is percentage correctly classified.

^c AUC is area under the receiver operating characteristic curve.

Table 7—Number of individual fires and sample pixels used in Random Forest statistical models for nonforest settings in each mapping region, along with the number of predictor variables (total and in the reduced, optimal model) and Random Forest model performance statistics. The horizontal line divides western from eastern mapping regions.

Region	MTBS fires ^a	Sample points	Number of predictors		Random Forest model performance	
			Full model	Optimal model	PCC ^b	AUC ^c
1	467	27,749	13	9	0.74	0.82
2	830	100,000	12	7	0.75	0.83
3	988	100,000	13	9	0.76	0.85
4	2,465	100,000	13	7	0.70	0.78
5	383	15,598	12	9	0.72	0.79
6	543	35,289	13	9	0.73	0.81
7	1,069	100,000	14	9	0.74	0.82
8	1,611	100,000	14	7	0.69	0.76
9	1,216	100,000	13	9	0.74	0.82
10	789	34,112	13	9	0.76	0.83
11	817	54,758	13	9	0.77	0.85
12	592	78,222	13	9	0.76	0.83
13	690	93,560	13	4	0.74	0.82
14	348	23,447	13	5	0.79	0.87
15	860	100,000	12	9	0.77	0.85
16	467	27,979	12	9	0.78	0.86
17	305	2,743	13	6	0.82	0.90
18	609	5,049	11	5	0.83	0.90
19	482	1,307	12	4	0.77	0.84
20	717	13,543	13	7	0.84	0.91
21	197	1,652	11	6	0.85	0.93
22	2,246	64,733	11	5	0.80	0.88
23	2,938	3,859	11	4	0.80	0.89
24	539	262	12	7	0.69	0.72
25	7	0	NA	NA	NA	NA

^a Many fires in the Monitoring Trends in Burn Severity (MTBS) database were used in more than one region. The total number of MTBS fires used across all regions was 11,958 (6,663 in the western United States, 5,295 in the eastern United States). Region 25 had insufficient data to construct a Random Forest model in nonforest areas.

^b PCC is percentage correctly classified.

^c AUC is area under the receiver operating characteristic curve.

3.1.2 *Relative Importance of Variables*

Our rigorous model selection routine confirmed that not all predictor variables added value to our models, and the most parsimonious prediction of SFP could in every case be accomplished with 10 or fewer predictors. The number of predictor variables used in the full Random Forest model, and variables selected in the optimal model, varied among modeling scenarios. Based on the correlation analysis (Spearman's rho) of candidate predictor variables, the full set of predictors used in each scenario ranged from 12 to 14 in the western study area, and 11 to 13 in the eastern study area (tables 6, 7). Solar radiation variables were highly correlated with each other, and only one was retained in most cases. Similarly, HLI was eliminated in all cases due to its correlation with solar radiation. Among candidate topographic variables, either ERR15 or ERR3 was removed in most cases due to their correlation with ERR27, DISS3, or DISS27. We also eliminated TPI2000, HSP, and DISS3 from certain eastern regions (tables 8, 9). Using Random Forest's statistics on the relative importance of each predictor variable, we ranked all predictors used in the models from most important (1) to least important (11–14, depending on the model) (tables 8, 9). The number of predictor variables retained in the optimal model for each region varied from 4 to 10 in the western study area, and from 4 to 9 in the eastern study area (tables 6–9).

The three most important variables in predicting SFP across all models were elevation, NDVI, and 1,000-hour fuel moisture (tables 8, 9), all of which make sense ecologically. These 3 variables were retained in the optimal model in all but 1 of the 49 models that we developed (fuel moisture was dropped in the nonforest model for region 24). In the western study area, elevation had the strongest effect on our forest models (average rank = 1.6) and was the second-ranked predictor in nonforest settings (average rank = 2.2). In the eastern study area, the effect of elevation was weaker, with an average rank of 3.0 in both forest and nonforest settings. NDVI, which represents the amount of green vegetation cover, was generally the second most important predictor, with average ranks of 2.1 in western forest models, and 2.5 and 2.4 in eastern forest and nonforest models, respectively. Notably, NDVI was the best predictor in nonforest settings in the western study area. In the eastern study area, 1,000-hour fuel moisture, indicating overall climatic conditions and drought, was the best predictor in both forest and nonforest settings, with average ranks of 2.1 in forests and 1.2 in nonforests. In the western study area, 1,000-hour fuel moisture was the third most important variable in both forests (average rank = 2.6) and nonforests (average rank = 3.0).

After the top three variables, the next most important predictors were generally some combination of slope, solar radiation, or topographic position. Some subset of these variables is included in every model, and average rankings for these variables generally are between 3 and 7. The only variable besides elevation, NDVI, and 1,000-hour fuel moisture that was included in all western models was the broad-scale topographic position index, TPI2000, with an average rank of 5.1 in forest models and 5.5 in nonforest models. No other variable, besides the top three, was included in all optimal models in the eastern study area.

The least important variables were those representing topographic complexity (dissection and elevation relief ratio). These variables were excluded from the optimal models in many scenarios, and when they were included they had the lowest rankings.

Table 8—Rankings of predictor variable importance from Random Forest statistical models for forest settings in each mapping region. The vertical line divides western from eastern mapping regions. ^aVariables are defined in table 4.

Variable	Region																										
	West												East														
	1	2	3	4	5	6	7	8	9	10	11	12	13	14	15	16	17	18	19	20	21	22	23	24	25		
Vegetation																											
NDVI	2	2	2	3	1	2	3	3	1	2	3	2	2	3	2	1	1	2	3	2	3	2	2	2	2	4	
Fuel moisture																											
FM1000	3	3	4	4	2	3	2	2	3	1	1	3	3	1	3	3	3	1	1	1	1	1	1	1	3	8	
Topography																											
DEM	1	1	1	1	4	1	1	1	2	3	2	1	1	2	1	2	2	3	2	3	2	3	2	3	4	3	
SLOPE	4	4	3	2	5	5	5	4	4	7	9	...	4	...	8	5	...	
RAD ^b	8	...	9	5	8	6	7	5	6	7	6	...	5	4	...	4	4	4	4	3	1	...	
GSPET ^c	6	—	—	—	5	—	4	4	...	4	...	6	4	—	5	—	4	—	—	—	—	—	—	—	—	—	
HLL	—	—	—	—	—	—	—	—	—	—	—	—	—	—	—	—	—	—	—	—	—	—	—	—	—	—	
TP1150	7	9	6	5	4	5	6	...		
TP12000	5	5	5	6	3	4	4	7	6	5	5	8	4	4	5	4	6		
HSP	8	8	8		
DISS3	5	1		
DISS27	7	...	6	7	7	8	6	5	6	7	...	9		
ERR3		
ERR15	—	—	—	—	—	—	—	—	—	—	—	—	—	—	—	—	—	5	5	...	2	
ERR27	9	6	10	8	9	6	9	9	7	9	8	5	7	3	2	3	2	3	2	3	4	3	

^a Ellipsis (...) = variables not selected in the optimal model for a region; dash (—) = variables not included in a particular region due to high correlations with other variables.

^b The "RAD" variable was different between the western and eastern regions (see text for full explanation).

^c The "GSPET" variable was not calculated in the East.

Table 9—Rankings of predictor variable importance from Random Forest statistical models for nonforest settings in each mapping region. The vertical line divides western from eastern mapping regions. ^a Variables are defined in table 4.

Variable	Region																								
	West												East												
	1	2	3	4	5	6	7	8	9	10	11	12	13	14	15	16	17	18	19	20	21	22	23	24	25
Vegetation																									
NDVI	1	1	1	1	2	2	2	1	1	1	1	1	1	1	1	1	1	2	3	2	1	2	4	3	
Fuel moisture																									
FM1000	2	3	3	5	3	3	3	4	3	2	3	3	3	3	2	3	3	1	1	1	2	1	1	...	
Topography																									
DEM	3	4	2	3	1	1	1	2	2	3	2	2	2	2	3	2	2	4	2	3	3	3	2	4	
SLOPE	5	6	6	6	7	6	6	9	7	6	9	8	8	5	6		
RAD ^b	—	2	7	4	5	6	5	5	4	4	6	7	4	5	3	...	4	4	4	3	2		
GSRAD ^c	4	—	—	—	—	—	—	—	—	—	—	—	—	—	—	—	—	—	—	—	—	—	—		
APET ^c	6	—	—	—	—	—	—	—	—	—	—	—	—	—	—	—	—	—	—	—	—	—	—		
GSPET ^c	—	—	5	2	—	4	4	3	4	5	4	—	5	—	—	4	—	—	—	—	—	—	—		
HLI	—	—	—	—	—	—	—	—	—	—	—	—	—	—	—	—	—	—	—	—	—	—	—		
TPI150	8		
TPI2000	7	5	4	7	4	5	7	7	6	6	7	5	4	4	4	6	6	...	4	7		
HSP	—	7		
DISS3	—		
DISS27	8	...	8	...	7	8	9	...	8	8	9	7	6	7	6	1	
ERR3	9	9	5	
ERR15	—	—	—	—	—	—	—	—	—	—	—	—	—	—	—	—	—	—	...	5	—	—	—		
ERR27	9	7	9	...	9	9	8	...	7	9	8	8	5	5	...	5	...	6	—	5	

^a There were too few samples to create a model for region 25. Ellipsis (...) = variables not selected in the optimal model for a region; dash (—) = variables not included in a particular region due to high correlations with other variables.

^b The "RAD" variable was different between the western and eastern regions (see text for full explanation).

^c The "GSRAD," "APET," and "GSPET" variables were not calculated in the East.

3.1.3 Random Forest Model Performance

Model performance statistics indicate that our forest models performed mostly in the fair to good range, with a few in the excellent range (fig. 10, table 6). In the western study area, eight regions had fair model performance (AUC 0.71–0.79; PCC 0.65–0.72; average sample size = 69,369). These regions are all in the northern two-thirds of the western study area. Eight western regions had good model performance (AUC 0.80–0.85; PCC 0.72–0.77; average sample size = 42,272), and were mostly in the southern third of the western United States. Only one western region had excellent model performance (AUC = 0.91, PCC = 0.83). This was region 17, which had the fewest samples (2,779). Of the eastern mapping regions, only one had fair model performance (AUC = 0.73, PCC = 0.70), but this was region 25, which had only 122 sample points, making the model very weak. Five eastern regions had good model performance (AUC 0.82–0.88; PCC 0.75–0.80; average sample size = 32,064), and two eastern regions had excellent model performance (AUC 0.91–0.93; PCC 0.84–0.87; average sample size = 13,290).

Nonforest models performed mostly in the good range, with a few regions each in the fair and excellent ranges (table 7, fig. 10). In the western study area, three regions had fair model performance (AUC 0.76–0.79; PCC 0.69–0.72; average sample size = 71,866). Thirteen western regions had good model performance (AUC 0.81–0.87; PCC 0.73–0.79; average sample size = 67,317). Again, region 17, which had the fewest sample pixels (2,743), was the only western region with excellent model performance (AUC = 0.90, PCC = 0.82). Of the seven eastern regions we were able to model, only one, the nonforest model for region 24, had fair model performance (AUC = 0.72, PCC = 0.69); it was built on a relatively small number of sample points (262). Three eastern regions had good model performance (AUC 0.84–0.89; PCC 0.77–0.80; average sample size = 23,300), and three eastern regions had excellent model performance (AUC 0.90–0.93; PCC 0.83–0.85; average sample size = 6,748).

3.2 Severe Fire Potential Map

The western SFP map (fig. 11) covers the entire western study area of roughly 427 million hectares (1.1 billion acres). It depicts the potential for high severity fire based on our Random Forest models, uniform 90th-percentile 1,000-hour fuel moisture conditions, and 2011 vegetation cover. Because we chose to use overlapping tile footprints for regional models, seamlines at regional boundaries are minimal. Individual tile footprints, however, are sometimes clearly visible due to our process for selecting the current NDVI month by tile based on fire occurrence records. These tile footprints are particularly visible in our outputs in the southern part of the study area (e.g., Texas).

Similarly, the eastern SFP map (fig. 12) covers the entire eastern study area of roughly 351 million hectares (868 million acres). It depicts the potential for moderate or high severity fire based on our Random Forest models, uniform 90th-percentile 1,000-hour fuel moisture conditions, and 2014 vegetation cover. Some seamlines are evident at regional boundaries, probably due to much sparser distribution of fires and larger mapping regions compared to the western study area. There is also considerably more area masked out as nonburnable, with the extensive agricultural areas in the upper Midwest and Mississippi Valley. Tile footprints are

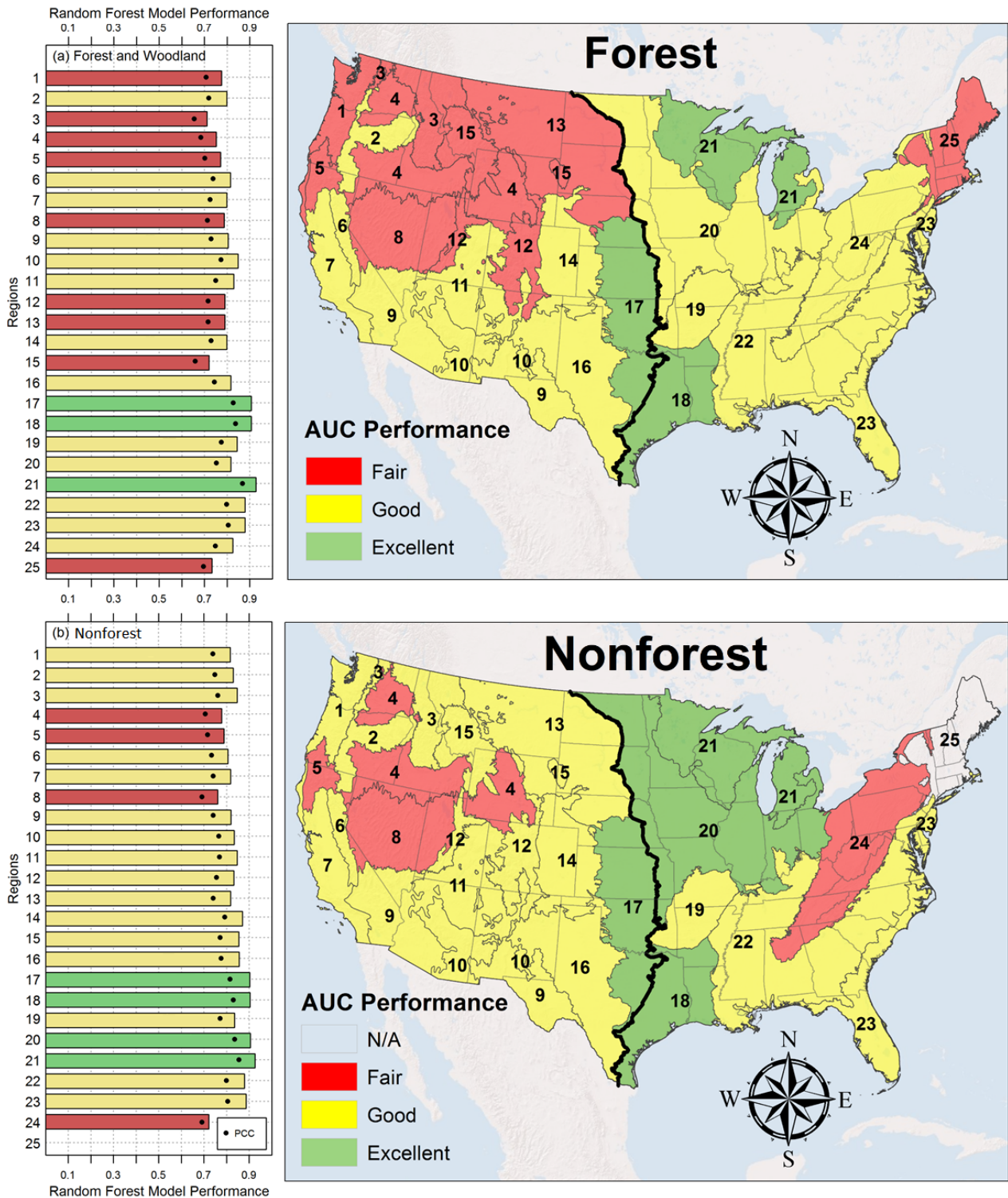


Figure 10—Model performance results from optimal Random Forest models in each region. Bars in the left panels show the area under the receiver operating characteristic curve (AUC) for each model, color-coded to reflect our interpretation of fair, good, or excellent performance. Percentage correctly classified (PCC) is also shown (PCC of 1 indicates 100%). Mapping regions in the maps are color-coded to match the bars.

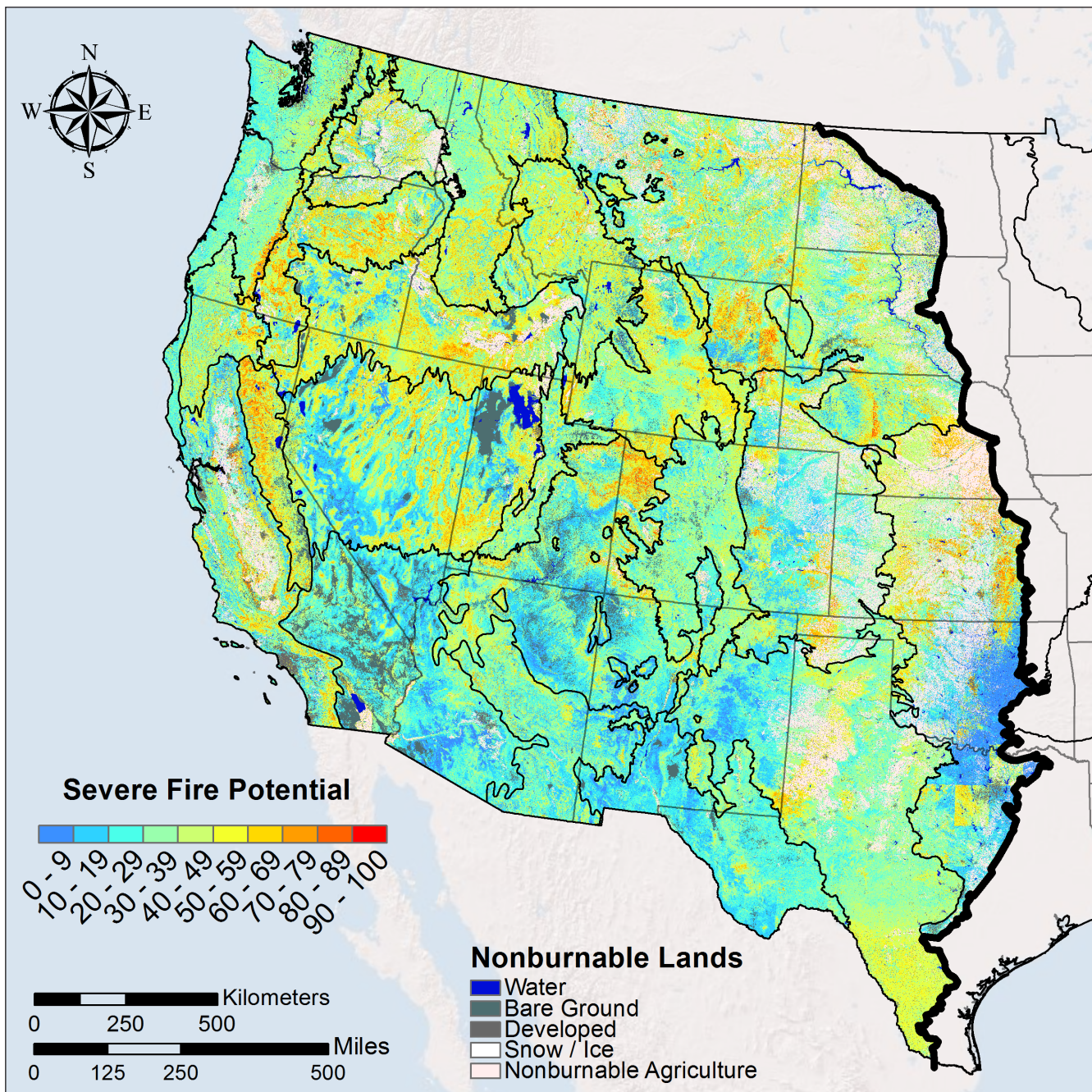


Figure 11—Potential for high severity fire in the western United States, modeled using 90th-percentile 1,000-hour fuel moistures and the normalized difference vegetation index developed from 2011 MODIS satellite imagery.

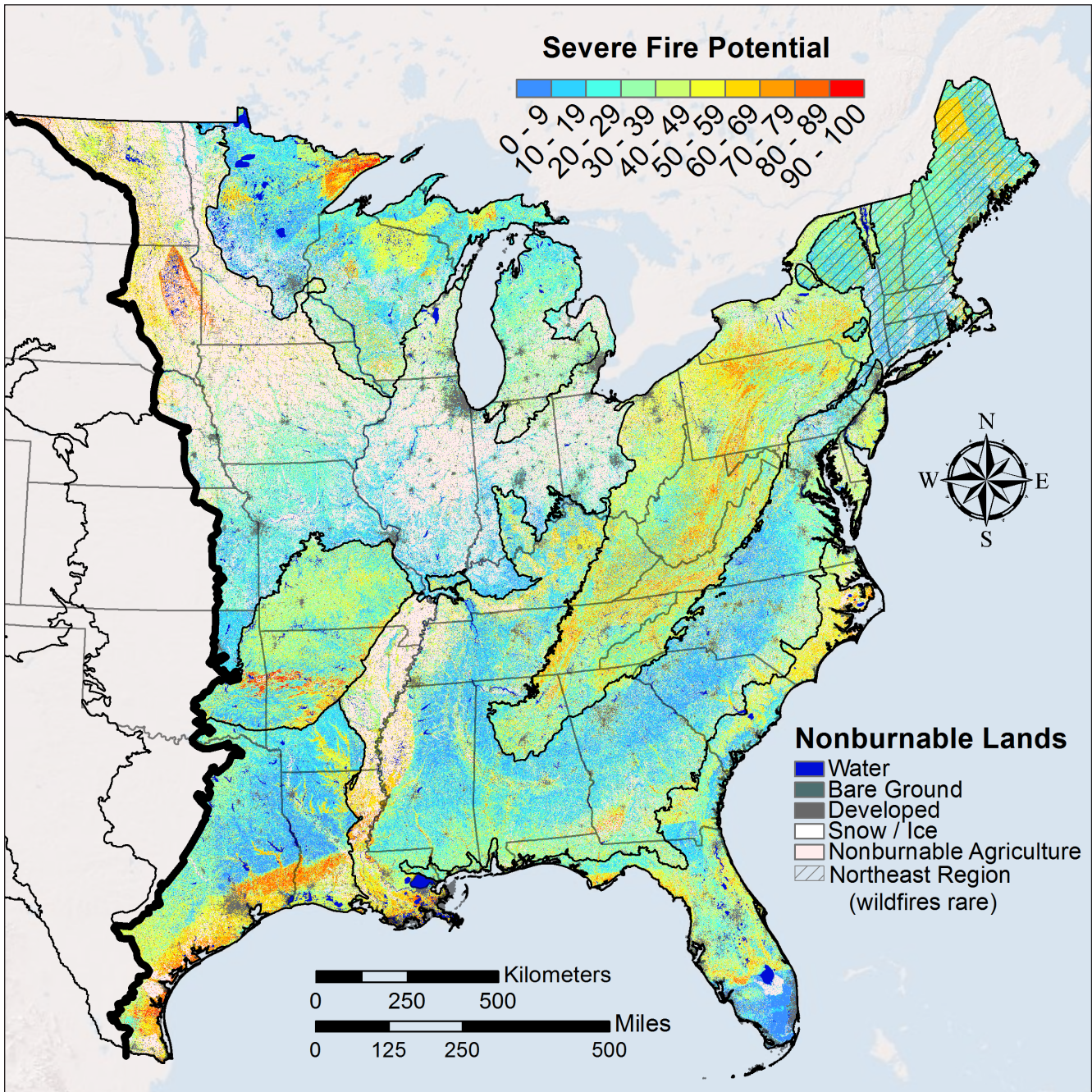


Figure 12—Potential for moderate to high severity fire in the eastern United States, modeled using 90th-percentile 1,000-hour fuel moistures and the normalized difference vegetation index developed from 2014 MODIS satellite imagery.

less visible in the eastern SFP product, with an exception in Maine, again due to our selection of current NDVI month by tile. It bears repeating that the SFP map in New England (region 25) is based on a model for forest settings created from very few data.

In both the western and eastern study areas, predicted SFP values were mostly below 50 and values above 80 are rare, indicating a relatively low potential for severe fire in most places (fig. 13). Across all western mapping regions the mean SFP index values are 38.4 for forest settings (standard deviation = 16.4, median = 37) and 36.4 for nonforest settings (standard deviation = 16.6, median = 35). When we break these distributions down by mapping region, the average predicted SFP values are typically between 20 and 50, with more variation among regions in the forest outputs than in the nonforest outputs (fig. 14). Forest settings in the eastern study area have the lowest average SFP value of 33.3 (standard deviation = 19.2, median = 30) and the most skewed distribution (fig. 13). Nonforest settings, in contrast, have the highest average SFP value of 41 (standard deviation = 16.9, median = 40) and a slightly more normal distribution. These patterns carry through to mapping regions, where forest SFP values are typically lower than in western regions and are somewhat less variable, while nonforest SFP values in the eastern mapping regions are comparable to, and in some cases higher than, values in western regions (fig. 15).

Across landform classes in the western study area, SFP values in forest settings are slightly higher on cool slopes (average = 45) and ridges (average = 42) than on other landforms, but several interesting patterns emerge when we look at landform classes by mapping region. Regions in Southern California, the Sierra Nevada, and the Southern Great Basin (6, 7, and 8) stand out as having higher than average SFP values in all landforms but cool slopes. In the Middle and Northern Rocky Mountain regions (13 and 15, and to a lesser degree 3 and 12), on the other hand, higher than average forest SFP values are most evident on cool slopes. Mapping regions in the Southwest and Southern Great Plains (9, 10, 11, 16, and 17) have consistently lower than average forest SFP values across all landforms.

Nonforest SFP values in western regions are also slightly higher on cool slopes (average = 50) and ridges (average = 44) than on other landform classes. In general, there is less variability in SFP values among regions and landforms for nonforest settings, compared to forest settings. However, the Southwest regions (9, 10, 11, and 16) again tend to have lower than average SFP values for any given landform class except ridges. A larger group of regions covering much of California and the arid Interior West (5, 6, 7, 8, 9, 10, 11, and 12) have below-average SFP values on cool slopes (fig. 14).

In forest settings across all eastern regions, ridges have higher SFP values (average = 38) than other landform classes (fig. 15). When we look at distributions by region, the Great Lakes region (21) has higher than average SFP values in most settings, particularly slopes and ridges. The Appalachian region (24) also has higher than average SFP values across landforms, but particularly on warm slopes and ridges. Interestingly, the Central and Eastern Great Plains region (20) has SFP values that are typically below average in forest settings and are very similar to neighboring region 17 in the western study area.

In eastern nonforest settings, general patterns in SFP values appear to be largely driven by

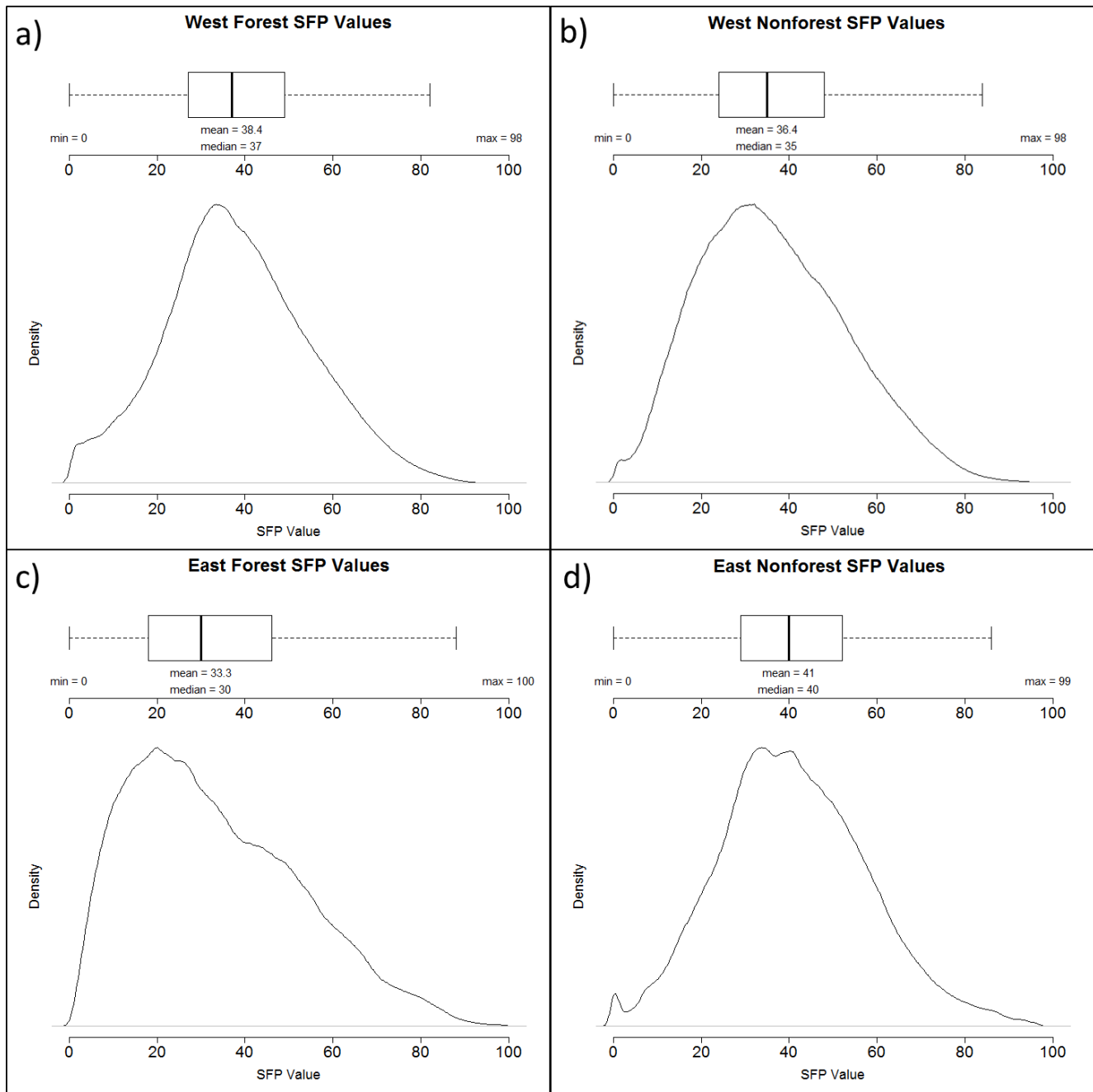


Figure 13—Statistical distributions of the Severe Fire Potential (SFP) index value for a) forests and b) nonforests in the western study area, and c) forests and d) nonforests in the eastern study area. In each panel, the box plot shows the inner quartile range (IQR; 25th–75th percentile) as the box width, the median value as a solid vertical line, and 1.5 × IQR as the whiskers. The histograms display a probability density function based on a large sample of the mapped SFP index values.

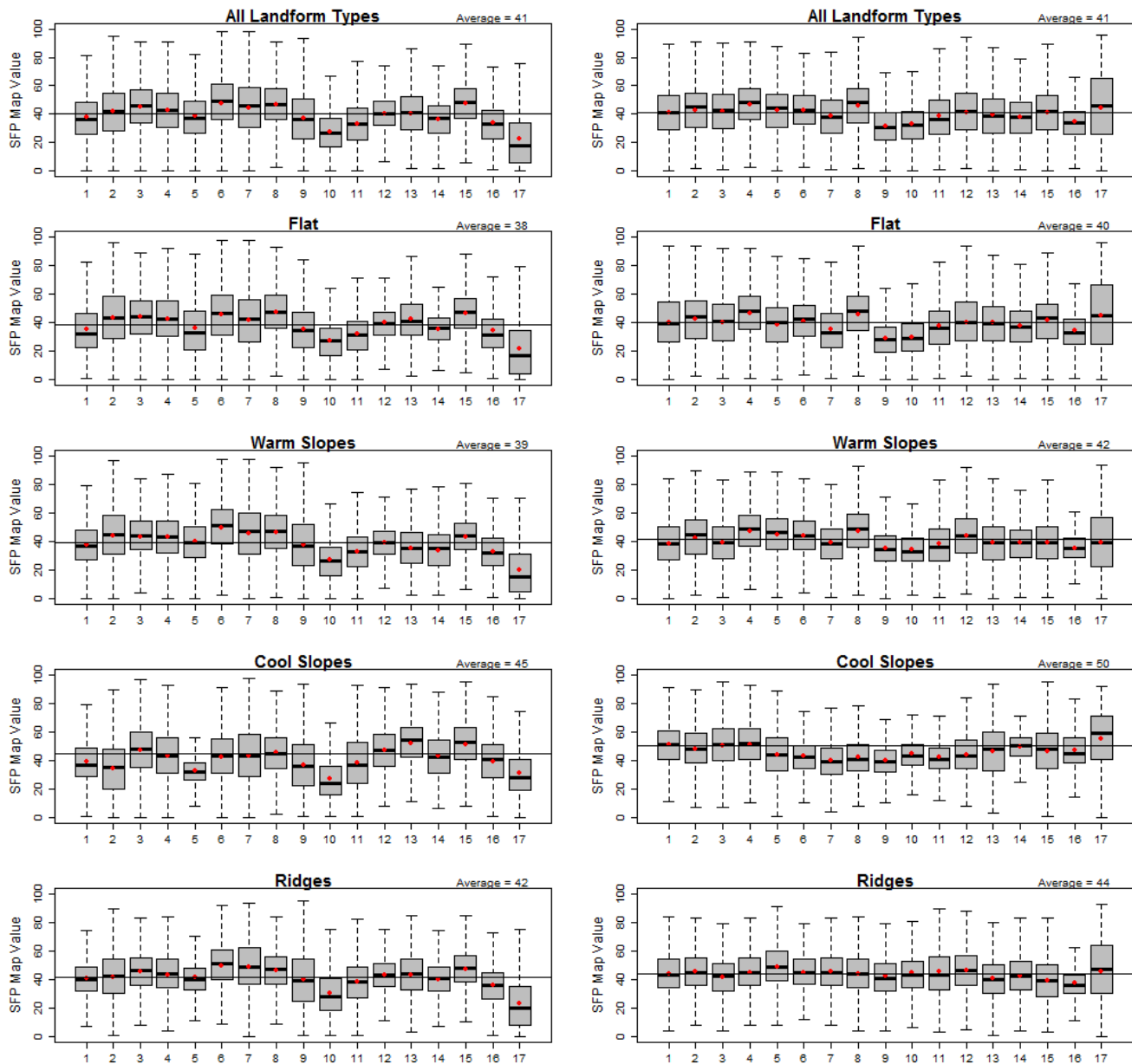


Figure 14—Distribution of Severe Fire Potential (SFP) index values for forest settings (left) and nonforest settings (right), by mapping regions and landform classes in the western study area. The inner quartile ranges (IQRs) of mapped SFP values are shown as gray boxes, with dotted lines extending to $1.5 \times$ IQR. Median values are shown as black horizontal bars, and the mean values are shown as red dots. In each graph, the average SFP value across all western regions for the data subset is reported and shown as a horizontal line.

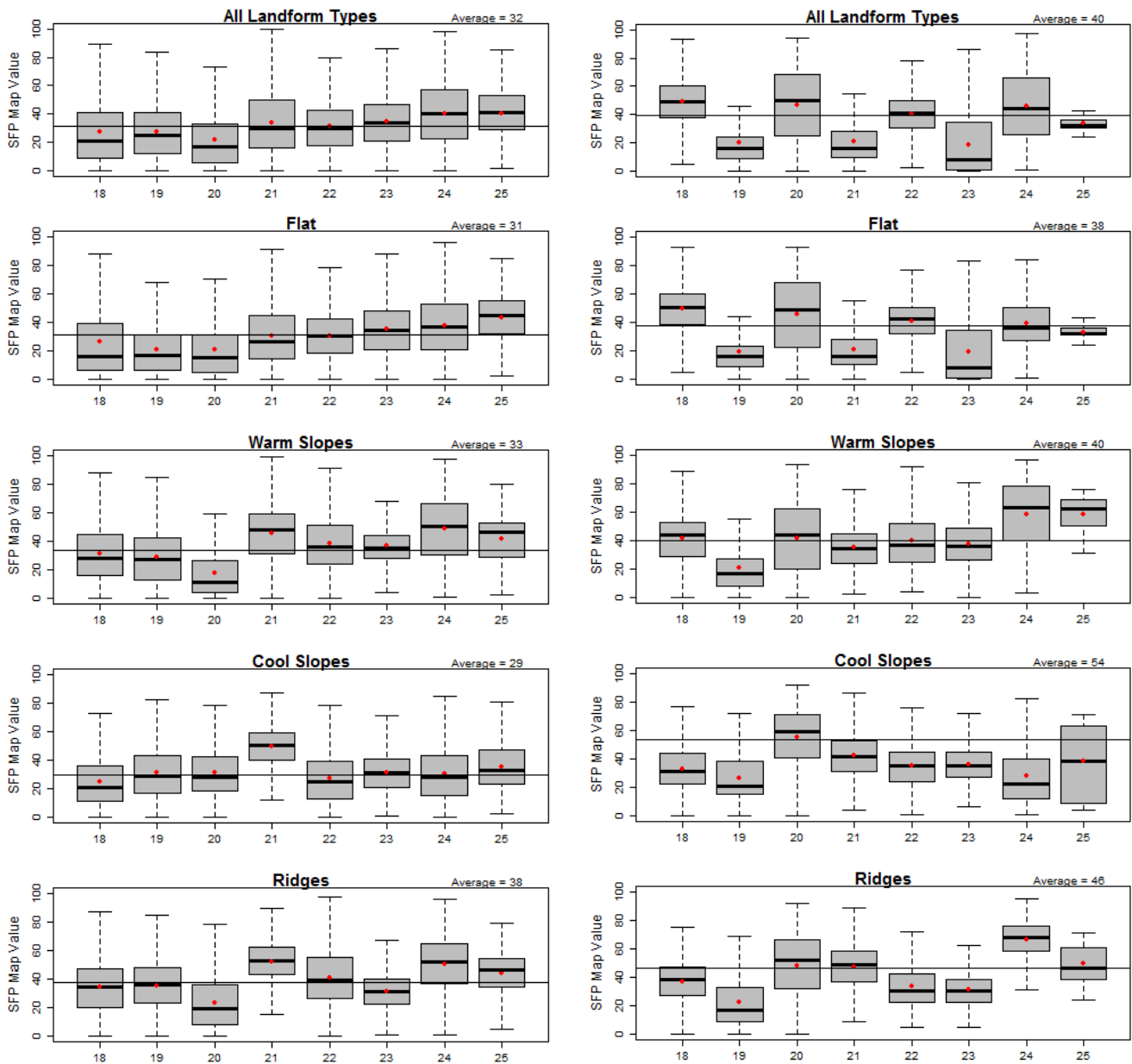


Figure 15—Distribution of Severe Fire Potential (SFP) index values for forest settings (left) and nonforest settings (right), by mapping regions and landform classes in the eastern study area. The inner quartile ranges (IQRs) of mapped SFP values are shown as gray boxes, with dotted lines extending to $1.5 \times$ IQR. Median values are shown as black horizontal bars, and the mean values are shown as red dots. In each graph, the average SFP value across all eastern regions for the data subset is reported and shown as a horizontal line.

the distributions in the flat landform class, while higher SFP values on cool slopes (average = 54) and ridges (average = 46) bring up overall average values (fig. 15). The Ozark Mountains, Great Lakes region, and Southeast Coastal Plain (19, 21, and 23) have below-average nonforest SFP values on flat landforms, and to some degree in all landform classes. Nonforest SFP values in all other regions tend to be above the average for any combination of region and landform class, with some exceptions on cool slopes and ridges.

3.3 Severe Fire Potential Map Validation

3.3.1 Comparisons of Predicted and Observed Binary Severity

The binary comparison of our predicted SFP and observed severity from MTBS at specific pixels showed lower accuracies than indicated by the Random Forest model performance statistics. Whereas the statistics from Random Forest showed all models in the fair (AUC > 0.7), good (AUC > 0.8), or even excellent (AUC > 0.9) range, this independent validation showed predicted SFP values for most models to be less accurate, with AUC values mostly below 0.7 (tables 10, 11).

In forest settings, the binary version of our SFP predictions agreed with observed severity just over half the time in most regions, with a few exceptions. The best AUC for individual regions in the western study area ranged from 0.50 to 0.68, with corresponding correct classification rates of 47 to 67% (table 10). The best-performing western region was region 11, the Colorado Plateau (AUC = 0.68, PCC = 0.67). In eastern regions, the best AUC ranged from 0.50 to 0.74, with corresponding correct classification rates of 56 to 86% (table 10). The best performing region in the eastern study area was region 18, the western Gulf coastal area (AUC = 0.74, PCC = 0.86). Across all CONUS mapping regions, the comparisons to binary MTBS severity in forest settings had on average a correct classification rate of 60% (AUC = 0.60, PCC = 0.60) (table 10).

The accuracy of SFP maps in nonforest settings was very similar to forest settings. In the western study area, the best AUC for individual regions ranged from 0.57 to 0.68, with corresponding correct classification rates of 49 to 67% (table 11). As with forest settings, the best performing region was region 11, the Colorado Plateau (AUC = 0.68, PCC = 0.67). In the eastern study area, AUC values for nonforest settings ranged from 0.50 to 0.79, and the proportion of validation samples correctly classified varied from 44 to 76% (table 11). The best performing region for nonforest settings in the eastern study area was region 21, the northern Great Lakes region (AUC = 0.79, PCC = 0.76). Across all mapping regions, 61% of the binary nonforest SFP predictions were correct (AUC = 0.61, PCC = 0.61) (table 11).

The best SFP breakpoints for binary classification of the SFP in both forest and nonforest settings were between 25 and 55, depending on the region (tables 10, 11). While the logical choice for a breakpoint would be 50, the slightly lower range of optimal breakpoints is consistent with our observation that SFP values are generally below 50. Across all CONUS mapping regions, the best breakpoint for a binary interpretation of SFP in forests was in the mid-30s (mean = 38, median = 35) (table 10), and slightly higher in nonforests (mean = 42, median = 45) (table 11).

Table 10—Results of pixel-scale validation of the Severe Fire Potential (SFP) map for forest settings, in relation to binary severity inferred from satellite imagery^a. The horizontal line divides western from eastern mapping regions. Fires used in this analysis were not included in Random Forest statistical model development.

Region	Fires	Samples	Best SFP breakpoint	Results for best breakpoint	
				AUC ^a	PCC ^b
1	125	2,250	40	0.58	0.61
2	119	1,959	45	0.61	0.60
3	277	6,052	40	0.54	0.51
4	243	3,990	50	0.58	0.60
5	98	1,539	40	0.64	0.63
6	82	1,243	35	0.59	0.59
7	161	1,834	45	0.61	0.60
8	126	916	35	0.55	0.52
9	93	1,061	30	0.61	0.60
10	66	981	25	0.55	0.55
11	87	1,035	35	0.68	0.67
12	54	625	25	0.54	0.46
13	57	1,150	50	0.58	0.59
14	6	144	25	0.53	0.50
15	184	3,151	50	0.58	0.59
16	13	301	25	0.50	0.47
17	2	4	NA	NA	NA
18	105	279	55	0.74	0.86
19	127	328	35	0.62	0.66
20	83	197	35	0.50	0.62
21	36	401	40	0.71	0.75
22	413	1,352	25	0.61	0.56
23	490	1,549	35	0.64	0.63
24	47	83	50	0.63	0.64
25	0	0	NA	NA	NA
Average	124	1,297	38	0.60	0.60

^a To compare SFP predictions (0–100 scale) to binary severity inferred from satellite imagery, we tested a range of breakpoints to reclassify the SFP to a binary scale. We selected the breakpoint that resulted in the highest area under the receiver operating characteristic curve (AUC) as the best breakpoint.

^b PCC is percentage correctly classified.

Table 11—Results of pixel-scale validation of the Severe Fire Potential (SFP) map for nonforest settings, compared against binary severity inferred from satellite imagery^a. The horizontal line divides western from eastern mapping regions. Fires used in this analysis were not included in Random Forest statistical model development.

Region	Fires	Samples	Results for best breakpoint		
			Best SFP breakpoint	AUC ^a	PCC ^b
1	97	959	45	0.60	0.60
2	244	3,986	50	0.58	0.60
3	312	4,947	35	0.60	0.56
4	771	18,593	50	0.60	0.61
5	68	436	45	0.64	0.62
6	106	934	35	0.60	0.52
7	258	2,989	40	0.62	0.62
8	473	9,110	50	0.57	0.57
9	323	4,867	35	0.63	0.62
10	127	1,044	40	0.65	0.67
11	116	1,215	45	0.68	0.67
12	129	1,528	45	0.59	0.55
13	148	1,871	45	0.58	0.59
14	28	274	50	0.58	0.58
15	205	3,403	40	0.61	0.60
16	38	226	25	0.61	0.49
17	7	15	NA	NA	NA
18	45	161	45	0.52	0.44
19	13	23	NA	NA	NA
20	115	431	35	0.50	0.75
21	24	71	40	0.79	0.76
22	48	65	55	0.60	0.63
23	73	149	25	0.72	0.70
24	4	5	NA	NA	NA
25	0	0	NA	NA	NA
Average	151	2,292	42	0.61	0.61

^a To compare SFP predictions (scale of 0–100) to binary severity inferred from satellite imagery, we tested a range of breakpoints to reclassify the SFP to a binary scale. We selected the breakpoint that resulted in the highest area under the receiver operating characteristic curve (AUC) as the best breakpoint.

^b PCC is percentage correctly classified.

The strength of this validation analysis was affected by sample sizes, which varied considerably among regions and were in some cases very small (tables 10, 11). We chose to exclude cases with fewer than 50 samples from the results. Most western regions had enough samples to evaluate performance in both forest settings ($n = 144\text{--}6,052$) and nonforest settings ($n = 226\text{--}18,593$), but we were unable to calculate validation statistics in region 17, where there were only 4 samples in forest (table 10) and 15 samples in nonforest (table 11). By comparison, most eastern regions had relatively few samples. We were able to calculate validation statistics for forest settings ($n = 83\text{--}1,549$) in all eastern regions except region 25, which had no samples (table 10). Nonforest settings in eastern regions had the smallest sample sizes; we were able to report validation statistics for five regions ($n = 65\text{--}431$), but had to exclude regions 19, 24, and 25 (table 11).

3.3.2 Relationship Between Predicted and Observed Continuous Severity Metrics

Linear regressions between the continuous SFP index value and the three continuous satellite-derived severity metrics used in this study (RdNBR, dNBR, NBR) all showed little to no relationship. Again, sample sizes for this analysis varied, and we eliminated results from any case with fewer than 20 sample points. In the western study area, regressions between RdNBR and the SFP index had R^2 values less than 0.18 (average = 0.05) in forest settings, and less than 0.12 (average = 0.05) in nonforest settings. In the eastern study area, regressions between dNBR and SFP performed similarly in forest settings ($R^2 < 0.13$, average = 0.05) and marginally better in nonforest settings ($R^2 < 0.32$, average = 0.13). We also regressed the postfire NBR against SFP in eastern regions and had similar results. Regressions with NBR had R^2 values less than 0.47 (average = 0.13) in forest settings, and less than 0.08 (average = 0.07) in nonforest settings. The strongest relationship in all the tests was between postfire NBR and SFP in forest settings in region 18 ($R^2 = 0.46$).

3.3.3 Assessing Variations in Observed Severity at the Landscape Scale

In almost all combinations of mapping region, forest or nonforest setting, and landform class, MTBS satellite-derived severity observations show that high severity fire occurs on a minority of burned area. Across all landform types, MTBS products mapped an average of 33% of burned area as high severity in both forest and nonforest settings in the western study area (fig. 16). In the eastern study area, an average of 20% of burned area in forest settings and 10% in nonforest settings was mapped as moderate or high severity (fig. 17).

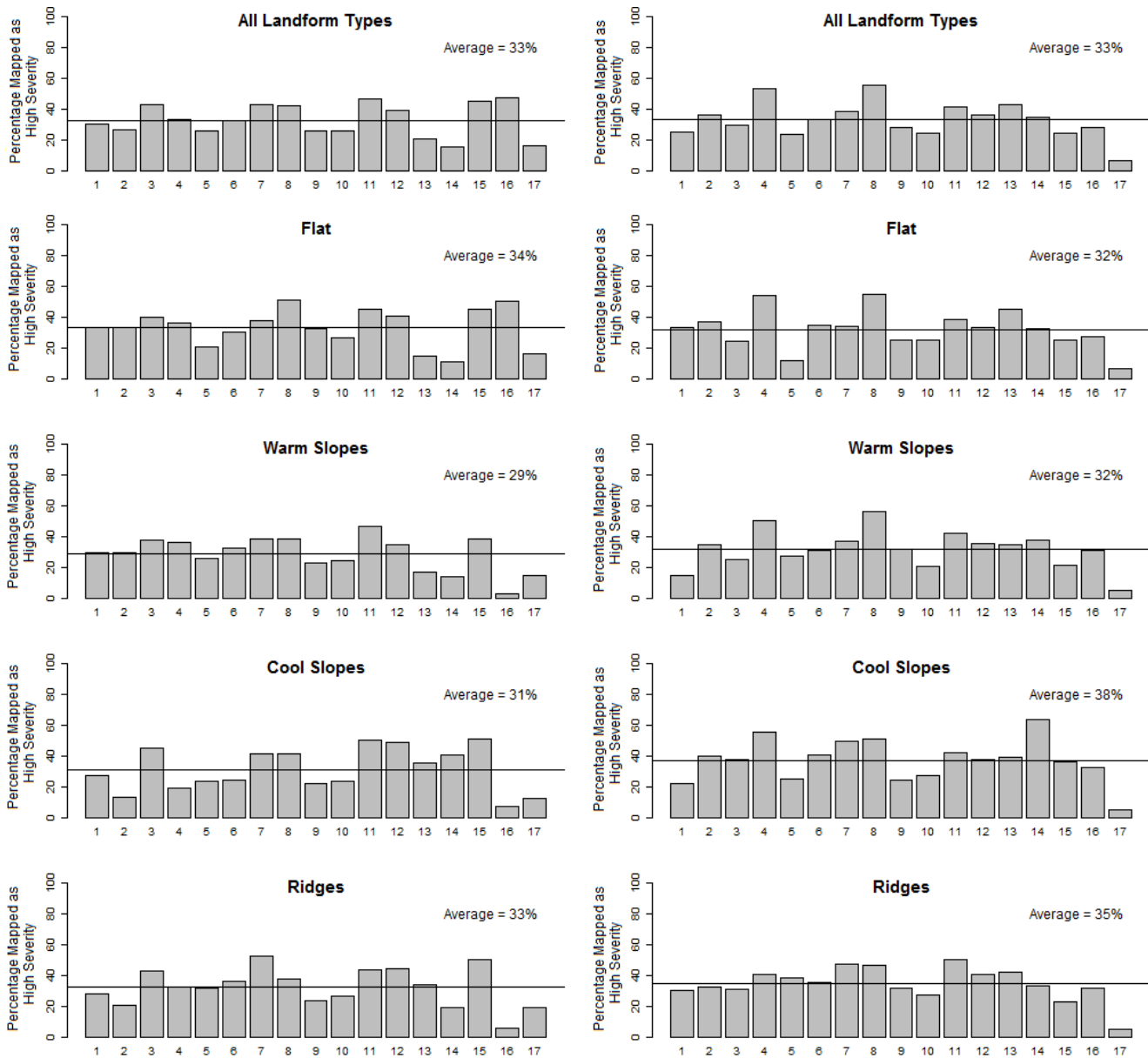


Figure 16—Percentage of burned area mapped by the Monitoring Trends in Burn Severity program classified as high severity using the relative differenced normalized burn ratio (RdNBR) thresholds calculated in this study. Bars represent individual mapping regions, and data are presented by forest settings (left) and nonforest settings (right) for mapping regions and landform classes in the western study area. In each graph, the average percentage mapped as high severity across all western regions for the data subset is reported and shown as a horizontal line.

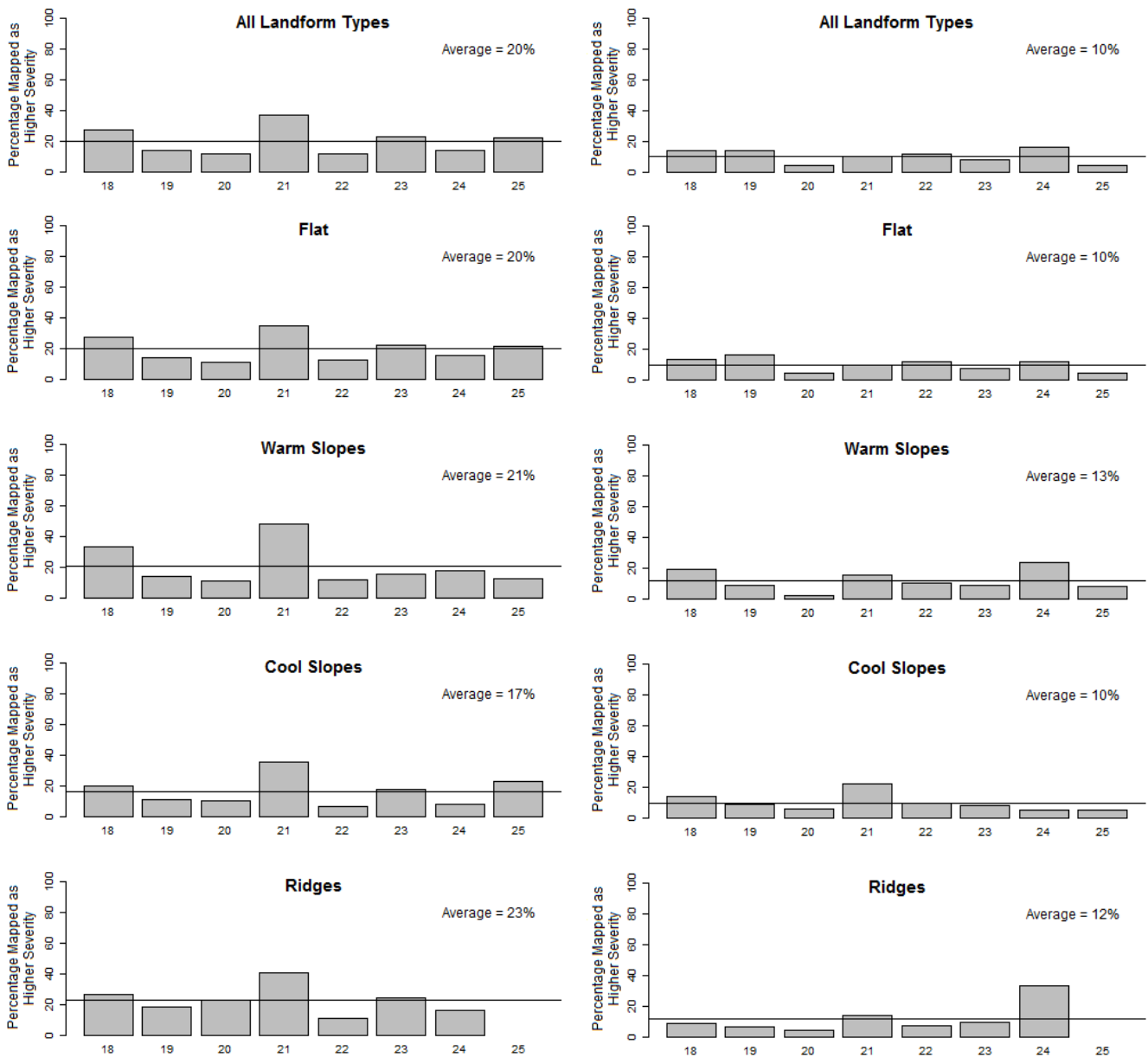


Figure 17—Percentage of burned area mapped by the Monitoring Trends in Burn Severity program classified as high or moderate severity using the normalized burn ratio (NBR) and differenced normalized burn ratio (dNBR) thresholds calculated in this study. Bars represent individual mapping regions, and data are presented by forest settings (left) and nonforest settings (right) for mapping regions and landform classes in the eastern study area. In each graph, the average percentage mapped as high severity across all western regions for the data subset is reported and shown as a horizontal line.

In the western study area, we found the lowest proportion of high severity (29%) on warm slopes in forest settings, and the highest proportion on cool slopes in nonforest settings (38%). Regions where percent high severity was consistently above average in forest settings were primarily in the Rocky Mountains, Southern Great Basin, and Southern California (3, 7, 8, 11, 12, and 15). Regions where proportion of high severity was consistently below average were in the Northwest, Southwest, and Southern Great Plains (1, 2, 5, 9, 10, and 17). For most regions that include parts of the Rocky Mountains (3, 11, 12, 13, 14, and 15), the proportion of high severity on forested cool slopes is slightly higher than on warm slopes. In regions located in parts of the Interior Northwest and the Sierra Nevada (2, 4, and 6), however, the percentage of high severity appears slightly higher on warm slopes relative to cool slopes in forest settings. On nonforest settings, regions with large extents of nonforest vegetation in Intermountain Basins, Central and Southern California, the Colorado Plateau, and Northern Plains (4, 7, 8, 11, 12, 13, and 14) consistently had a higher than average proportion of high severity, while regions in the Pacific Northwest, Northern Rockies, and Southwest generally had less high severity than the average for any landform class.

In eastern mapping regions, the observed proportion of moderate and high severity combined (i.e., higher severity) was consistently much lower than the proportion of just high severity in western regions (fig. 17). Ridges in forest settings had the highest proportion of higher severity (23%), while flat landforms and cool slopes in nonforest settings had the lowest proportion (10%). Across all landforms in forest settings, the Western Gulf Coast and Great Lakes Regions (18 and 21) had a consistently larger proportion of higher severity than average, while the Ozark Mountains, Central and Eastern Great Plains, Piedmont and Mississippi Valley, and Appalachians (18, 20, 22, and 24) had lower than average percentages of higher severity fire. Observed amounts of higher severity fire on nonforest settings in eastern regions were very low (typically below 15%), and sample sizes were too small to draw much inference from observed patterns.

4. Discussion

We achieved our objective in this study of creating a predictive map of severe fire potential for all lands in the contiguous United States. This is an unprecedented accomplishment, and reflects the exciting possibilities enabled by MTBS data to consistently analyze the ecological effects of wildfire over large areas. Others have analyzed temporal trends in fire occurrence and area burned, and generalized severity from MTBS data (Dennison et al. 2014; Picotte et al. 2016) but stopped short of developing statistical models to help us better understand the biophysical conditions driving burn severity. Many researchers have evaluated burn severity from different angles in recent years (Arkle et al. 2012; Estes et al. 2017; Harvey et al. 2016; Keyser and Westerling 2017; Lutz et al. 2011; Mallek et al. 2013; Miller et al. 2012; Parks et al. 2018; Picotte and Robertson 2011b; Stevens-Rumann et al. 2018; Thode et al. 2011; Veraverbeke et al. 2011), and some have produced maps depicting high severity fire potential (e.g., Holden et al. 2009; Keyser and Westerling 2017; Parks et al. 2018). Many of these studies, however, have a narrower geographic scope, from a single fire up to fires within one region. Keyser and Westerling (2017) mapped the potential for high severity fire across the western United States, but at a very coarse spatial resolution (approximately 12 kilometers, or 7.5 miles) and with a focus on examining the influence of interannual climate variability. Parks et al. (2018) also mapped high severity fire potential in the western United States, but only for forest and woodland settings. Most burn severity studies consider forested landscapes in the western United States, with very few studies in the eastern United States (but see Picotte and Robertson 2011b). Ours is the only project to date to analyze burn severity across all ecosystems in the contiguous United States and produce fine-grained (i.e., 30-meter resolution) predictive maps across a domain of that size. With our analysis, we can explore questions of where and why wildfires are severe; greater understanding of these questions can inform future fire management, which is increasingly focused on balancing ecological values with protecting people and property (Scott et al. 2013; Thompson et al. 2016).

Burn severity is a complex phenomenon, and evaluating it across different ecosystems requires some flexibility and adaptability. Many of the challenges with defining and mapping severity in different contexts were articulated by Morgan et al. (2014) in a publication that was informed by our work on this study. Picotte and Robertson (2011a) showed that in the southeastern United States even selecting satellite imagery and mapping severity with dNBR and NBR requires different timing of image capture and other considerations than one might use in the western United States. Similarly, we found that the choice of index (RdNBR, dNBR, NBR) and the methods for determining thresholds for severity classes must be context-specific (i.e., forest vs. nonforest, initial vs. extended assessments, eastern vs. western United States). We were fortunate to have the rich MTBS dataset to use in this study, and now we hope our information about thresholds can help others interested in working with those data across broad areas. Likewise, some of the predictor data we developed for this study can lay the groundwork for others. Parks et al. (2018), for example, were able to leverage the topographic datasets that we created, including modeled solar radiation, and build upon lessons learned by this study to produce improved models and maps of high severity potential.

We gained insight into the influence of specific drivers of severity, and confirmed that burn severity is affected by fuels, topography, and climate. We found, as others have, that vegetation and topography as well as site-specific fuel moistures have an effect on burn severity. We

included predictor variables representing prefire vegetation, fuel moisture, and topography, and our results showed that elements of all three were important to varying degrees in different settings. We found elevation to be the most important variable in western U.S. forests (overall and in 10 out of 17 regions), which could indicate some inherent topographic controls on fire occurrence (i.e., more ignitions on ridgelines) or fire behavior (i.e., higher intensity fire as fire moves upslope). The same could be said for the presence, and moderate importance, of broad-scale topographic position in all western forest models. It is more likely, however, that both elevation and topographic position are serving as surrogates for vegetation distribution and broad-scale climatic patterns, which are strongly affected by elevational gradients. The variable we used to represent vegetation condition, NDVI, was second in importance overall in western forest models (and most important in 4 of 17 regions), further suggesting that the amount of prefire green vegetation affects severity. Notably, NDVI was the most important variable in western nonforest models (overall and in 14 of 17 regions). This result makes sense in ecosystems where vegetation cover can be more sparse and discontinuous, with variable distribution of fuels; fires can burn hotter at sites with more available fuels, and these sites therefore have more potential for high severity. In contrast, our modeling results for eastern U.S. regions indicated that fuel moisture has the largest influence on severity in both forest and nonforest settings (overall and in six of eight regions for forests and five of eight regions for nonforest), ahead of NDVI and elevation. We believe this finding reflects a generally climate-limited scenario for wildfire in the eastern United States. In other words, the amount of available fuel is more consistent in most eastern U.S. settings (despite being highly variable from broadleaf deciduous forest in much of the East to conifers in the upper Midwest and coastal plain), and less driven by topographic gradients. Subsequently, the occurrence and severity of wildfire is driven more by how hot and dry conditions are, which is reflected in fuel moisture. This relationship could become very important as climate changes into the future.

Our findings about the influence of specific variables on SFP are mostly consistent with what other researchers have found. Parks et al. (2018) conducted perhaps the most in-depth analysis of the relative influence of variables representing live fuels, topography, climate, and fire weather on burn severity to date, and argue that live fuels (i.e., green vegetation) have the largest effect on severity in western U.S. forests, followed in importance by fire weather tied to the specific day of burning, then long-term climate, and finally topography. Their results contrasted with previous studies that found topography to be one of the more important drivers of severity (e.g., Birch et al. 2015; Dillon et al. 2011; Estes et al. 2017). Parks et al. (2018) point out, as do Dillon et al. (2011), that topography is an indirect measure of vegetation and fuel distribution and can appear more important when specific variables representing vegetation are not included. Our results generally support the conclusion of Parks et al. (2018) that the amount of prefire vegetation is more important than any inherent topographic factor. Nonetheless, some combination of topographic variables did add value to our models in every scenario, even after accounting for vegetation and fuel moisture. These results suggest that manipulating the fuels, such as through fuels treatments or through accumulation in the absence of other disturbance, influences fire impacts on ecosystems.

Burn severity is affected by factors other than those included in our models. For instance, we know that climate can play an important role (Birch et al. 2015; Dillon et al. 2011; Keyser

and Westerling 2017), and with changing climate that role is likely to increase (Parks et al. 2016). We did not include any true climate variables (i.e., 30-year normals). Our fuel moisture variable was more an indicator of seasonal weather conditions than of long-term climatology, and we may have only indirectly captured climate impacts on vegetation distribution with elevation and topographic position variables. Similarly, time since previous fire or other disturbance also influences the severity with which an area burns (Parks et al. 2014b; Stevens-Rumann et al. 2016), but the effects of previous disturbances and subsequent time for vegetation are related primarily to the amount of fuels available to burn. Explicitly including time since last disturbance in models may be unnecessary if satellite indices such as NDVI can adequately capture prefire vegetation and fuel conditions. In many ecosystems, however, such indices are sensitive to timing of imagery with respect to the growing season and represent only a top-down look at greenness and biomass. They do not capture vertical structure (e.g., ladder fuels), individual tree species (some species are more resistant to fires than others), understory plant composition, or surface fuels, all of which are important factors in the ecological consequences of fire (Morgan et al. 2014, 2015).

A general challenge to modeling burn severity across broad geographic areas is the distribution of available data. The MTBS program provides a tremendous resource in the United States for satellite-derived severity data, but there are still large areas, particularly in the eastern two-thirds of the country, with very sparse coverage. Few wildland fires occur in these areas that are large enough to be mapped from satellite data. This presents a challenge to our objective of modeling and mapping burn severity potential for all lands. Because of gaps in the spatial coverage of burn severity data, other studies with a broad geographic scope have typically limited modeling to forests and woodlands in the western United States, where sufficient data exist (Dillon et al. 2011; Parks et al. 2018). A related challenge with satellite-derived burn severity data is that they can be very noisy and have significant variation, as indicated by our finding that model performance was inversely proportional to sample size. The appearance of better performance with fewer samples is misleading. When we struggle to have enough samples, then we also struggle to adequately capture the variability of conditions under which fires burn. The result is models that might reasonably explain the observed set of conditions but may not be applicable to new fires in different locations, some of which will burn under conditions very different from those included in the databases on which our statistical models are based.

Our statistical models performed relatively well, but our analysis highlights the importance of independent validation. Based strictly on performance statistics calculated within Random Forest, our models performed well (average AUC = 0.81 for forest models and 0.84 for nonforest models). Had we stopped there, our results would have been comparable to those from other studies (Dillon et al. 2011; Holden et al. 2009). However, the results of our independent validation using sample pixels withheld from model development were lower (average AUC = 0.60 for forests and 0.63 for nonforest). Models based on machine learning can be susceptible to overfitting. In other words, a model adheres too closely to relationships found in the training data but is not transferable to new observations. Although the Random Forest algorithm was developed in part to reduce overfitting, it has not eliminated this possibility entirely (Hastie et al. 2009), particularly when the training data do not capture

enough variability. Parks et al. (2018) specifically addressed this problem, building in independent cross-validation to their modeling by withholding data from entire fires (rather than pixels within the same fires) during model development, thus ensuring models that are more transferable and produce more reliable predictions. Their cross-validated AUCs (average AUC = 0.72) were generally lower than what we achieved in our models, but were more reflective of the predictive ability of the models. By using a semi-independent validation dataset in our study (i.e., independent pixels withheld from the same fires used for model development), we found that the internal Random Forest performance measures did not accurately reflect the predictive ability of the models.

This study yielded many positive outcomes, including resources for fire researchers and managers. The field data that we assembled are one such outcome. The CBI data that we accumulated from other scientists and managers cover a wide range of ecosystems. From a national perspective, however, they are highly clustered and poorly distributed. We filled in some gaps with the field data collected specifically for this study (Sikkink et al. 2013), and strongly encourage further postfire monitoring efforts to continue building a more complete distribution of field-based burn severity data. With our field sampling, we built upon protocols for the CBI (Key and Benson 2006) and GeoCBI (De Santis and Chuvieco 2009) metrics, and offered improvements such as incorporating continuous measurements (e.g., percent change) where possible, including fraction green and fraction charred (Hudak et al. 2007; Lentile et al. 2009), size of the smallest remaining twig in shrublands (Keeley et al. 2008), and other indicators of burn severity (see supplemental files in Sikkink et al. (2013) for complete protocol descriptions and field forms).

Another outcome of our study is the foundation that we laid for broad-scale analysis of burn severity. We hope that our study provides a resource for further analyses and refinement of methods, such as work by Parks et al. (2018). Given the importance of the ecological effects of fire, similar analyses to understand how and where fires are likely to burn with higher severity within a region would be valuable to support both fire management and natural resource management. Predictive models and maps of burn severity, and the understanding they engender about fire ecology, could also inform assessments of ecosystem vulnerability to wildfires now and into the future (e.g., Walker et al. 2018). In cases where high levels of tree mortality (Hicke et al. 2016) are coincident with poor postfire tree regeneration (Stevens-Rumann and Morgan 2019; Stevens-Rumann et al. 2018), for example, projections of areas susceptible to high severity fire could be combined with future climate projections to assess potential ecosystem shifts due to changing climate.

Importantly, our analysis showed that high burn severity occurs on a relatively small portion of the total area burned in wildfires (figs. 16, 17). Previous evaluations of MTBS data have shown that typically less than one-third of burned area is high severity (Finco et al. 2012; Picotte et al. 2016). Despite using different thresholds to classify the MTBS data, we found the same to be true. Our results also highlight that even the combination of moderate and high severity fire is much less common in ecosystems of the eastern United States, compared to high severity fire in the western United States. Since 1984, when Landsat-based observations of burn severity became available, the proportion of area burning with high severity has been relatively stable (Dillon et al. 2011), although some researchers have reported trends toward

increasing high severity in some settings (Miller et al. 2009a, 2012). Focusing on individual burn days on 42 fires, Birch et al. (2014, 2015) also found that only about 13% of area burned with high severity on most days, and even on rare days with large fire runs, high severity always accounted for less than half of burned area. Further, others have found that most large fires include unburned areas and areas burned with low to moderate severity that are especially important to the survival and recovery of plants and animals (Krawchuk et al. 2016; Meddens et al. 2016, 2018a). Monitoring parameters such as the proportion of burned area with high severity, along with corresponding information on the amount of unburned area within fire perimeters (7–10% on average; Meddens et al. 2018b), and the size and shape of burned patches (Kemp et al. 2016), can help managers and scientists understand whether shifts in fire regimes are occurring over time.

Our analysis of burn severity observations and predictions in different geographic settings also provides some insight into regional and topographic differences in burn severity at a landscape scale. As an example, for forests in the western United States, satellite observations suggest that high severity occurs on a comparatively higher amount of burned area in the Rocky Mountains, Central and Southern California, and the Southern Great Basin; and that high severity is less prevalent in the Pacific Northwest, Southwest, and Great Plains (fig. 16). These findings are consistent with the fire ecology of the predominant ecosystems in these regions (Keane et al. 2008). Our findings from observed severity and our SFP predictions further suggest that forests on cooler, northerly aspects experience slightly more high severity fire than other topographic settings in the Rocky Mountains, but not in California and the Southwest. Similarly, our data suggest that in the Interior Northwest and Sierra Nevada, slightly more high severity fire occurs in forests on warm, southerly aspects compared to other settings. To summarize, not all areas are likely to burn with high severity, and severe fire potential varies geographically.

4.1 Limitations

Our work has limitations, many of which have been addressed elsewhere in the text. Here we summarize those limitations and how we addressed them. We also provide some suggestions for overcoming our limitations through future research and monitoring work.

One of the biggest limitations to being able to model burn severity across all lands in the contiguous United States was the availability of data. Despite our efforts to acquire all available satellite and field data, there were large areas where we lacked sufficient information to build good models, particularly in the eastern United States (fig. 6). To address this, we made our mapping regions large enough to ensure each region would have satellite-derived severity data and we also included fires from the 1-degree tiles that touched each region's boundary. However, this approach created the problem of sometimes extrapolating across large, diverse areas based on samples concentrated in small corners of the regions. Region 20 (Central and Eastern Great Plains) illustrates this problem. The model for region 20 was built with samples from the Flint Hills of Kansas and the northwest corner of Minnesota, yet extends from eastern North Dakota to western Ohio and down to northeast Oklahoma. While the satellite-derived data provided by the MTBS program is invaluable, their minimum fire size of 500 acres

(202 hectares) east of the 97th meridian leaves many small fires in the eastern United States unmapped. Future efforts to analyze burn severity at the scale in this study would benefit from retrospective mapping of many more smaller fires.

Our lack of field data on fire effects, particularly in many parts of the eastern United States, also hampered our modeling efforts. Field data on fire effects are needed to improve the interpretation of burn severity from remotely sensed imagery across a greater variety of ecosystems (Kolden et al. 2015). There were few CBI data available for many ecoregions and for particular geographic settings within ecoregions; these are the places where our SFP map is likely to perform poorly simply because input data used for modeling are few. Specifically, regions 13 (Northwest Plains), 14 (Western Great Plains), 16 (Southwest Plains and Hill Country), and 17 (Southern Great Plains) in the western study area, and regions 18 (Western Gulf Coast), 20 (Northcentral Great Plains), and 25 (New England) in the eastern study area had no field data. Where CBI data were available, they were typically tightly concentrated around specific study areas and within large wildfires that may not always be representative of severity or burning conditions across an entire region (fig. 6). In the western study area, we addressed this problem by pooling all field data to calculate thresholds for classifying satellite-derived severity data. To deal with the limited number of field data in the eastern United States, we used a different thresholding method (section 2.1.5.2). We suggest that putting CBI data and other field data on fire effects into a public, centralized data repository would help future studies like ours. Programs for monitoring fire effects could both contribute to and benefit from such a data repository as well (Kolden et al. 2015).

Another major limitation of our study is the challenge of choosing the predictor variables and assembling datasets that align both spatially and temporally. Other researchers have found that variables representing weather at the time of fire (Birch et al. 2015; Parks et al. 2018), long-term climate (Keyser and Westerling 2017; Parks et al. 2016), or time since previous disturbance (Parks et al. 2014b; Stevens-Rumann et al. 2016) are useful in describing burn severity patterns. We chose to use 1,000-hour fuel moisture as a single, integrative variable to capture elements of fire weather and climate, and NDVI as a measure of vegetation that would theoretically reflect the influences of landscape disturbances. In future research, we recommend using a more diverse set of predictor variables, as Parks et al. (2018) did, and ideally selecting variables based on regional knowledge of key drivers of severity.

Aligning the timing of variables representing fire weather with observed severity is a persistent challenge in studies like ours. We used 1,000-hour fuel moisture values extracted from a 10-day window following the detection date of a wildfire, but this does not necessarily correspond to the dates when the fire burned the most area with high or moderate severity. In hindsight, the choice to use a 10-day window represents a major weakness of our modeling. Another way to mitigate this timing problem would be to choose the lowest fuel moisture that occurred between the start and end dates of a fire. Better still would be to incorporate satellite fire detection data from sensors like MODIS or the Visible Infrared Imaging Radiometer Suite (VIIRS) to roughly determine the day each pixel burned and use the 1,000-hour fuel moisture for that day (Birch et al. 2015; Parks 2014; Parks et al. 2018).

Similarly, aligning the spatial resolution of multiple raster datasets presents a challenge. In our case, our burn severity data, elevation, and topographic derivatives all had a 30-meter

pixel size, while the MODIS NDVI that we used had 250-meter pixels, and the 1,000-hour fuel moisture had 4-kilometer pixels. Using a mixture of 30-meter Landsat-derived NDVI for model development and 250-meter MODIS-derived NDVI for predictions in the western study area very likely affected our SFP predictions, despite our careful efforts to mitigate this (see Appendix D). In the eastern study area we used only 250-meter MODIS NDVI because prefire Landsat images were often not available with MTBS data, but this resulted in vegetation data that were consistently of coarser resolution than our burn severity observations. In a more recent study, Parks et al. (2018) were able to efficiently select and process NDVI from Landsat scenes for model prediction using Google Earth Engine, a technology that was not available when we began this study. Recent advances in downscaling daily climatology data (Holden and Jolly 2011; Holden et al. 2016) also indicate that technological advances may soon solve some of our technical limitations. With climatology and vegetation data more closely matched to the resolution of burn severity and topography data, model results in future studies are likely to improve.

Last, the statistical modeling methods we used have some inherent limitations. While Random Forest has some advantages for modeling complex ecological phenomena (Cutler et al. 2007), it can also produce models that are tightly fit to training data but not reliable for predictions with new data. These problems are not uncommon for machine-learning algorithms in general, and Parks et al. (2018) showed that incorporating independent cross-validation into the model development process can at least provide a better indication of the predictive ability of a model.

4.2 Management Implications

In developing the SFP map, we sought to provide managers with a readily available tool to help identify where high severity fire effects are most likely, thereby allowing for ecological effects to be more easily considered in fire management and planning. Given our results, we see the greatest value of the SFP map in broad-scale land management and strategic planning applications. The geographic patterns in severe fire likelihood, as well as knowledge of biophysical conditions driving high severity fire effects, can help managers more fully incorporate fire ecology into their planning efforts. Given our relatively low map validation results, however, we must temper our recommendations about using the SFP map in a wildfire operations context. The strength of our analysis comes from looking at burn severity patterns in aggregate. Throughout the duration of an individual wildfire, there are simply too many site- and time-specific variables affecting fire behavior and resulting severity that we did not include in our models, and too much uncertainty in our SFP predictions to base tactical decisions on them. This is unfortunate, for the existing tools commonly used in fire operations are focused more on fire behavior than on the effects of those fires on landscapes. We recommend that managers use thorough analysis of potential fire behavior at the time of a fire, including evaluation of weather, topography, fuel moisture, and applicable fire danger indices such as ERC and Burning Index to gauge potential fire effects. Operational systems such as the Wildland Fire Assessment System (WFAS; <https://m.wfas.net/>), as well as fire behavior

modeling tools available through the Wildland Fire Decision Support System (WFDSS; https://wfdss.usgs.gov/wfdss/WFDSS_Home.shtml) and the Interagency Fuel Treatment Decision Support System (IFTDSS; https://iftdss.firenet.gov/landing_page/) can provide this kind of information.

Our specific recommendations for how managers can use the maps and information from this study include:

1. The best use of the SFP map is for long-term assessments and strategic planning. Do not base tactical decisions for a particular fire event on our results because they do not reflect the specific conditions under which any one fire will burn, but instead provide a more holistic overview. Burn severity is complex and the SFP map does not capture the full range of site- and time-specific factors required for tactical decisionmaking.
2. Compare spatial patterns in the continuous SFP map with observed patterns of severity on your landscape. Do the general patterns match what someone with local knowledge of past fires would expect to see in terms of higher severity being more likely on certain parts of the landscape? Were there a reasonable number of fires and sample points for our models in your area? If so, then use the general patterns reflected in the SFP map to guide expectations about where future fires may result in higher severity. The strength of the SFP map is in these generalized patterns in potential severity rather than interpreting individual pixels as definitive projections of where high severity fire will occur. At best, about 60% of binary interpretations of the SFP map in this study were correct, but there is significant complexity and nuance in our models that we believe provides useful information.
3. Understand that the SFP index depicts the likelihood of high severity fire in the western United States (or moderate and high severity fire in the eastern United States) but says nothing about the likelihood of low severity fire. Do not try to interpret the SFP map as a continuous measure of severity potential. Our comparisons between continuous satellite-derived severity measures (e.g., dNBR or RdNBR) and the 0 to 100 values of the SFP index clearly show that they are not correlated. Likewise, do not interpret the SFP as probability of fire occurrence—it is the probability that when a fire occurs, it will burn with high severity.
4. The SFP map could provide a starting point to indicate where landscape fuels treatments aimed at moderating severe fire potential could be placed. Broadly speaking, our finding that prefire vegetation is an important factor influencing burn severity, combined with the findings of others (e.g., Parks et al. 2018; Stevens-Rumann et al. 2016), implies that vegetation management and natural disturbances like wildfire may be effective at altering severity of future fires in certain circumstances. Our results, however, do not support any specific recommendations for how to treat fuels in a specific location to reduce the potential for severe fire. Managers should consult the vast information available on fuels treatment design for specific objectives (Fulé et al. 2012; Hudak et al. 2011; Kalies and Yocom Kent 2016) and perform a thorough analysis of local conditions and potential treatment effects using tools available in IFTDSS and elsewhere.

5. Conclusions

Burn severity is important because it provides a framework for thinking about the ecological footprint of wildfires. We focused on high severity because of the many potential changes to ecosystem values and subsequent vegetation response that can result from high severity fire (Morgan et al. 2014). But high burn severity (plus moderate severity in the eastern United States) occurs on only a portion of area burned in wildfires. Our analysis of satellite-derived burn severity observations was consistent with previous investigations (Finco et al. 2012; Picotte et al. 2016) in demonstrating that high severity fire accounts for about one-third of burned area, on average, in the western United States and much less in the eastern United States. At most, up to about 50% of burned area can burn with high severity in rare events (Birch et al. 2014) and in certain geographic settings. We can conclude that all wildfires are patchy and include unburned areas interspersed with patches of low, moderate, and high burn severity.

We met our objective in this study of producing the first-ever map of severe fire potential (SFP) at 30-meter spatial resolution across all lands in the contiguous United States. The SFP index we mapped has values from 0 to 100, but predicted SFP values were typically less than 50, with averages from 33 to 41 depending on forest or nonforest settings in the western or eastern United States. These values support the conclusion that potential for high severity fire is relatively low (<50%) in most settings, consistent with our analysis of MTBS data. The distribution of SFP values by mapping region, forest or nonforest setting, and landform also mimics, to some degree, patterns we found in satellite-derived measurements of severity. Still, the relatively low predictive ability of our models highlights the challenges of modeling such a complex and stochastic phenomenon. Our study and others have shown that burn severity is influenced by many factors including vegetation, climate, fuel moisture, weather, and the legacy of prior fires and other disturbances. Burn severity is also variable over the diverse ecosystems and topographic settings in an area as large as the contiguous United States. Based on our experience, we suggest continued field monitoring of fire effects and mapping of burn severity from satellite imagery to improve upon our efforts. Uses of our SFP map should be consistent with its limitations and the management recommendations that we have outlined.

High severity fire will continue to be of concern because of the heightened ecological impacts, both positive and negative, that accompany it relative to places that burn with low or moderate severity. Terms like “severe” and “high severity” have negative connotations and preventing these types of fires will continue to be a common fire management objective. It is nonetheless important to recognize that many plants and animals thrive in areas burned with high severity (DellaSala and Hanson 2015; Hutto et al. 2016), and many ecosystem services that people value are provided by burned areas (Schoennagel et al. 2017). Equally important, however, is the potential for high severity fire to be a catalyst for ecosystem change in the face of changing climate (Stevens-Rumann and Morgan 2019; Walker et al. 2018). Understanding where and when fires are more likely to burn severely now and into the future can inform both science and management. We hope the work presented here contributes to that understanding.

6. References

- Abatzoglou, John T. 2013. Development of gridded surface meteorological data for ecological applications and modelling. *International Journal of Climatology*. 33(1): 121–131. doi: 10.1002/joc.3413.
- Abatzoglou, John T.; Williams, A. Park. 2016. Impact of anthropogenic climate change on wildfire across western US forests. *Proceedings of the National Academy of Sciences*. 113(42): 11770–11775. doi: 10.1073/pnas.1607171113.
- Andrews, Patricia L.; Loftsgaarden, Don O.; Bradshaw, Larry S. 2003. Evaluation of fire danger rating indexes using logistic regression and percentile analysis. *International Journal of Wildland Fire*. 12(2): 213–226. doi: 10.1071/WF02059.
- Arkle, Robert S.; Pilliod, David S.; Welty, Justin L. 2012. Pattern and process of prescribed fires influence effectiveness at reducing wildfire severity in dry coniferous forests. *Forest Ecology and Management*. 276: 174–184. doi: 10.1016/j.foreco.2012.04.002.
- Bessie, W.C.; Johnson, E.A. 1995. The relative importance of fuels and weather on fire behavior in subalpine forests. *Ecology*. 76(3): 747–762. doi: 10.2307/1939341.
- Birch, Donovan S.; Morgan, Penelope; Kolden, Crystal A.; [et al.]. 2014. Is proportion burned severely related to daily area burned? *Environmental Research Letters*. 9(6): 064011. doi: 10.1088/1748-9326/9/6/064011.
- Birch, Donovan S.; Morgan, Penelope; Kolden, Crystal A.; [et al.]. 2015. Vegetation, topography and daily weather influenced burn severity in central Idaho and western Montana forests. *Ecosphere*. 6(1): 1–23. doi: 10.1890/es14-00213.1.
- Breiman, L. 2001. Random forests. *Machine Learning*. 45: 5–32.
- Cansler, C. Alina; McKenzie, Donald. 2012. How robust are burn severity indices when applied in a new region? Evaluation of alternate field-based and remote-sensing methods. *Remote Sensing*. 4(2): 456–483. doi: 10.3390/rs4020456.
- Commission for Environmental Cooperation [CEC]. 2007. Ecological regions of North America: Toward a common perspective. Montreal, QC: CEC. 71 p.
- Cutler, D. Richard; Edwards, Thomas C.; Beard, Karen H.; [et al.]. 2007. Random Forests for classification in ecology. *Ecology*. 88(11): 2783–2792. doi: 10.1890/07-0539.1.
- De Santis, Angela; Chuvieco, Emilio. 2009. GeoCBI: A modified version of the Composite Burn Index for the initial assessment of the short-term burn severity from remotely sensed data. *Remote Sensing of Environment*. 113(3): 554–562. doi: 10.1016/j.rse.2008.10.011.

DellaSala, Dominick A.; Hanson, Chad T., eds. 2015. The ecological importance of mixed-severity fires: Nature's phoenix. Amsterdam, the Netherlands: Elsevier. 450 p.

Dennison, Philip E.; Brewer, Simon C.; Arnold, James D.; Moritz, Max A. 2014. Large wildfire trends in the western United States, 1984–2011. *Geophysical Research Letters*. 41(8): 2014GL059576. doi: 10.1002/2014gl059576.

Didan, Kamel. 2015. MOD13Q1 MODIS/Terra vegetation indices 16-day L3 global 250m SIN grid V006 [dataset]. NASA EOSDIS Land Processes DAAC. <https://lpdaac.usgs.gov/products/mod13q1v006/> [Accessed 30 March 2020].

Didan, Kamel; Barreto Munoz, Armando; Solano, Ramon; [et al.]. 2015. MODIS Vegetation Index User's Guide (MOD13 Series). Tucson, AZ: University of Arizona, Vegetation Index and Phenology Lab. https://vip.arizona.edu/MODIS_UsersGuide.php [Accessed 5 December 2018].

Dillon, Gregory K.; Holden, Zachary A.; Morgan, Penelope; [et al.]. 2011. Both topography and climate affected forest and woodland burn severity in two regions of the western US, 1984 to 2006. *Ecosphere*. 2(12): art130. doi: 10.1890/es11-00271.1.

Dwyer, John; Schmidt, Gail. 2006. The MODIS Reprojection Tool. In: Qu, John J.; Gao, Wei; Kafatos, Menas, [et al.], eds. *Earth science satellite remote sensing*. Berlin, Heidelberg: Springer: 162–177.

Eidenshink, Jeff; Schwind, Brian; Brewer, Ken.; [et al.]. 2007. A project for monitoring trends in burn severity. *Fire Ecology*. 3(1): 3–21. doi: 10.4996/fireecology.0301003.

Estes, Becky L.; Knapp, Eric E.; Skinner, Carl N.; [et al.]. 2017. Factors influencing fire severity under moderate burning conditions in the Klamath Mountains, northern California, USA. *Ecosphere*. 8(5): e01794. doi: 10.1002/ecs2.1794.

Evans, Ian S. 1972. General geomorphometry, derivatives of altitude, and descriptive statistics. In: Chorley, Richard J., ed. *Spatial analysis in geomorphology*. New York: Harper and Row: 17–90.

Finco, Mark; Quayle, Brad; Zhang, Yuan; [et al.]. 2012. Monitoring Trends in Burn Severity (MTBS): Monitoring wildfire activity for the past quarter century using Landsat data. In: Morin, Randall S.; Liknes, Greg C., comps. *Moving from status to trends: Forest Inventory and Analysis (FIA) symposium 2012*. Gen. Tech. Rep. NRS-P-105. Newtown Square, PA: U.S. Department of Agriculture, Forest Service, Northern Research Station: 222–228.

Flint, Alan L.; Childs, Stuart W. 1987. Calculation of solar radiation in mountainous terrain. *Agricultural and Forest Meteorology*. 40(3): 233–249. doi: 10.1016/0168-1923(87)90061-X.

-
- Fulé, Peter Z.; Crouse, Joseph E.; Roccaforte, John Paul; Kalies, Elizabeth L. 2012. Do thinning and/or burning treatments in western USA ponderosa or Jeffrey pine-dominated forests help restore natural fire behavior? *Forest Ecology and Management*. 269: 68–81. doi: 10.1016/j.foreco.2011.12.025.
- Gesch, Dean B. 2007. Chapter 4—The National Elevation Dataset. In: Maune, David, ed. *Digital elevational model technologies and applications: The DEM Users Manual* (2nd ed.). Bethesda, MD: American Society of Photogrammetry and Remote Sensing: 99–118.
- Harvey, Brian J.; Donato, Daniel C.; Turner, Monica G. 2016. Drivers and trends in landscape patterns of stand-replacing fire in forests of the US Northern Rocky Mountains (1984–2010). *Landscape Ecology*. 31(10): 2367–2383. doi: 10.1007/s10980-016-0408-4.
- Hastie, Trevor; Tibshirani, Robert; Friedman, Jerome. 2009. *The elements of statistical learning: Data mining, inference, and prediction*. 2nd ed. New York: Springer-Verlag. 746 p.
- Hicke, Jeffrey A.; Meddens, Arjan J.H.; Kolden, Crystal A. 2016. Recent tree mortality in the western United States from bark beetles and forest fires. *Forest Science*. 62(2): 141–153. doi: 10.5849/forsci.15-086.
- Hijmans, Robert J.; van Etten, Jacob; Sumner, Michael; [et al.]. 2016. Package ‘raster’. <https://cran.r-project.org/web/packages/raster/raster.pdf> [Accessed 31 March 2020].
- Holden, Zachary A.; Jolly, W. Matt. 2011. Modeling topographic influences on fuel moisture and fire danger in complex terrain to improve wildland fire management decision support. *Forest Ecology and Management*. 262(12): 2133–2141. doi: 10.1016/j.foreco.2011.08.002.
- Holden, Zachary A.; Morgan, Penelope; Evans, Jeffrey S. 2009. A predictive model of burn severity based on 20-year satellite-inferred burn severity data in a large southwestern US wilderness area. *Forest Ecology and Management*. 258(11): 2399–2406. doi: 10.1016/j.foreco.2009.08.017.
- Holden, Zachary A.; Swanson, Alan; Klene, Anna E.; [et al.]. 2016. Development of high-resolution (250 m) historical daily gridded air temperature data using reanalysis and distributed sensor networks for the US Northern Rocky Mountains. *International Journal of Climatology*. 36(10): 3620–3632. doi: 10.1002/joc.4580.
- Huang, Chengquan; Goward, Samuel N.; Masek, Jeffrey G.; [et al.]. 2010. An automated approach for reconstructing recent forest disturbance history using dense Landsat time series stacks. *Remote Sensing of Environment*. 114(1): 183–198. doi: 10.1016/j.rse.2009.08.017.

Hudak, Andrew T.; Morgan, Penelope; Bobbitt, Michael J.; [et al.]. 2007. The relationship of multispectral satellite imagery to immediate fire effects. *Fire Ecology*. 3(1): 64–90. doi: 10.4996/fireecology.0301064.

Hudak, Andrew T.; Rickert, Ian; Morgan, Penelope; [et al.]. 2011. Review of fuel treatment effectiveness in forests and rangelands and a case study from the 2007 megafires in central Idaho, USA. Gen. Tech. Rep. RMRS-GTR-252. Fort Collins, CO: U.S. Department of Agriculture, Forest Service, Rocky Mountain Research Station. 60 p.

Hutto, Richard L.; Keane, Robert E.; Sherriff, Rosemary L.; [et al.]. 2016. Toward a more ecologically informed view of severe forest fires. *Ecosphere*. 7(2): e01255. doi: 10.1002/ecs2.1255.

Iqbal, Muhammed. 2012. An introduction to solar radiation. New York: Elsevier. 408 p.

Jolly, W. Matt; Freeborn, Patrick H. 2017. Towards improving wildland firefighter situational awareness through daily fire behaviour risk assessments in the US Northern Rockies and Northern Great Basin. *International Journal of Wildland Fire*. 26(7): 574–586. doi: 10.1071/WF16153.

Jolly, William M.; Graham, Jonathan M.; Michaelis, Andrew; [et al.]. 2005. A flexible, integrated system for generating meteorological surfaces derived from point sources across multiple geographic scales. *Environmental Modelling & Software*. 20(7): 873–882. doi: 10.1016/j.envsoft.2004.05.003.

Kalies, Elizabeth L.; Yocom Kent, Larissa L. 2016. Tamm Review: Are fuel treatments effective at achieving ecological and social objectives? A systematic review. *Forest Ecology and Management*. 375: 84–95. doi: 10.1016/j.foreco.2016.05.021.

Karau, Eva C.; Sikkink, Pamela G.; Keane, Robert E.; Dillon, G.K. 2014. Integrating satellite imagery with simulation modeling to improve burn severity mapping. *Environmental Management*. 54(1): 98–111. doi: 10.1007/s00267-014-0279-x.

Keane, Robert E.; Agee, James; Fulé, Peter; [et al.]. 2008. Ecological effects of large fires on US landscapes: Benefit or catastrophe? *International Journal of Wildland Fire*. 17(6): 696–712. doi: 10.1071/WF07148.

Keane, Robert E.; Dillon, Greg; Drury, Stacy; [et al.]. 2014. New and revised fire effects tools for fire management. *Fire Management Today*. 73(3): 37–47.

Keeley, J. E. 2009. Fire intensity, fire severity and burn severity: A brief review and suggested usage. *International Journal of Wildland Fire*. 18(1): 116–126. doi:10.1071/WF07049.

Keeley, Jon E.; Brennan, Teresa; Pfaff, Anne H. 2008. Fire severity and ecosystem responses following crown fires in California shrublands. *Ecological Applications*. 18(6): 1530-1546. doi: 10.1890/07-0836.1.

Kemp, Kerry B.; Higuera, Philip E.; Morgan, Penelope. 2016. Fire legacies impact conifer regeneration across environmental gradients in the U.S. northern Rockies. *Landscape Ecology*. 31(3): 619–636. doi: 10.1007/s10980-015-0268-3.

Key, Carl H. 2006. Ecological and sampling constraints on defining landscape fire severity. *Fire Ecology*. 2(2): 34–59. doi: 10.4996/fireecology.0202034

Key, Carl H.; Benson, Nathan C. 2006. Landscape assessment: sampling and analysis methods. In: Lutes, Duncan C.; Keane, Robert E.; Caratti, John F.; [et al.], eds. FIREMON: Fire Effects Monitoring and Inventory System. Gen. Tech. Rep. RMRS-GTR-164-CD. Fort Collins, CO: U.S. Department of Agriculture, Forest Service, Rocky Mountain Research Station: LA1-LA51.

Keyser, Alisa; Westerling, Anthony LeRoy. 2017. Climate drives inter-annual variability in probability of high severity fire occurrence in the western United States. *Environmental Research Letters*. 12(6): 065003. doi: 10.1088/1748-9326/aa6b10.

Kolden, Crystal A.; Lutz, James A.; Key, Carl H.; [et al.]. 2012. Mapped versus actual burned area within wildfire perimeters: Characterizing the unburned. *Forest Ecology and Management*. 286: 38–47. doi: 10.1016/j.foreco.2012.08.020.

Kolden, Crystal A.; Smith, Alistair M.S.; Abatzoglou, John T. 2015. Limitations and utilisation of Monitoring Trends in Burn Severity products for assessing wildfire severity in the USA. *International Journal of Wildland Fire*. 24(7): 1023–1028. doi: 10.1071/WF15082.

Krawchuk, Meg A.; Haire, Sandra L.; Coop, Jonathan; [et al.]. 2016. Topographic and fire weather controls of fire refugia in forested ecosystems of northwestern North America. *Ecosphere*. 7(12): e01632. doi:10.1002/ecs2.1632.

Lentile, Leigh B.; Holden, Zachary A.; Smith, Alistair M.S.; [et al.]. 2006. Remote sensing techniques to assess active fire characteristics and post-fire effects. *International Journal of Wildland Fire*. 15(3): 319–345. doi: 10.1071/WF05097.

Lentile, Leigh B.; Morgan, Penelope; Hudak, Andrew T.; [et al.]. 2007. Post-fire burn severity and vegetation response following eight large wildfires across the western United States. *Fire Ecology*. 3(1): 91–101. doi: 10.4996/fireecology.0301091.

Lentile, Leigh B.; Smith, Alistair M.S.; Hudak, Andrew T.; [et al.]. 2009. Remote sensing for prediction of 1-year post-fire ecosystem condition. *International Journal of Wildland Fire*. 18(5): 594–608. doi: 10.1071/WF07091.

-
- Lewis, Sarah A.; Hudak, Andrew T.; Robichaud, Peter R.; [et al.]. 2017. Indicators of burn severity at extended temporal scales: A decade of ecosystem response in mixed-conifer forests of western Montana. *International Journal of Wildland Fire*. 26(9): 755–771. doi: 10.1071/WF17019.
- Liaw, Andy; Wiener, Matthew. 2002. Classification and regression by randomForest. *R news: The newsletter of the R project*. 2(3): 18–22.
- Littell, Jeremy S.; McKenzie, Donald; Peterson, David L.; Westerling, Anthony L. 2009. Climate and wildfire area burned in western U.S. ecoprovinces, 1916–2003. *Ecological Applications*. 19(4): 1003–1021. doi: 10.1890/07-1183.1.
- Lutz, James A.; Key, Carl H.; Kolden, Crystal A.; [et al.]. 2011. Fire frequency, area burned, and severity: A quantitative approach to defining a normal fire year. *The Journal of the Association for Fire Ecology*. 7(2): 51–65. doi: 10.4996/fireecology.0702051.
- Lydersen, Jamie M.; Collins, Brandon M.; Miller, Jay D.; [et al.]. 2016. Relating fire-caused change in forest structure to remotely sensed estimates of fire severity. *Fire Ecology*. 12(3): 99–116. doi: 10.4996/fireecology.1203099.
- Mallek, Chris; Safford, Hugh; Viers, Joshua; Miller, Jay. 2013. Modern departures in fire severity and area vary by forest type, Sierra Nevada and southern Cascades, California, USA. *Ecosphere*. 4(12): 1–28. doi: 10.1890/es13-00217.1.
- McCune, B.; Keon, D. 2002. Equations for potential annual direct incident radiation and heat load. *Journal of Vegetation Science*. 13(4): 603–606. doi: 10.1111/j.1654-1103.2002.tb02087.x.
- Meddens, Arjan J.H.; Kolden, Crystal A.; Lutz, James A. 2016. Detecting unburned areas within wildfire perimeters using Landsat and ancillary data across the northwestern United States. *Remote Sensing of Environment*. 186: 275–285. doi: 10.1016/j.rse.2016.08.023.
- Meddens, Arjan J.H.; Kolden, Crystal A.; Lutz, James A.; [et al.]. 2018a. Fire refugia: What are they, and why do they matter for global change? *BioScience*. 68(12): 944–954. doi: 10.1093/biosci/biy103.
- Meddens, Arjan J.H.; Kolden, Crystal A.; Lutz, James A.; [et al.]. 2018b. Spatiotemporal patterns of unburned areas within fire perimeters in the northwestern United States from 1984 to 2014. *Ecosphere*. 9(2): e02029. doi: 10.1002/ecs2.2029.
- Miller, J.D.; Safford, H.D.; Crimmins, M.; Thode, A.E. 2009a. Quantitative evidence for increasing forest fire severity in the Sierra Nevada and Southern Cascade Mountains, California and Nevada, USA. *Ecosystems*. 12(1): 16–32. doi: 10.1007/s10021-008-9201-9.

Miller, J.D.; Skinner, C.N.; Safford, H.D.; [et al.]. 2012. Trends and causes of severity, size, and number of fires in northwestern California, USA. *Ecological Applications*. 22(1): 184–203. doi: 10.1890/10-2108.1.

Miller, Jay D.; Knapp, Eric E.; Key, Carl H.; [et al.]. 2009b. Calibration and validation of the relative differenced normalized burn ratio (RdNBR) to three measures of fire severity in the Sierra Nevada and Klamath Mountains, California, USA. *Remote Sensing of Environment*. 113(3): 645–656. doi: 10.1016/j.rse.2008.11.009.

Miller, Jay D.; Thode, Andrea E. 2007. Quantifying burn severity in a heterogeneous landscape with a relative version of the delta normalized burn ratio (dNBR). *Remote Sensing of Environment*. 109(1): 66–80. doi: 10.1016/j.rse.2006.12.006.

Monitoring Trends in Burn Severity [MTBS]. 2016. Monitoring Trends in Burn Severity (MTBS) mapping protocol. Unpublished guidebook prepared by MTBS staff. <https://mtbs.gov>. 19 p. [Accessed 10 October 2018].

Morgan, Penelope; Keane, Robert E.; Dillon, Gregory K.; [et al.]. 2014. Challenges of assessing fire and burn severity using field measures, remote sensing and modelling. *International Journal of Wildland Fire*. 23(8): 1045–1060. doi: 10.1071/WF13058.

Morgan, Penelope; Moy, Marshall; Droske, Christine A.; [et al.]. 2015. Vegetation response to burn severity, native grass seeding, and salvage logging. *The Journal of the Association for Fire Ecology*. 11(2): 31–58. doi: 10.4996/fireecology.1102031.

Murphy, Melanie A.; Evans, Jeffrey S.; Storfer, Andrew. 2010. Quantifying *Bufo boreas* connectivity in Yellowstone National Park with landscape genetics. *Ecology*. 91(1): 252–261. doi: 10.1890/08-0879.1.

National Interagency Fire Center [NIFC]. 2018. Interagency standards for fire and fire aviation operations (Redbook). Boise, ID: Interagency Standards for Fire and Fire Aviation Operations Group, National Interagency Fire Center. https://www.nifc.gov/policies/pol_ref_redbook_2018.html [Accessed 30 March 2020].

Omernik, James M.; Griffith, Glenn E. 2014. Ecoregions of the conterminous United States: Evolution of a hierarchical spatial framework. *Environmental Management*. 54(6): 1249–1266. doi: 10.1007/s00267-014-0364-1.

Pabst, Kari L. 2010. Quantifying burn severity in a heterogeneous landscape: A comparison of the differenced normalized burn ratio and the relative differenced normalized burn ratio in the Grand Canyon National Park, Arizona. Brookings, SD: South Dakota State University. Thesis. 95 p.

-
- Parks, Sean; Dillon, Gregory; Miller, Carol. 2014a. A new metric for quantifying burn severity: The relativized burn ratio. *Remote Sensing*. 6(3): 1827–1844. doi: 10.3390/rs6031827.
- Parks, Sean A. 2014. Mapping day-of-burning with coarse-resolution satellite fire-detection data. *International Journal of Wildland Fire*. 23(2): 215–223. doi: 10.1071/WF13138.
- Parks, Sean A.; Miller, Carol; Abatzoglou, John T.; [et al.]. 2016. How will climate change affect wildland fire severity in the western US? *Environmental Research Letters*. 11(3): 035002. doi: 10.1088/1748-9326/11/3/035002.
- Parks, Sean A.; Holsinger, Lisa M.; Panunto, Matthew H.; [et al.]. 2018. High-severity fire: Evaluating its key drivers and mapping its probability across western US forests. *Environmental Research Letters*. 13(4): 044037. doi: 10.1088/1748-9326/aab791.
- Parks, Sean A.; Miller, Carol; Nelson, Cara R.; [et al.]. 2014b. Previous fires moderate burn severity of subsequent wildland fires in two large western US wilderness areas. *Ecosystems*. 17(1): 29–42. doi: 10.1007/s10021-013-9704-x.
- Parks, Sean A.; Parisien, Marc-André; Miller, Carol; Dobrowski, Solomon Z. 2014c. Fire activity and severity in the western US vary along proxy gradients representing fuel amount and fuel moisture. *PLoS ONE*. 9(6): e99699. doi: 10.1371/journal.pone.0099699.
- Parsons, Annette; Robichaud, P.R.; Lewis, S.A.; Clark, Jess T. 2010. Field guide for mapping post-fire soil burn severity. Gen. Tech. Rep. RMRS-GTR-243. Fort Collins, CO: U.S. Department of Agriculture, Forest Service, Rocky Mountain Research Station. 49 p.
- Picotte, Joshua J.; Peterson, Birgit; Meier, Gretchen; Howard, Stephen M. 2016. 1984–2010 trends in fire burn severity and area for the conterminous US. *International Journal of Wildland Fire*. 25(4): 413–420. doi: 10.1071/WF15039.
- Picotte, Joshua J.; Robertson, Kevin. 2011a. Timing constraints on remote sensing of wildland fire burned area in the southeastern US. *Remote Sensing*. 3(8): 1680–1690. doi: 10.3390/rs3081680.
- Picotte, Joshua J.; Robertson, Kevin M. 2011b. Validation of remote sensing of burn severity in south-eastern US ecosystems. *International Journal of Wildland Fire*. 20(3): 453–464. doi: 10.1071/WF10013.
- Pike, R.J.; Wilson, S.E. 1971. Elevation relief ratio, hypsometric integral and geomorphic area altitude analysis. *Bulletin of the Geological Society of America*. 82(4): 1079–1084. doi: 10.1130/0016-7606(1971)82[1079:erhiag]2.0.co;2.

Prasad, Anantha; Iverson, Louis; Liaw, Andy. 2006. Newer classification and regression tree techniques: Bagging and Random Forests for ecological prediction. *Ecosystems*. 9(2): 181–199. doi: 10.1007/s10021-005-0054-1.

Prichard, Susan J.; Stevens-Rumann, Camille S.; Hessburg, Paul F. 2017. Tamm Review: Shifting global fire regimes: Lessons from reburns and research needs. *Forest Ecology and Management*. 396: 217–233. doi: 10.1016/j.foreco.2017.03.035.

Pyne, Stephen J.; Andrews, Patricia L.; Laven, Richard D. 1996. *Introduction to wildland fire*. 2nd ed. New York: John Wiley and Sons. 808 p.

R Development Core Team. 2015. *R: A language and environment for statistical computing*. Vienna, Austria: R Foundation for Statistical Computing. Available at <http://www.R-project.org> [Accessed 16 March 2020].

Robichaud, Peter R.; Lewis, Sarah A.; Wagenbrenner, Joseph W.; [et al.]. 2013. Post-fire mulching for runoff and erosion mitigation: Part I: Effectiveness at reducing hillslope erosion rates. *Catena*. 105: 75–92. doi: 10.1016/j.catena.2012.11.015.

Rollins, Matthew G. 2009. LANDFIRE: A nationally consistent vegetation, wildland fire, and fuel assessment. *International Journal of Wildland Fire*. 18(3): 235–249. doi: 10.1071/WFo8o88.

Romme, William H.; Boyce, Mark S.; Gresswell, Robert; [et al.]. 2011. Twenty years after the 1988 Yellowstone fires: Lessons about disturbance and ecosystems. *Ecosystems*. 14(7): 1196–1215. doi: 10.1007/s10021-011-9470-6.

Rouse, J.W.; Haas, R.H.; Schell, J.A. [et al.]. 1974. Monitoring vegetation systems in the Great Plains with ERTS. In: Freden, Stanley C.; Mercanti, Enrico P.; Becker, Margaret A., eds. *Third ERTS Satellite-1 Symposium. Volume 1: Technical Presentations, Section A*. Washington, DC: National Aeronautics and Space Administration: 309–317 (Paper-A20).

Schlobohm, Paul; Brian, Jim, comps. 2002. *Gaining an understanding of the National Fire Danger Rating system: Report PMS 932*. Boise, ID: National Wildfire Coordinating Group. 72 p.

Schoennagel, Tania; Balch, Jennifer K.; Brenkert-Smith, Hannah; [et al.]. 2017. Adapt to more wildfire in western North American forests as climate changes. *Proceedings of the National Academy of Sciences*. 114(18): 4582–4590. doi: 10.1073/pnas.1617464114.

Scott, Joe H.; Burgan, Robert E. 2005. Standard fire behavior fuel models: A comprehensive set for use with Rothermel's surface fire spread model. Gen. Tech. Rep. RMRS-GTR-153. Fort Collins, CO: U.S. Department of Agriculture, Forest Service, Rocky Mountain Research Station. 72 p.

Scott, Joe H.; Thompson, Matthew P.; Calkin, David E. 2013. A wildfire risk assessment framework for land and resource management. Gen. Tech. Rep. RMRS-GTR-315. Fort Collins, CO: U.S. Department of Agriculture, Forest Service, Rocky Mountain Research Station. 83 p.

Sikkink, Pamela G.; Dillon, Gregory K.; Keane, Robert E.; [et al.]. 2013. Composite Burn Index (CBI) data and field photos collected for the FIRESEV project, western United States. Fort Collins, CO: Forest Service Research Data Archive. <https://doi.org/10.2737/RDS-2013-0017>.

Stage, A.R. 1976. Notes: An expression for the effect of aspect, slope, and habitat type on tree growth. *Forest Science*. 22(4): 457–460.

Stevens-Rumann, Camille S.; Kemp, Kerry B.; Higuera, Philip E.; [et al.]. 2018. Evidence for declining forest resilience to wildfires under climate change. *Ecology Letters*. 21(2): 243–252. doi: 10.1111/ele.12889.

Stevens-Rumann, Camille S.; Morgan, Penelope. 2019. Tree regeneration following wildfires in the western US: A review. *Fire Ecology*. 15(1): 15. doi: 10.1186/s42408-019-0032-1.

Stevens-Rumann, Camille S.; Prichard, Susan J.; Strand, Eva K.; [et al.]. 2016. Prior wildfires influence burn severity of subsequent large fires. *Canadian Journal of Forest Research*. 46(11): 1375–1385. doi: 10.1139/cjfr-2016-0185.

Svetnik, Vladimir; Liaw, Andy; Tong, Christopher; [et al.]. 2004. Application of Breiman's Random Forest to modeling structure-activity relationships of pharmaceutical molecules. In: Roli, Fabio; Kittler, Josef; Windeatt, Terry, eds. Multiple classifier systems. *Lecture Notes in Computer Science*. Vol. 3077. Berlin and Heidelberg, Germany: Springer: 334–343.

Swets, J.A. 1988. Measuring the accuracy of diagnostic systems. *Science*. 240(4857): 1285–1293. doi: 10.1126/science.3287615.

Theobald, David; Stevens, Don L., Jr.; White, Denis; [et al.]. 2007. Using GIS to generate spatially balanced random survey designs for natural resource applications. *Environmental Management*. 40(1): 134–146. doi: 10.1007/s00267-005-0199-x.

Thode, Andrea E.; van Wagendonk, Jan W.; Miller, Jay D.; Quinn, J.F. 2011. Quantifying the fire regime distributions for severity in Yosemite National Park, California, USA. *International Journal of Wildland Fire*. 20(2): 223–239. doi: 10.1071/WFO9060.

-
- Thomas, Nancy E.; Huang, Chengquan; Goward, Samuel N.; [et al.]. 2011. Validation of North American forest disturbance dynamics derived from Landsat time series stacks. *Remote Sensing of Environment*. 115(1): 19–32. doi: 10.1016/j.rse.2010.07.009.
- Thompson, Matthew; Bowden, Phil; Brough, April; [et al.]. 2016. Application of wildfire risk assessment results to wildfire response planning in the Southern Sierra Nevada, California, USA. *Forests*. 7(3): 64. doi: 10.3390/f7030064.
- Turner, Monica G.; Romme, William H.; Gardner, Robert H.; Hargrove, William W. 1997. Effects of fire size and pattern on early succession in Yellowstone National Park. *Ecological Monographs*. 67(4): 411–433. doi: 10.1890/0012-9615(1997)067[0411:EOFSAP]2.0.CO;2.
- Veraverbeke, S.; Lhermitte, S.; Verstraeten, W.W.; Goossens, R. 2011. A time-integrated MODIS burn severity assessment using the multi-temporal differenced normalized burn ratio (dNBRMT). *International Journal of Applied Earth Observation and Geoinformation*. 13(1): 52–58. doi: 10.1016/j.jag.2010.06.006.
- Walker, Ryan B.; Coop, Jonathan D.; Parks, Sean A.; Trader, Laura. 2018. Fire regimes approaching historic norms reduce wildfire-facilitated conversion from forest to non-forest. *Ecosphere*. 9(4): e02182. doi: 10.1002/ecs2.2182.
- Waring, Richard H.; Schlesinger, William H. 1985. *Forest ecosystems: Concepts and management*. Orlando, FL: Academic Press. 340 p.
- Weiss, A. 2001. Topographic position and landforms analysis. Poster presentation. ESRI user conference; 9–13 July 2001; San Diego, CA.
- Westerling, A.L.; Hidalgo, H.G.; Cayan, D.R.; Swetnam, T.W. 2006. Warming and earlier spring increase western US forest wildfire activity. *Science*. 313(5789): 940–943. doi: 10.1126/science.1128834.
- Western Forestry Leadership Coalition. 2010. *The true cost of wildfire in the western U.S.* Lakewood, CO. 15 p. https://www.thewflc.org/sites/default/files/324_pdf.pdf [Accessed 5 December 2018].
- Whittaker, Robert H. 1970. *Communities and ecosystems*. New York: Macmillan. 162 p.
- Wiken, Ed; Jimenez Nava, Francisco; Griffith, Glenn. 2011. *North American Terrestrial Ecosystems—Level III*. Montreal, QC: Commission for Environmental Cooperation. 149 p.

Appendix A: Solar Radiation Modeling

Modeling solar radiation across large areas is a complex and computationally intensive process. Due to different computing resources and time available during our work on the western versus eastern study areas, we used different modeling methods that are described here.

Solar Radiation Modeling in the Western Study Area

For the western study area we used a complex solar radiation model to calculate incoming solar radiation, net radiation, and potential evapotranspiration (PET). The model we used, SOLPET6, was a set of Fortran computer programs that evolved from hydrologic research in California and the Desert Southwest (Flint and Childs 1987; Flint and Flint 2008; Flint et al. 2004). We chose SOLPET6 for its thoroughness: It incorporates inputs for geographic position, topography, and monthly temperatures to calculate sun angles, atmospheric transmittance, and topographic shading throughout each day. SOLPET6 models direct, diffuse, and reflected radiation, and produces output raster layers representing solar radiation, net radiation, and PET. Net radiation, as defined here, is equivalent to insolation minus the shortwave radiation reflected by the Earth's surface plus net longwave radiation emitted and absorbed by the Earth's surface and the atmosphere. Potential evapotranspiration is the amount of water that would be evaporated and transpired by vegetation if enough water were available.

Using our digital elevation model (DEM) data, along with 30-year normal (1971–2000) mean monthly minimum and maximum temperature data from the PRISM (Parameter-elevation Relationships on Independent Slopes Model) Climate Group (Daly et al. 2002; PRISM Climate Group 2010), we calculated potential surface insolation for every pixel in the western study area. We performed a number of processing steps for each tile, including: (1) running both the DEM and temperature data through several standalone computer programs specifically written to create input data for SOLPET6 (A. Flint, Research Hydrologist, USGS California Water Science Center, Sacramento, CA, pers. comm., June 2010), (2) calculating surface insolation with SOLPET6 on hourly timesteps for each day of the year and summing those by month, and (3) processing and summing outputs into growing season (April–October) and annual rasters.

Modeling solar radiation in this way was an extremely computer-intensive process that required certain tradeoffs. Minimum and maximum temperature data are used in this process only to estimate atmospheric transmittance (Flint and Flint 2008) based on methodologies developed by Bristow and Campbell (1984). Using PRISM data, which were summarized as monthly means and have a 4-kilometer (approximately 2.5 mile) spatial resolution, was sufficient to capture variation in transmittance throughout the year. To calculate shading at any pixel from nearby topography, we needed to set a horizontal search radius. This distance specified the distance the program would look in each direction for topography that could potentially block the sun. After initial testing, we set this distance to 2 kilometers (approximately 1.2 miles), compromising between including as much area as possible and having reasonable processing times. Despite these tradeoffs, this approach to modeling solar radiation took extensive time and computational resources. The result of this modeling process was six predictor variables for each 1-degree DEM tile: annual and growing season versions of

solar radiation, net radiation, and PET. However, total solar radiation and net radiation had an almost one-to-one correlation, so we did not use net radiation in any of our statistical models.

Solar Radiation Modeling in the Eastern Study Area

Due to constraints on time and computing resources during the eastern phase of the project, we needed to use a less computationally intensive solar radiation model. In place of SOLPET6 we used the Area Solar Radiation (ASR) tool in ArcGIS, which is based on methods developed by Rich et al. (1994) and refined and implemented in the Solar Analyst model by Fu and Rich (2000, 2002). Using ASR, we calculated incoming solar radiation for 3 days of the calendar year, the two solstices and an equinox, for every 30-meter (98-foot) cell in each of the 471 tiles in the eastern study area. The ASR tool models direct and diffuse radiation and outputs global radiation (direct + diffuse) for each of the 3 days we selected. The global radiation output is conceptually similar to the solar radiation output modeled with SOLPET6 for the West with one primary exception. The western measure is an approximation of total annual or growing season insolation, while the eastern measure is simply a spatially relative index.

After the DEMs were buffered and projected, we calculated solar radiation with ASR at multiple timesteps throughout each processing day, and processed outputs into an averaged index of relative solar radiation for that day (winter solstice, equinox, or summer solstice). Our final output was a single solar radiation index for each tile representing the average global insolation across the 3 modeled days. Settings for parameters to the ASR tool included: sky size = 200 cells (i.e., a square area 6 kilometers [3.8 miles] on a side); hour interval = 0.2; calculation directions = 32; diffuse model type = uniform sky; diffuse proportion = 0.3; and transmissivity = 0.5 (Fu and Rich 2000).

References

Bristow, Keith L.; Campbell, Gaylon S. 1984. On the relationship between incoming solar radiation and daily maximum and minimum temperature. *Agricultural and Forest Meteorology*. 31(2): 159–166. doi: 10.1016/0168-1923(84)90017-0.

Daly, Christopher; Gibson, Wayne P.; Taylor, George H.; [et al.]. 2002. A knowledge-based approach to the statistical mapping of climate. *Climate Research*. 22: 99–113. doi: 10.3354/cro22099.

Flint, Alan L.; Childs, Stuart W. 1987. Calculation of solar radiation in mountainous terrain. *Agricultural and Forest Meteorology*. 40(3): 233–249. doi: 10.1016/0168-1923(87)90061-X.

Flint, Alan L.; Flint, Lorraine E.; Hevesi, Joseph A.; [et al.]. 2004. Fundamental concepts of recharge in the Desert Southwest: A regional modeling perspective. In: Hogan, James F.; Phillips, Fred M.; Scanlon, Bridget R., eds. *Groundwater recharge in a desert environment: The southwestern United States*. Washington, DC: American Geophysical Union: 159–184.

Flint, Lorraine E.; Flint, Alan L. 2008. A basin-scale approach to estimating stream temperatures of tributaries to the Lower Klamath River, California. *Journal of Environmental Quality*. 37(1): 57–68. doi: 10.2134/jeq2006.0341.

Fu, Pinde; Rich, Paul M. 2000. *The Solar Analyst 1.0 user manual*. Lawrence, KS: Helios Environmental Modeling Institute, LLC. 53 p.

Fu, Pinde; Rich, Paul M. 2002. A geometric solar radiation model with applications in agriculture and forestry. *Computers and Electronics in Agriculture*. 37(1–3): 25–35. doi: 10.1016/S0168-1699(02)00115-1.

PRISM Climate Group. 2010. United States average monthly minimum and maximum temperature, 1971–2000 (4km; ASC). Oregon State University. <http://prism.oregonstate.edu> [Accessed June 2010].

Rich, Paul M.; Hetrick, W.A.; Saving, S.C. 1994. Using viewshed models to calculate intercepted solar radiation: Applications in ecology. *American Society for Photogrammetry and Remote Sensing Technical Papers*. 4: 524–529.

Appendix B: Prefire NDVI Pixel Reliability for the Eastern Study Area

Our choice to include single-scene fires in the eastern study area necessitated a different approach to generating prefire normalized difference vegetation index (NDVI) data because single-scene (NBR) fires from Monitoring Trends in Burn Severity (MTBS) do not come with prefire Landsat NDVI data. Therefore, we decided to use precalculated NDVI from the Moderate-Resolution Imaging Spectroradiometer (MODIS) instead. We acquired the MODIS NDVI data (MOD13Q1 V006) (Didan 2015), then used the MODIS Reprojection Tool (Dwyer and Schmidt 2006) to extract, project, and convert the NDVI and associated raster layers to our Albers equal-area conic projection and the GeoTiff format.

MODIS vegetation index data contain many layers of information, including NDVI and a measure of pixel reliability. The pixel reliability layer indicates whether NDVI for each pixel is good or whether it has been affected by clouds, cloud shadows, and other atmospheric interference such as smoke. To ensure that we were using only the most accurate prefire vegetation data, we decided to use only those pixels with a reliability rank of 0—“Good Data—Use with confidence” as described in the MODIS Vegetation Index User’s Guide (Didan et al. 2015).

To select the prefire MODIS scene to use as our vegetation predictor variable, we analyzed the pixel reliability data for scenes preceding the start date of each fire in our study. With this analysis we sought to answer two primary questions. First, how many prefire MODIS images should we consider when we are searching for the best representation of prefire vegetation? And second, how can pixel reliability values help determine which MODIS scene to choose?

For the first question, we needed to determine how many prefire MODIS scenes to consider in our analysis. Vegetation index data are available from MODIS every 16 days. Ideally, the scene from just before the fire start date would be used to represent prefire vegetation conditions. However, this was not always possible due to our requirement of using only pixels with a reliability rank of zero. But moving too far back in time (within the fire occurrence year) is undesirable because NDVI would become less representative of conditions at the time of the fire. To gauge how far back we would go in considering prefire NDVI data, we evaluated prefire imagery dates for all the multiscene (dNBR) fires included in our eastern study area dataset (2,789 of the 5,412 fires in the eastern study area). We calculated the difference between the prefire image capture date and the fire start date to identify the general patterns of prefire scene selection timing made by the MTBS project.

We confined our analysis to only those MTBS prefire images captured in the same year as the fire. Often, the prefire imagery can come from a year or two prior to the fire start date as long as it comes from a similar point in the growing season. This is based on the assumption that vegetation phenology is similar from year to year. We decided not to consider prior years for two main reasons: practical considerations related to acquiring and processing many NDVI scenes, and concerns about possible overlapping fires over multiple years. In many mapping regions, both wildfire and prescribed fire are frequent events and can overlap from year to year due to rapid vegetation regrowth. This was especially a concern in the Southeast, where vegetative cover can change dramatically over the course of a few weeks.

When we considered only same-year prefire imagery, the difference between prefire scene capture date and fire start date was almost entirely clustered around 0 to 60 days (fig. B.1). Approximately 90 percent of fires in this 60-day subset fell within the 0- to 32-day range,

which coincides with one to two prefire MODIS NDVI images. Based on this analysis and our desire to minimize phenological differences in prefire vegetation, we decided to limit our consideration of prefire images to only the first or second MODIS NDVI scenes prior to the fire start date.

For the second question in our analysis, we did a quantitative comparison of pixel reliability values between the two prefire MODIS scenes for each fire. For each scene, we calculated the percentage of cells within a fire’s perimeter that had a pixel reliability rank of 0 (“Good Data”). In cases where both MODIS images yielded a comparable percentage of good quality pixels, we assumed that an image date closer to the fire start date would provide a more accurate depiction of prefire conditions. Therefore, we implemented a rule that, in order for the second prior scene to be used it would have to provide at least a 10-percent improvement in the number of “Good Data” pixels.

Once we selected the optimum prefire MODIS scene, we extracted NDVI values from the selected prefire NDVI scene for each fire. We extracted NDVI values only where pixel reliability was described as “Good Data.” We inserted a “no data” value anywhere the pixel reliability had a description other than “Good Data.” We eliminated 117 fires from the eastern study area due to a lack of good pixels anywhere in the burned area. The first prior scene was selected for 4,516 fires and the second prior scene for 779 fires. Using this methodology to consider two prior scenes rather than just the first prior scene increased the number of burned pixels that had usable NDVI values from 83 percent to 93 percent.

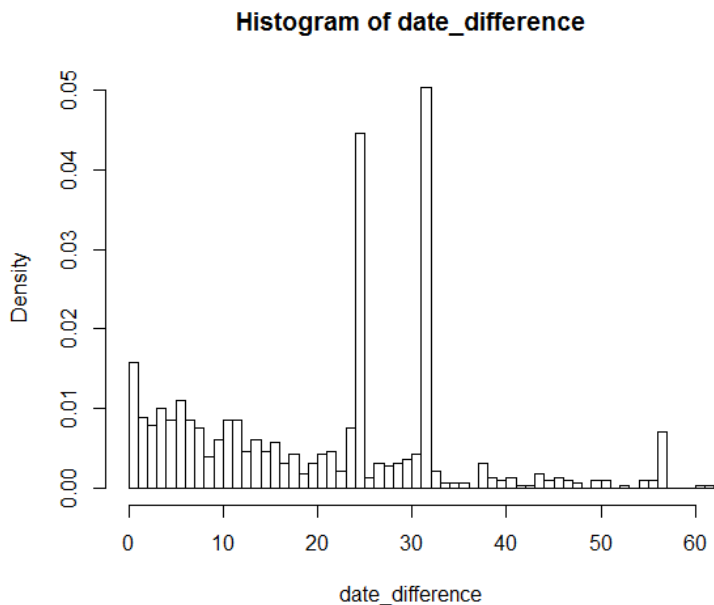


Figure B.1—Distribution of the difference between Monitoring Trends in Burn Severity prefire imagery capture date and fire start date.

References

Didan, Kamel. 2015. MOD13Q1 MODIS/Terra vegetation indices 16-day L3 global 250m SIN Grid V006 [dataset]. NASA EOSDIS Land Processes DAAC.

<https://lpdaac.usgs.gov/products/mod13q1v006/> [Accessed 30 March 2020].

Didan, Kamel; Barreto Munoz, Armando; Solano, Ramon; Huete, Alfredo. 2015. MODIS Vegetation Index User's Guide (MOD13 Series). Tucson, AZ: University of Arizona, Vegetation Index and Phenology Lab. https://vip.arizona.edu/MODIS_UsersGuide.php [Accessed 5 December 2018].

Dwyer, John; Schmidt, Gail. 2006. The MODIS Reprojection Tool. In: Qu, John J.; Gao, Wei; Kafatos, Menas; [et al.], eds. Earth science satellite remote sensing. Berlin, Heidelberg, Germany: Springer. 335 p.

Appendix C: Defining Fire Season for Each Mapping Region

We delineated fire seasons for each region to help us develop a 1,000-hour fuel moisture index that was relative to the fire season itself (see section 2.1.6). We calculated fire seasons using the Fire Program Analysis fire occurrence database (FPA FOD; Short 2013, 2014).

For the 17 regions in the western study area we defined fire seasons based on a frequency analysis of the fire detection dates found in the FPA FOD (fig. C.1). We defined start and end dates for fire seasons in the western study area as the 10th to 95th percentiles, respectively, of the Julian fire detection dates for all wildfires within each region (table C.1).

We also attempted to delineate fire seasons for the eastern study area from a frequency analysis of the FPA FOD. However, we decided not to apply the percentile restrictions on the regional fire season start and end dates due to difficulties in clearly identifying singular fire seasons. Most fire seasons in the eastern regions exhibit a multimodal nature in which there is more than one peak in fire occurrence (fig. C.2). Therefore, we decided to use the entire year to define fire seasons for the eight regions in the East.

Table C.1—Results of Fire Program Analysis fire occurrence database fire detection date analysis for the western mapping regions. For each region, we chose the 10th percentile (10th Perc) as the season start date (10th Date) and the 95th percentile (95th Perc) as the season end date (95th Date).

Region	Median	Mean	Standard deviation	10 th Perc	95 th Perc	10 th Date	95 th Date
----- Julian day -----							
1	219	216	50.1	156	291	4-Jun	17-Oct
2	214	214	41.6	167	287	15-Jun	13-Oct
3	217	217	39.7	164	269	12-Jun	25-Sep
4	208	205	44.1	156	274	4-Jun	30-Sep
5	209	211	48.6	154	289	2-Jun	15-Oct
6	214	211	56.6	140	299	19-May	25-Oct
7	199	202	65.4	126	308	5-May	3-Nov
8	207	206	42.3	159	269	7-Jun	25-Sep
9	174	175	71.5	83	304	23-Mar	30-Oct
10	188	186	54.6	121	278	30-Apr	4-Oct
11	195	188	53.9	112	265	21-Apr	21-Sep
12	202	200	48.2	145	276	24-May	2-Oct
13	197	192	67.0	91	302	31-Mar	28-Oct
14	182	172	86.2	57	318	26-Feb	13-Nov
15	215	208	53.2	138	286	17-May	12-Oct
16	124	143	102.8	23	345	23-Jan	10-Dec
17	109	148	114.0	15	354	15-Jan	19-Dec

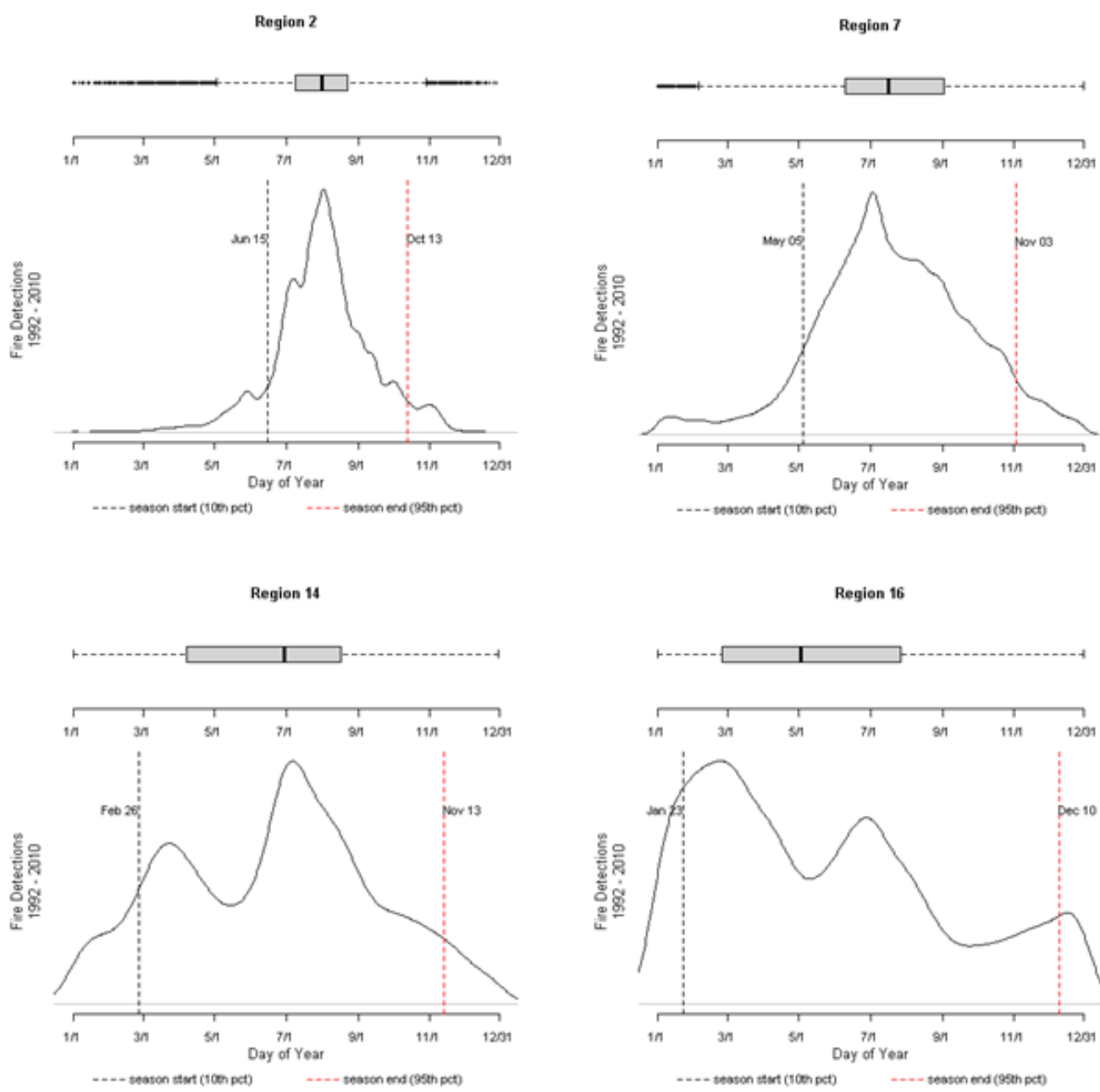


Figure C.1—Histograms of fire detection dates for all fires in the Fire Program Analysis fire occurrence database from 1992 through 2010 for four regions in the western study area. These illustrate the 4 broad fire season distributions seen across the 17 western mapping regions. Season start and end dates are shown with dashed vertical lines.

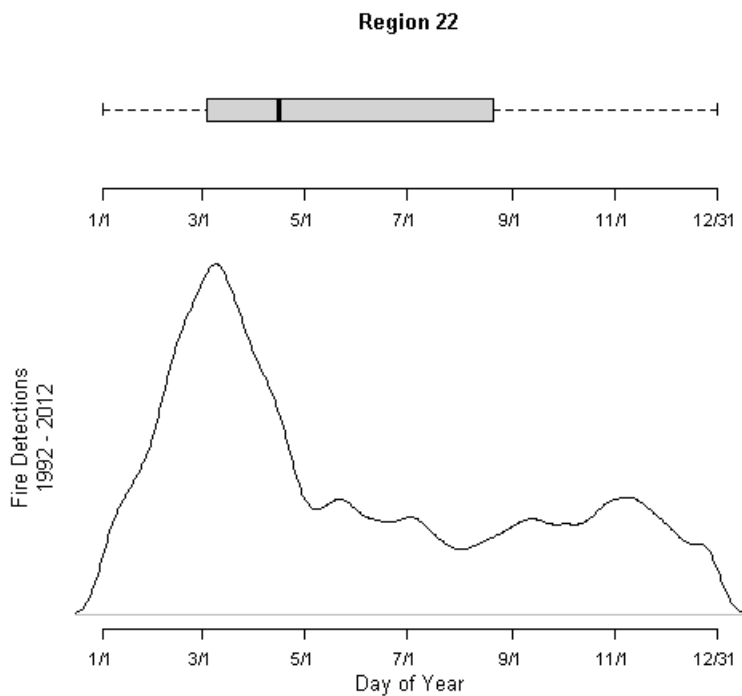


Figure C.2—Histogram of fire detection dates for all fires in the Fire Program Analysis fire occurrence database from 1992 through 2012 for one example region in the eastern study area. All regions in the eastern study area had a multimodal distribution with a peak in the spring and another in the fall. Although the heights and timing of those peaks varied among regions, we decided to consider the entire year as the fire season for eastern mapping regions.

References

Short, K.C. 2014. A spatial database of wildfires in the United States, 1992–2011. *Earth System Science Data*. 6(1): 1–27. doi: 10.5194/essd-6-1-2014.

Short, Karen C. 2013. Spatial wildfire occurrence data for the United States, 1992–2011 [FPA_FOD_20130422]. 1st ed. Fort Collins, CO: U.S. Department of Agriculture, Forest Service, Rocky Mountain Research Station. doi: 10.2737/RDS-2013-0009.

Appendix D: Landsat and MODIS NDVI Normalization—Western Study Area

Despite being conceptually similar, the normalized difference vegetation index (NDVI) calculated from Landsat imagery and NDVI calculated from Moderate-Resolution Imaging Spectroradiometer (MODIS) imagery have some important differences. Because we used Landsat as our source for prefire NDVI in the western study area but used MODIS NDVI to represent current conditions (2011) for predictions, some adjustment of the data was necessary to bring them into alignment. During the model development phase, we first ran a filter (9×9 cell average) over the Landsat NDVI in anticipation of using coarser resolution MODIS data for spatial prediction. This helped to smooth out 30-meter (approximately 98 feet) pixelation in the Landsat data and spread values out to the approximately 250-meter (approximately 820 feet) resolution of MODIS pixels. In preparing to do spatial predictions, however, we realized that further adjustments to both the spatial resolution and the statistical distribution of values in the MODIS NDVI data would be necessary. In this appendix, we outline the process used to do these adjustments, and the results from the statistical analyses involved.

To make the pixel size of the MODIS data match the Landsat data, we resampled the MODIS data from their native 250-meter resolution down to 30-meter resolution. We did this using the resample command in ArcGIS Workstation, with bilinear interpolation. In each mapping region in the western study area, we resampled the monthly NDVI mosaics needed for prediction in that region (table D.1). By setting the spatial extent in each case to the tile-based mapping footprint for the region, the output of this process was a set of 30-meter resolution NDVI rasters for each region, covering the full mapping footprint of the region.

As with our Random Forest modeling, we needed to select a sample of pixels from NDVI rasters for analyzing the statistical distributions. Within each mapping region, we drew a 1-percent spatially balanced random sample of pixels that were never classified as high severity in our MTBS dataset. We used the Create Spatially Balanced Points tool in ArcGIS to do this (Theobald et al. 2007).

At each pixel in our 1-percent sample, we extracted the value of the prefire Landsat NDVI and the 2011 monthly MODIS NDVI for each month needed for predictions in each region. We also extracted the classified (four-class) relative differenced normalized burn ratio (RdNBR) burn severity value for each fire. We compiled extracted values into data tables ready for statistical analysis.

Because the Landsat NDVI data were used in our Random Forest model development, we used those as our base values and adjusted MODIS NDVI values to match the Landsat NDVI distribution. Therefore, we developed regression models with Landsat NDVI as the response and MODIS NDVI as the predictor. We selected out just samples where the classified burn severity indicated no change so our models would be comparing relatively undisturbed pixels both before fire and in 2011. We fit two types of regression models, a simple ordinary least squares (OLS) regression and a major axis (MA) regression (Legendre 2013). Major axis regression has advantages over OLS for image normalization in remote sensing (Goslee 2011). In each mapping region, we fit regressions for each month separately and for all months combined.

The MA regression methods require certain assumptions about the distribution of the data to be met, particularly that they have roughly a bivariate normal distribution. In some mapping regions this assumption was not met and we felt we needed an alternate method for matching the MODIS NDVI distribution to the Landsat NDVI distribution. Therefore, we also performed histogram matching on the monthly and overall data for each region. Histogram matching forces the distribution of values from one image to match another and is commonly used in image processing (Goslee 2011). In performing histogram matching, we used all pixels available in the prefire NDVI images except those that recorded high burn severity.

In the final step, we used the MA regression and histogram matching models to create adjusted versions of the MODIS NDVI rasters. In all cases, we chose to use the models that combined data across the months within each region because they had better model fit. The adjusted outputs had statistical distributions that much more closely fit the distribution of values found in corresponding Landsat prefire NDVI images. In 14 of 17 regions the correlation coefficient (R) between Landsat and MODIS NDVI values was greater than 0.8, leading to relatively good fit in the regressions ($R^2 > 0.7$) (fig. D.1, table D.1). The three regions in the Great Plains (13, 14, and 17), however, had much lower correlation and poorer regression model fit ($R^2 < 0.4$) (fig. D.1, table D.1). In every region, we compared basic descriptive statistics such as mean, median, inner quartile range, minimum, and maximum values for the original MODIS NDVI values, Landsat NDVI, OLS-adjusted MODIS NDVI, MA-adjusted MODIS NDVI, and histogram-matching-adjusted MODIS NDVI (figs. D.2–D.18). In every case, the MODIS values adjusted with histogram matching were closest to the Landsat NDVI values. Therefore, we ultimately decided to use the histogram-matching-adjusted MODIS NDVI for severe fire potential predictions in every western mapping region.

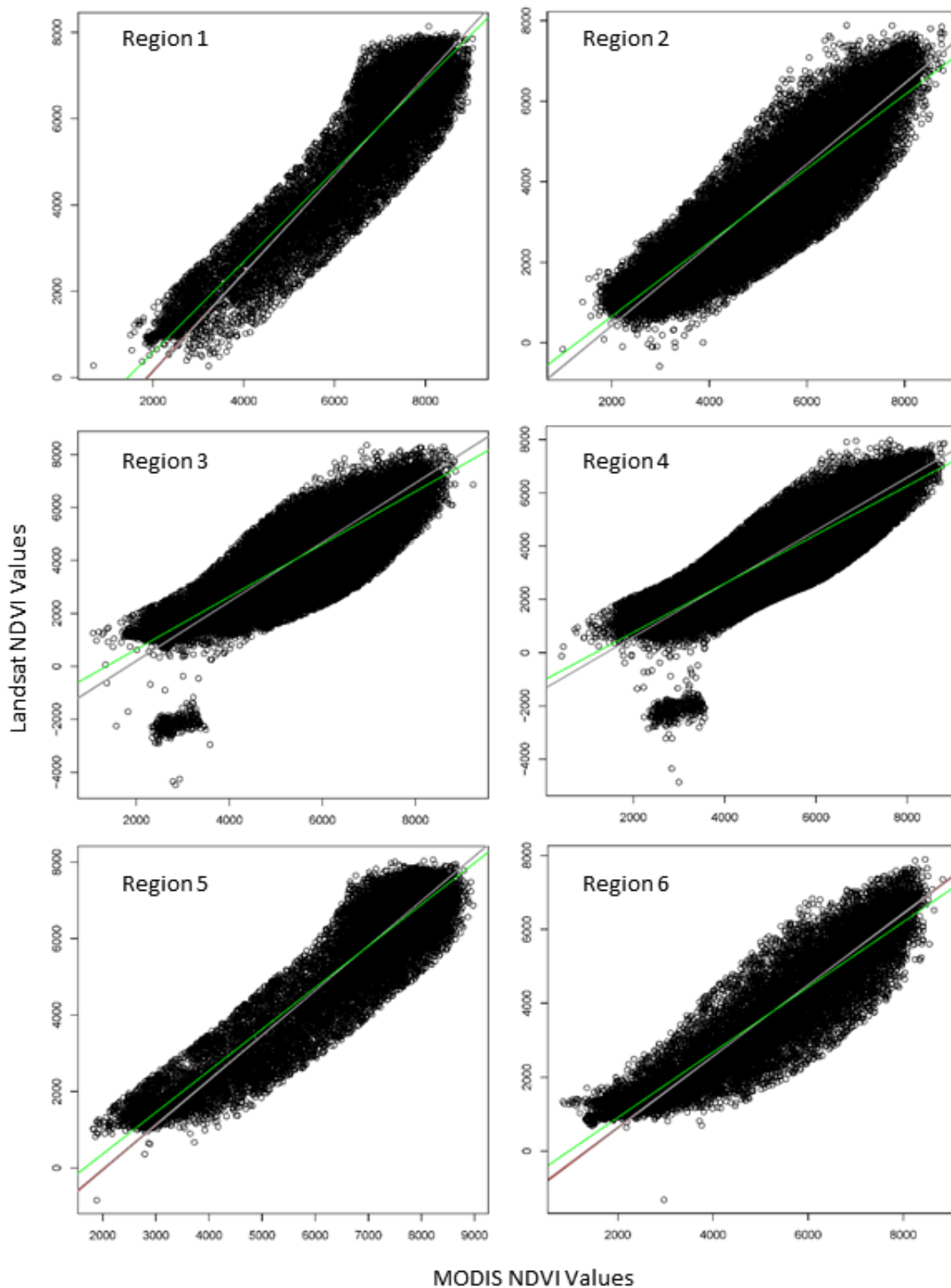


Figure D.1 Regions 1-6—Scatter plots of 2011 MODIS normalized difference vegetation index (NDVI) values (x-axis) and prefire Landsat NDVI values (y-axis) at sample pixel locations for each region. Green lines show the ordinary least squares (OLS) regression fit and red lines show the major axis (MA) regression fit. A 95% confidence interval for the MA regression is shown as gray lines. In many cases the confidence interval is so tight that the red line is not visible.

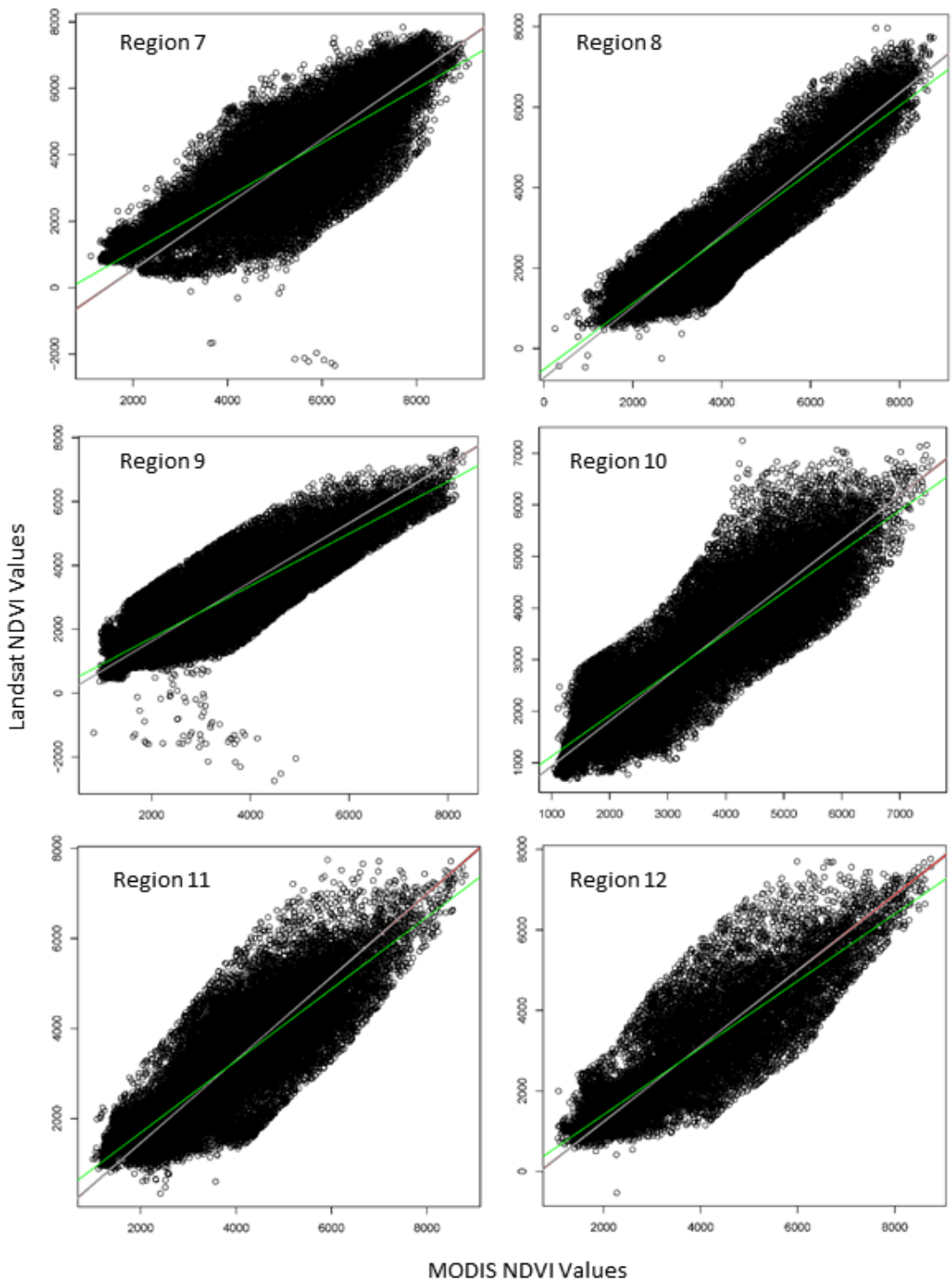


Figure D.1 Regions 7-12—Scatter plots of 2011 MODIS normalized difference vegetation index (NDVI) values (x-axis) and prefire Landsat NDVI values (y-axis) at sample pixel locations for each region. Green lines show the ordinary least squares (OLS) regression fit and red lines show the major axis (MA) regression fit. A 95% confidence interval for the MA regression is shown as gray lines. In many cases the confidence interval is so tight that the red line is not visible.

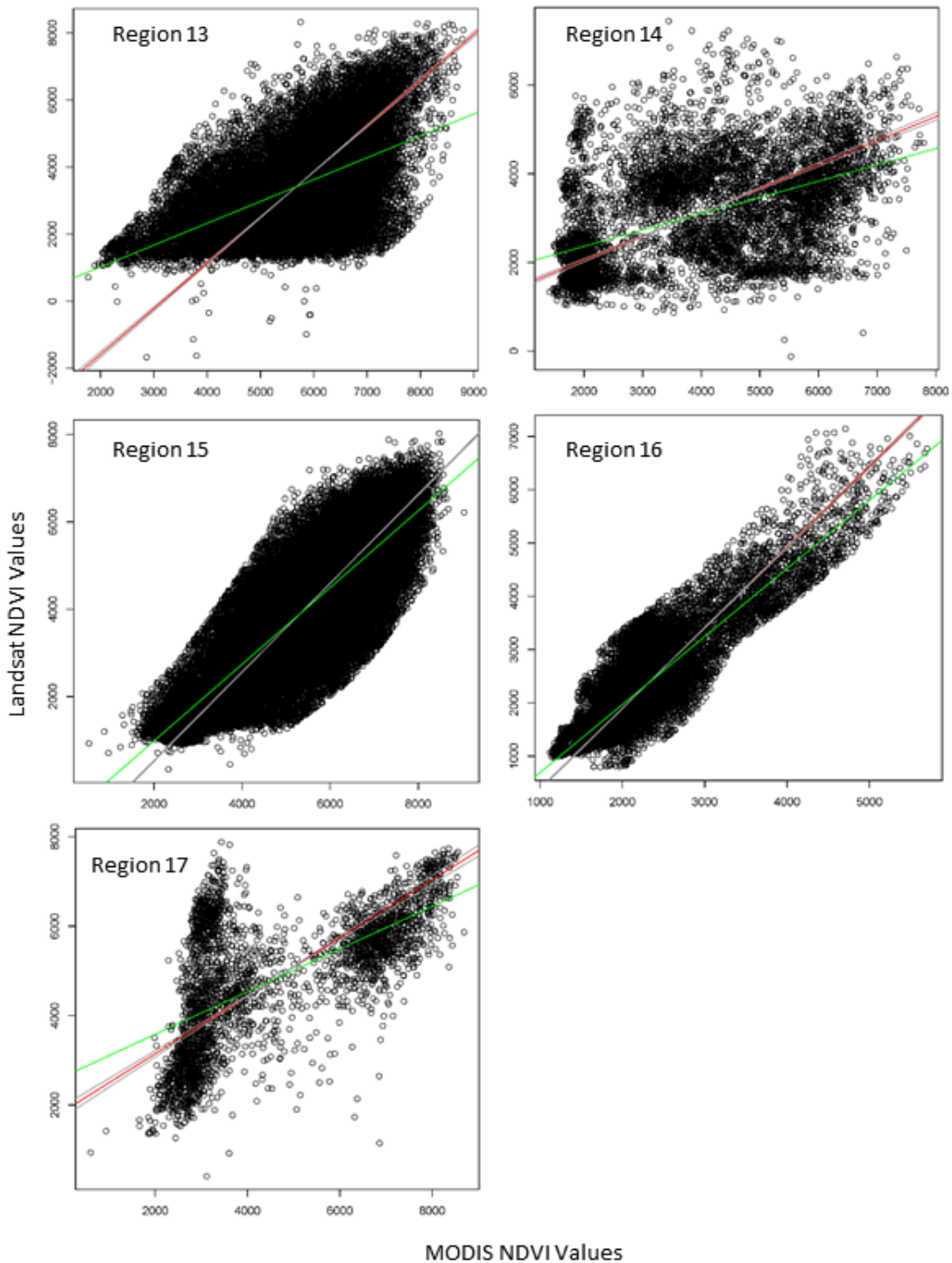


Figure D.1 Regions 13-18—Scatter plots of 2011 MODIS normalized difference vegetation index (NDVI) values (x-axis) and prefire Landsat NDVI values (y-axis) at sample pixel locations for each region. Green lines show the ordinary least squares (OLS) regression fit and red lines show the major axis (MA) regression fit. A 95% confidence interval for the MA regression is shown as gray lines. In many cases the confidence interval is so tight that the red line is not visible.

Table D.1—Results of regression analyses between prefire Landsat normalized differenced vegetation index (NDVI) and current (2011) MODIS NDVI rasters for the western mapping regions. Months for each region are the months of MODIS NDVI used for predicting severe fire potential based on the most common fire occurrence dates in 1-degree mapping tiles within the region. Sample size (n) is the number of pixels sampled for generating regression models. Correlation coefficient (r) reflects the general correlation between prefire Landsat NDVI and 2011 MODIS NDVI across all sample pixels, and the coefficient of determination (OLS r^2) from the ordinary least squares regression indicates regression model fit.

Region	Months	n	r	OLS r^2
1	June, July, August	26,824	0.868	0.932
2	July	46,745	0.837	0.915
3	July, August	68,134	0.805	0.897
4	June, July, August	125,296	0.843	0.918
5	June, July, August	25,727	0.879	0.937
6	June, July	16,077	0.829	0.910
7	June, July, August	45,587	0.688	0.830
8	June, July, August	58,950	0.839	0.916
9	March, April, May, June, July	62,144	0.765	0.874
10	April, May, June, July	45,703	0.801	0.895
11	April, May, June, July	39,061	0.732	0.856
12	April, May, June, July, August	20,387	0.770	0.878
13	April, May, June, July, August	29,696	0.301	0.548
14	March, April, May, June, July	7,990	0.261	0.511
15	June, July, August	63,896	0.750	0.866
16	March, April, May, June	16,614	0.781	0.884
17	March, April, May, June	3,278	0.397	0.630

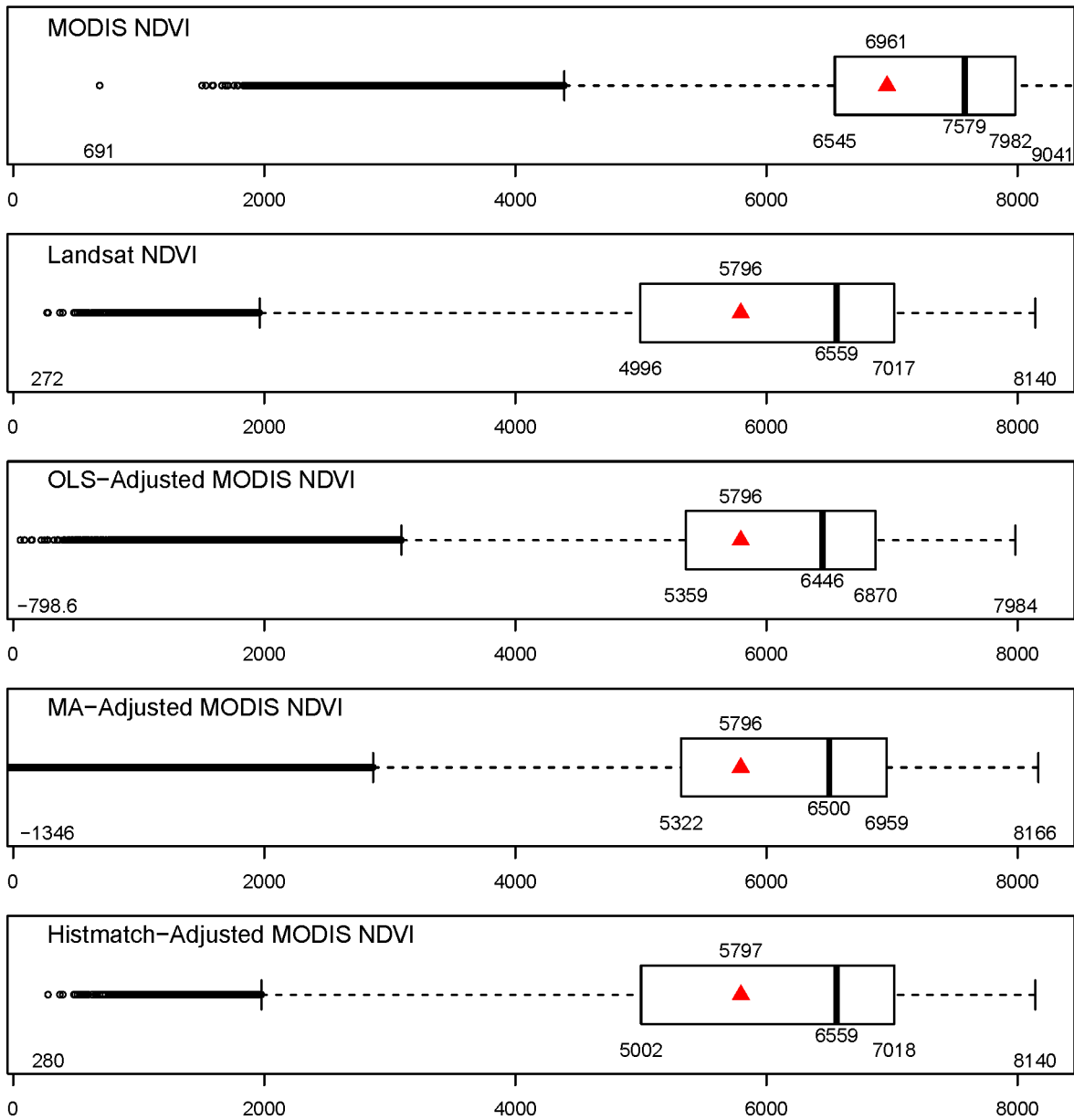


Figure D.2—Comparison of the distribution of values in the original 2011 MODIS normalized difference vegetation index (NDVI), prefire Landsat NDVI, and three versions of adjusted MODIS NDVI rasters for region 1. The adjusted MODIS rasters were created using ordinary least squares (OLS) regression, major axis (MA) regression, and histogram matching (histmatch) methods. In each boxplot, the box represents the inner quartile range (25th–75th percentiles), the solid vertical bar is the median, and the red triangle is the mean.

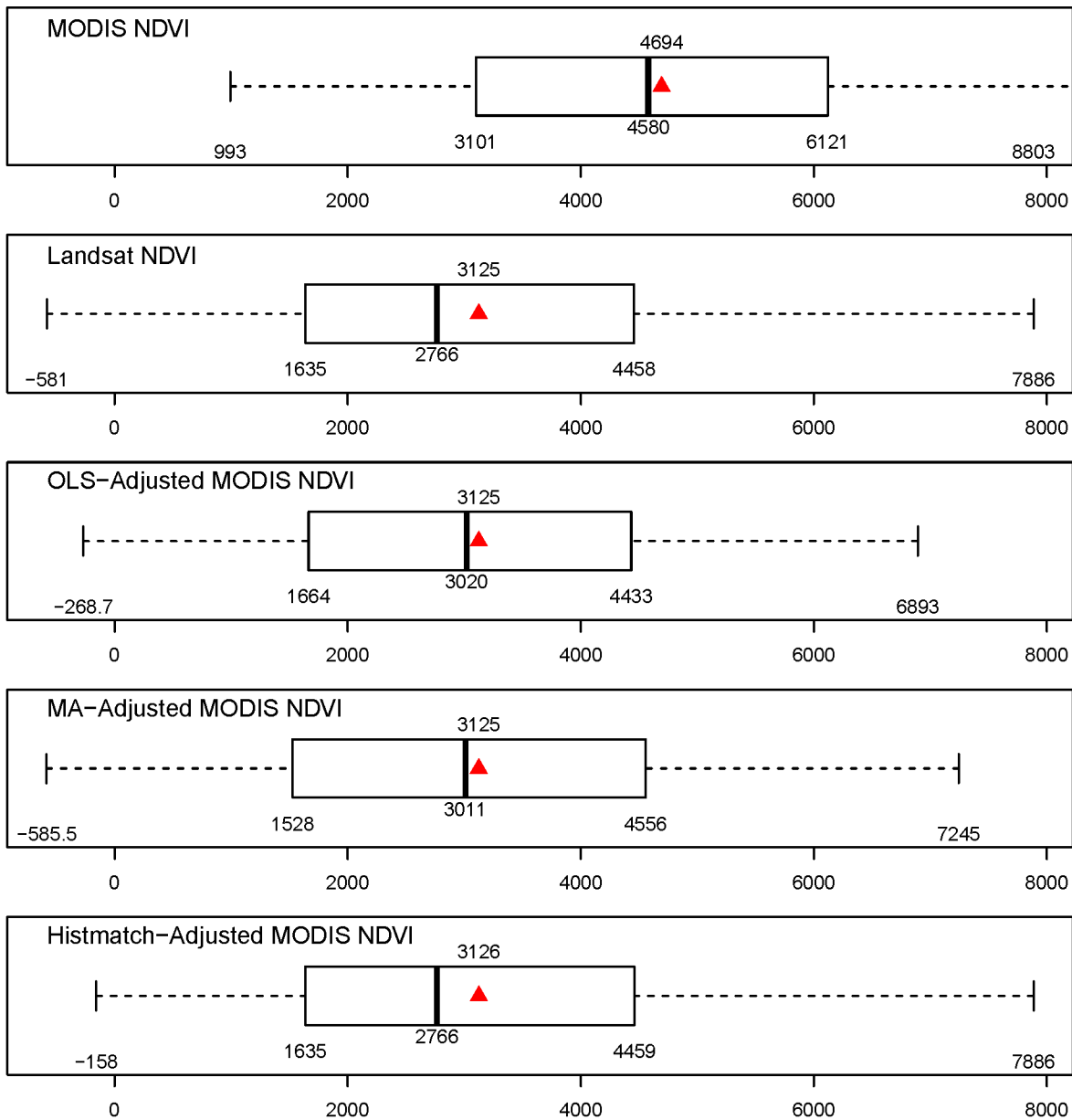


Figure D.3—Comparison of the distribution of values in the original 2011 MODIS normalized difference vegetation index (NDVI), prefire Landsat NDVI, and three versions of adjusted MODIS NDVI rasters for region 2. The adjusted MODIS rasters were created using ordinary least squares (OLS) regression, major axis (MA) regression, and histogram matching (histmatch) methods. In each boxplot, the box represents the inner quartile range (25th–75th percentiles), the solid vertical bar is the median, and the red triangle is the mean.

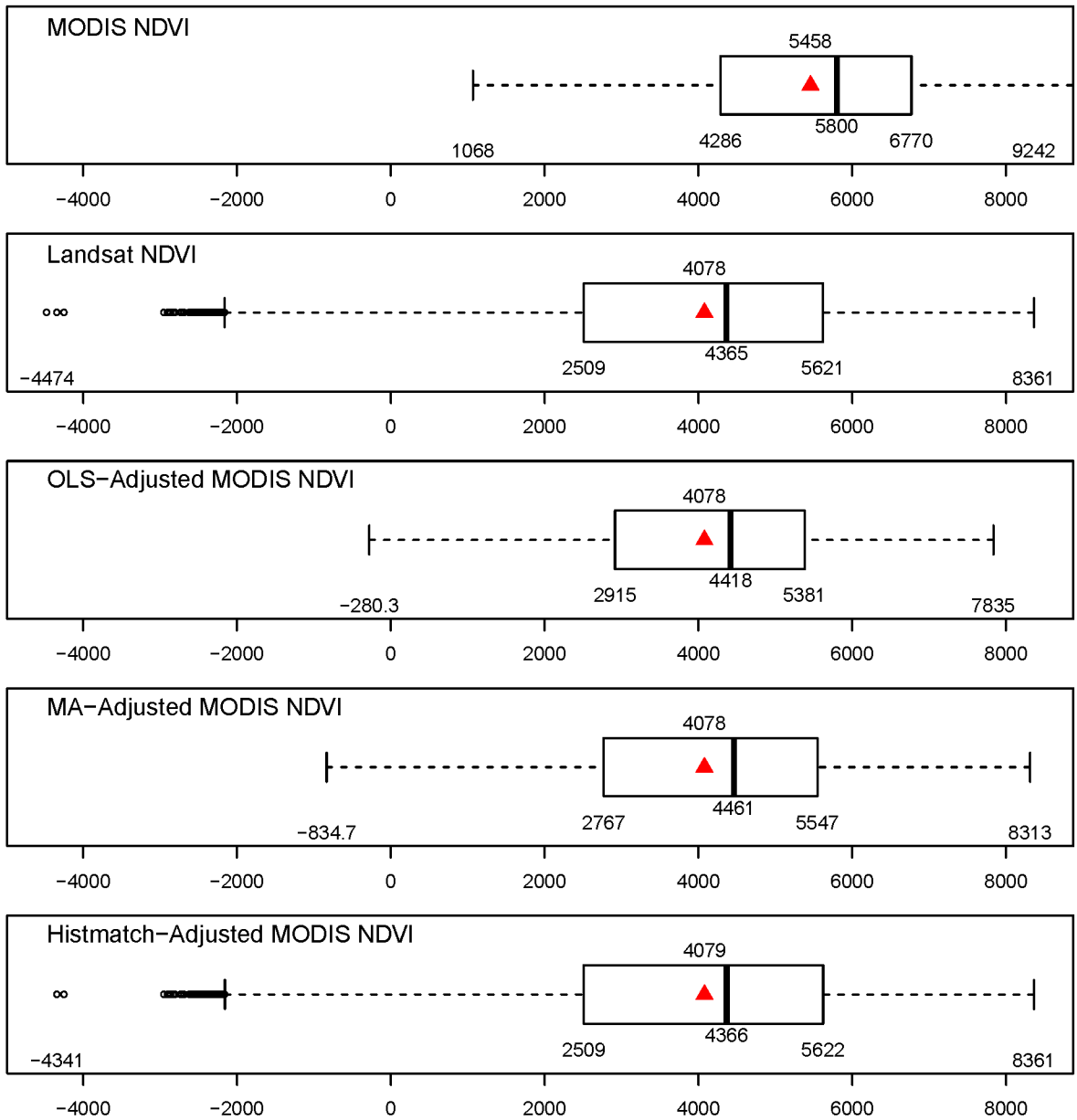


Figure D.4—Comparison of the distribution of values in the original 2011 MODIS normalized difference vegetation index (NDVI), prefire Landsat NDVI, and three versions of adjusted MODIS NDVI rasters for region 3. The adjusted MODIS rasters were created using ordinary least squares (OLS) regression, major axis (MA) regression, and histogram matching (histmatch) methods. In each boxplot, the box represents the inner quartile range (25th–75th percentiles), the solid vertical bar is the median, and the red triangle is the mean.

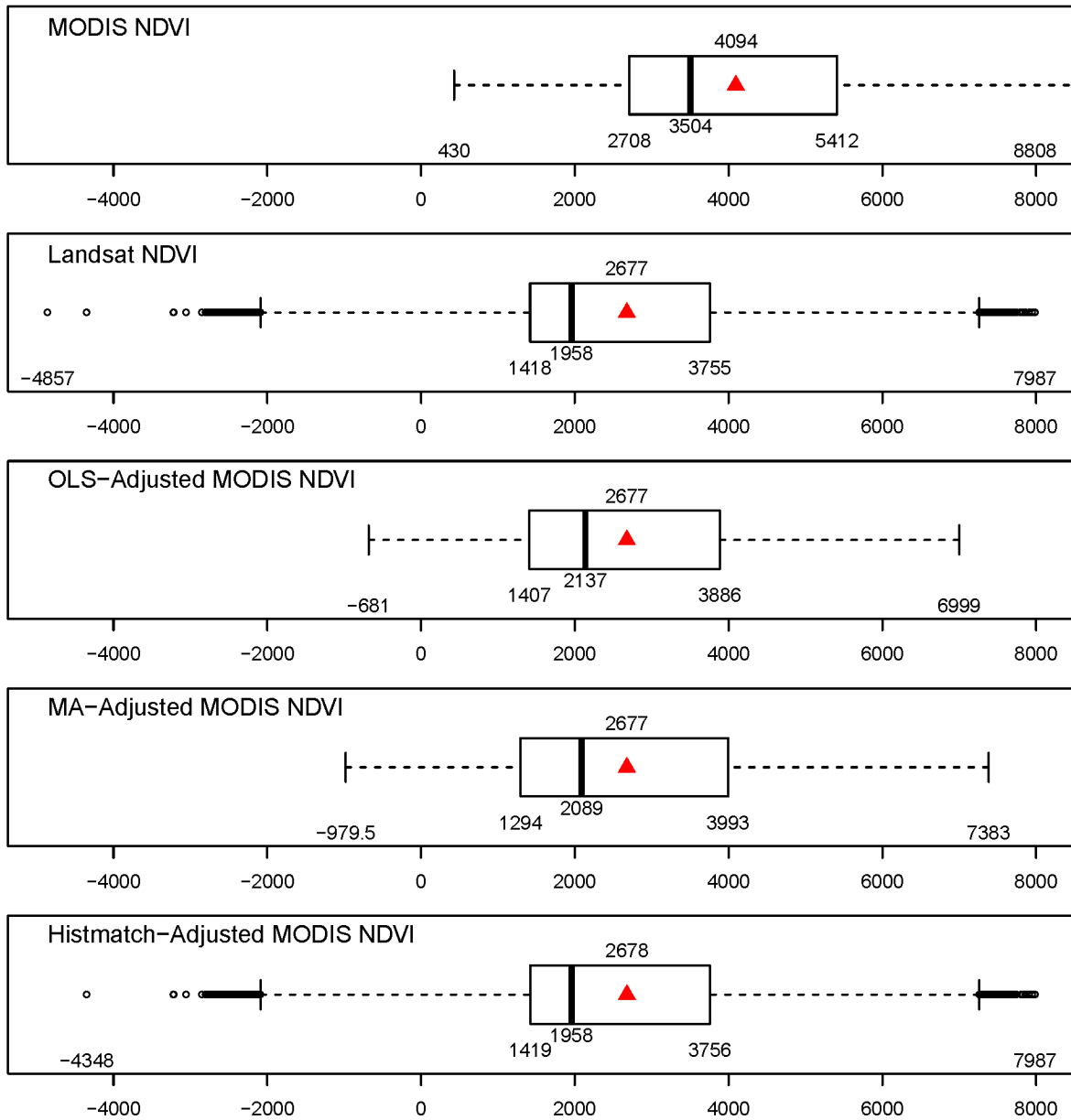


Figure D.5—Comparison of the distribution of values in the original 2011 MODIS normalized difference vegetation index (NDVI), prefire Landsat NDVI, and three versions of adjusted MODIS NDVI rasters for region 4. The adjusted MODIS rasters were created using ordinary least squares (OLS) regression, major axis (MA) regression, and histogram matching (histmatch) methods. In each boxplot, the box represents the inner quartile range (25th–75th percentiles), the solid vertical bar is the median, and the red triangle is the mean.

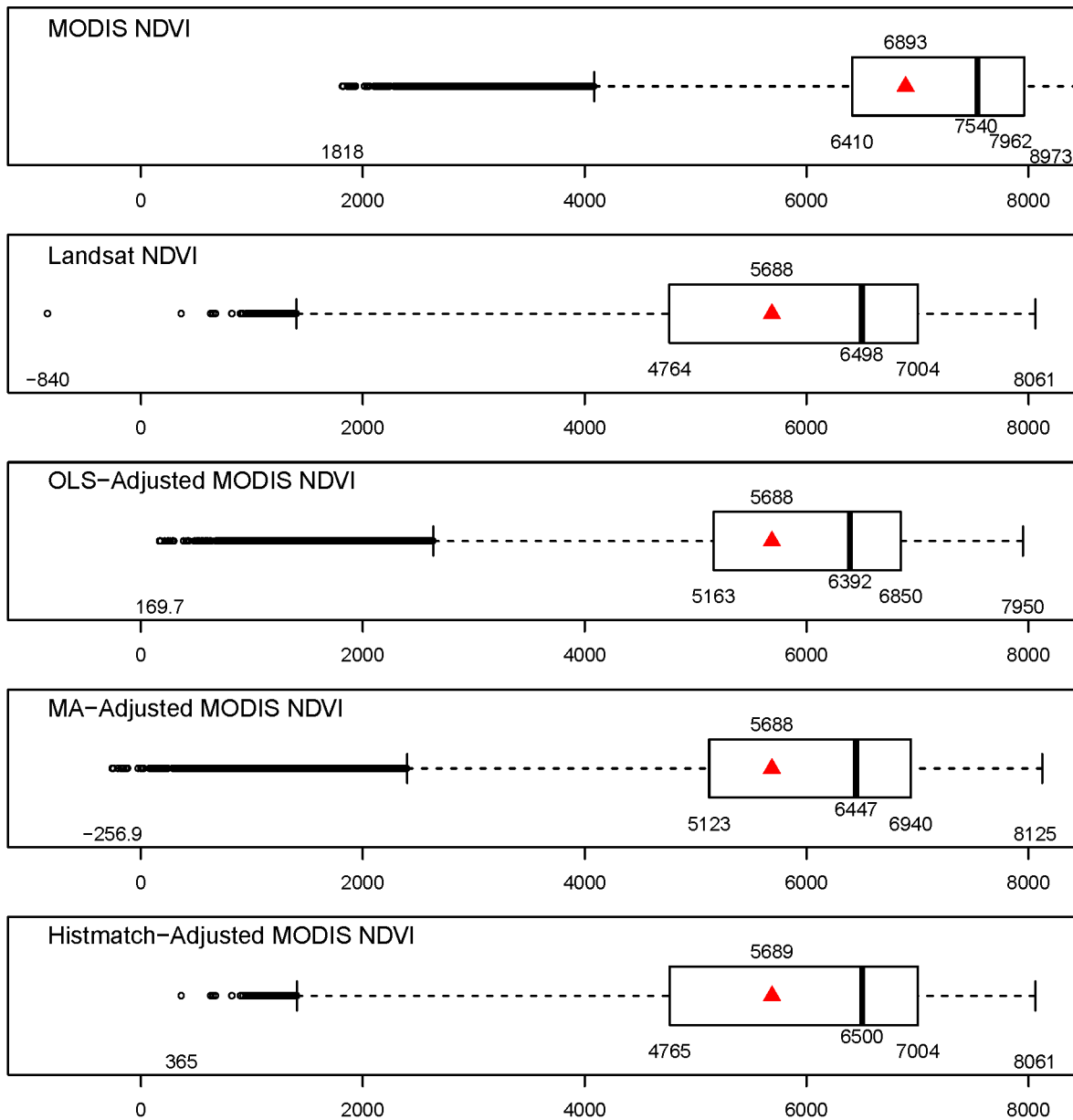


Figure D.6—Comparison of the distribution of values in the original 2011 MODIS normalized difference vegetation index (NDVI), prefire Landsat NDVI, and three versions of adjusted MODIS NDVI rasters for region 5. The adjusted MODIS rasters were created using ordinary least squares (OLS) regression, major axis (MA) regression, and histogram matching (histatch) methods. In each boxplot, the box represents the inner quartile range (25th–75th percentiles), the solid vertical bar is the median, and the red triangle is the mean.

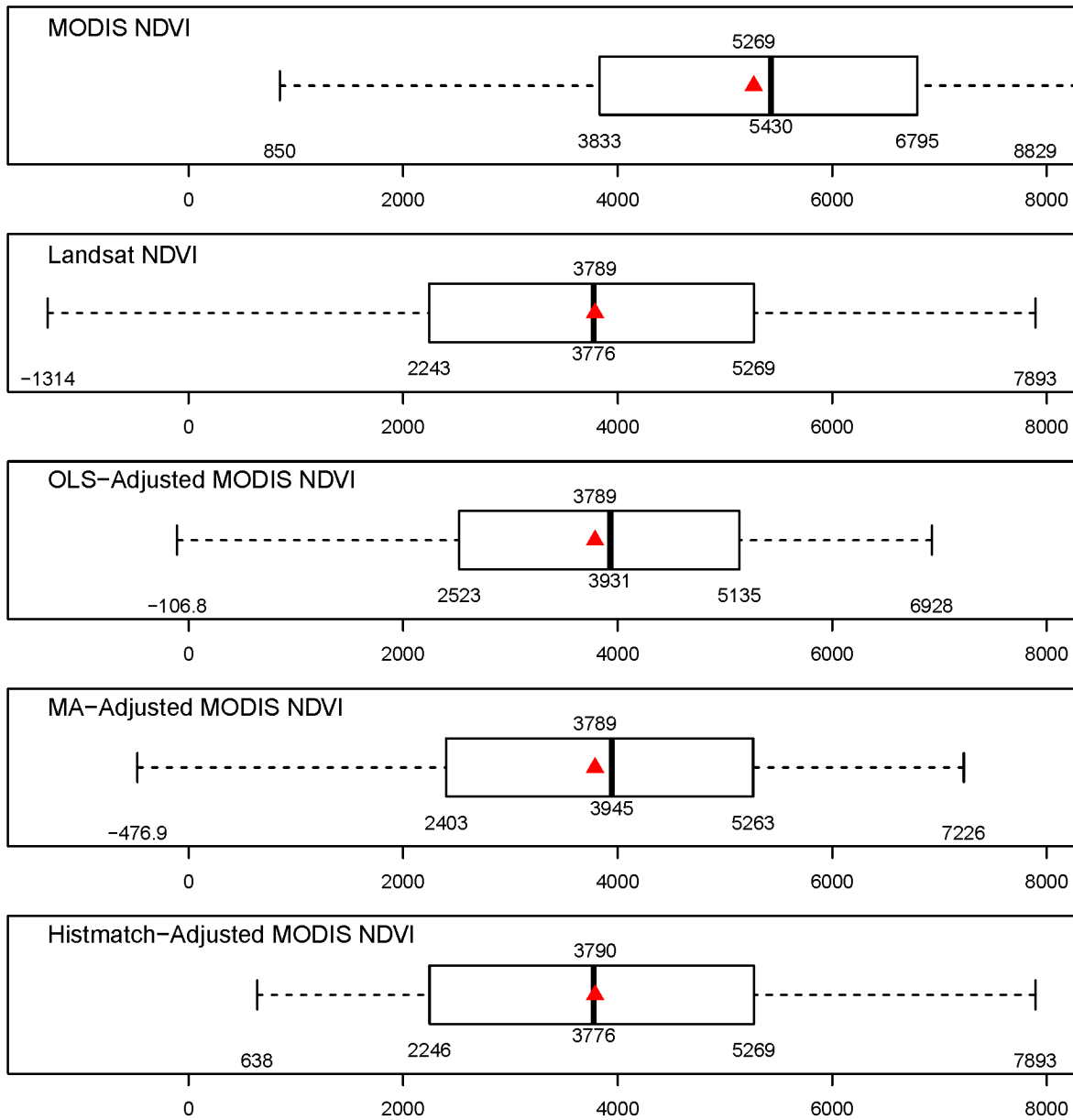


Figure D.7—Comparison of the distribution of values in the original 2011 MODIS normalized difference vegetation index (NDVI), prefire Landsat NDVI, and three versions of adjusted MODIS NDVI rasters for region 6. The adjusted MODIS rasters were created using ordinary least squares (OLS) regression, major axis (MA) regression, and histogram matching (histmatch) methods. In each boxplot, the box represents the inner quartile range (25th–75th percentiles), the solid vertical bar is the median, and the red triangle is the mean.

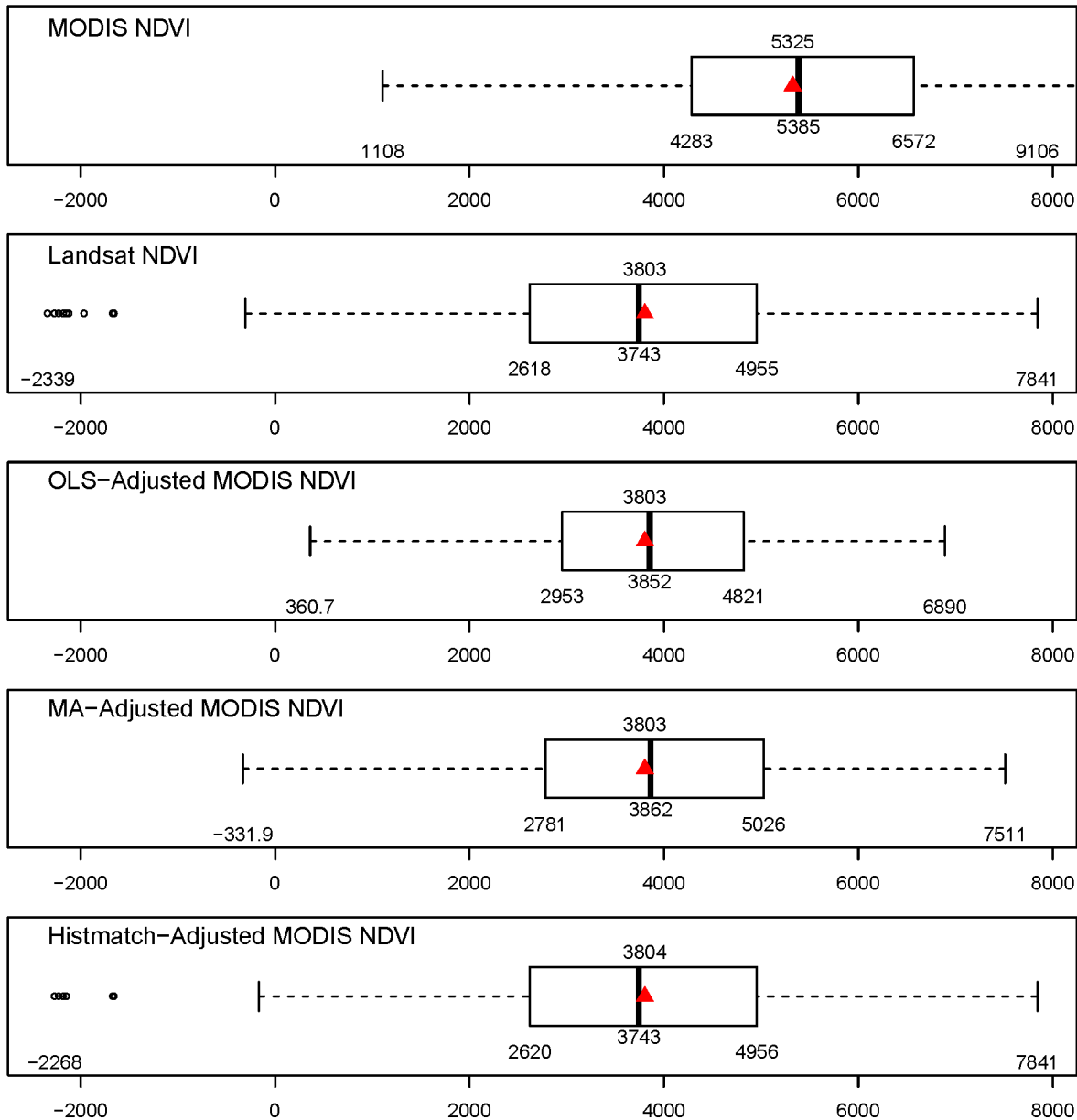


Figure D.8—Comparison of the distribution of values in the original 2011 MODIS normalized difference vegetation index (NDVI), prefire Landsat NDVI, and three versions of adjusted MODIS NDVI rasters for region 7. The adjusted MODIS rasters were created using ordinary least squares (OLS) regression, major axis (MA) regression, and histogram matching (histmatch) methods. In each boxplot, the box represents the inner quartile range (25th–75th percentiles), the solid vertical bar is the median, and the red triangle is the mean.

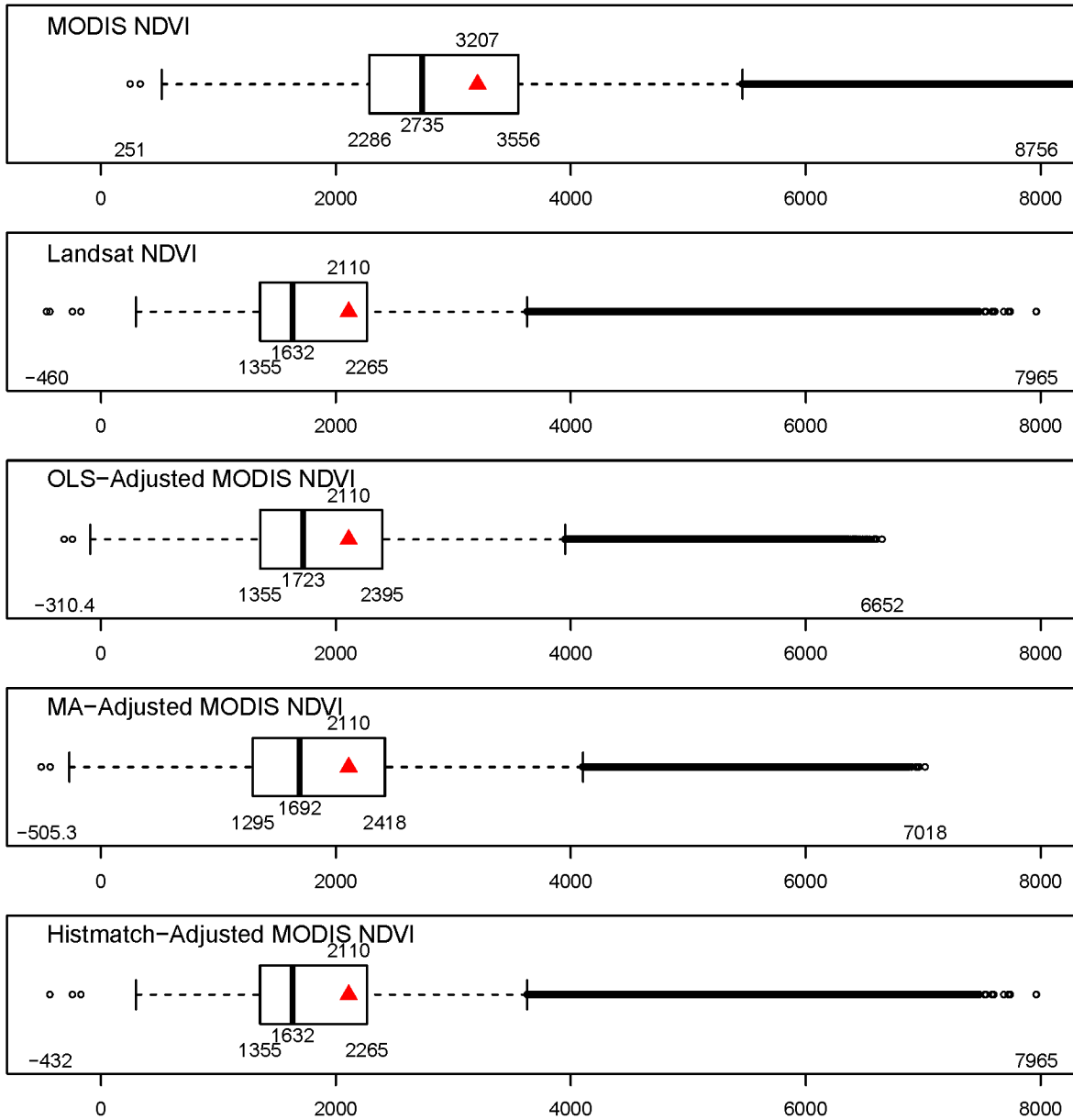


Figure D.9—Comparison of the distribution of values in the original 2011 MODIS normalized difference vegetation index (NDVI), prefire Landsat NDVI, and three versions of adjusted MODIS NDVI rasters for region 8. The adjusted MODIS rasters were created using ordinary least squares (OLS) regression, major axis (MA) regression, and histogram matching (histmatch) methods. In each boxplot, the box represents the inner quartile range (25th–75th percentiles), the solid vertical bar is the median, and the red triangle is the mean.

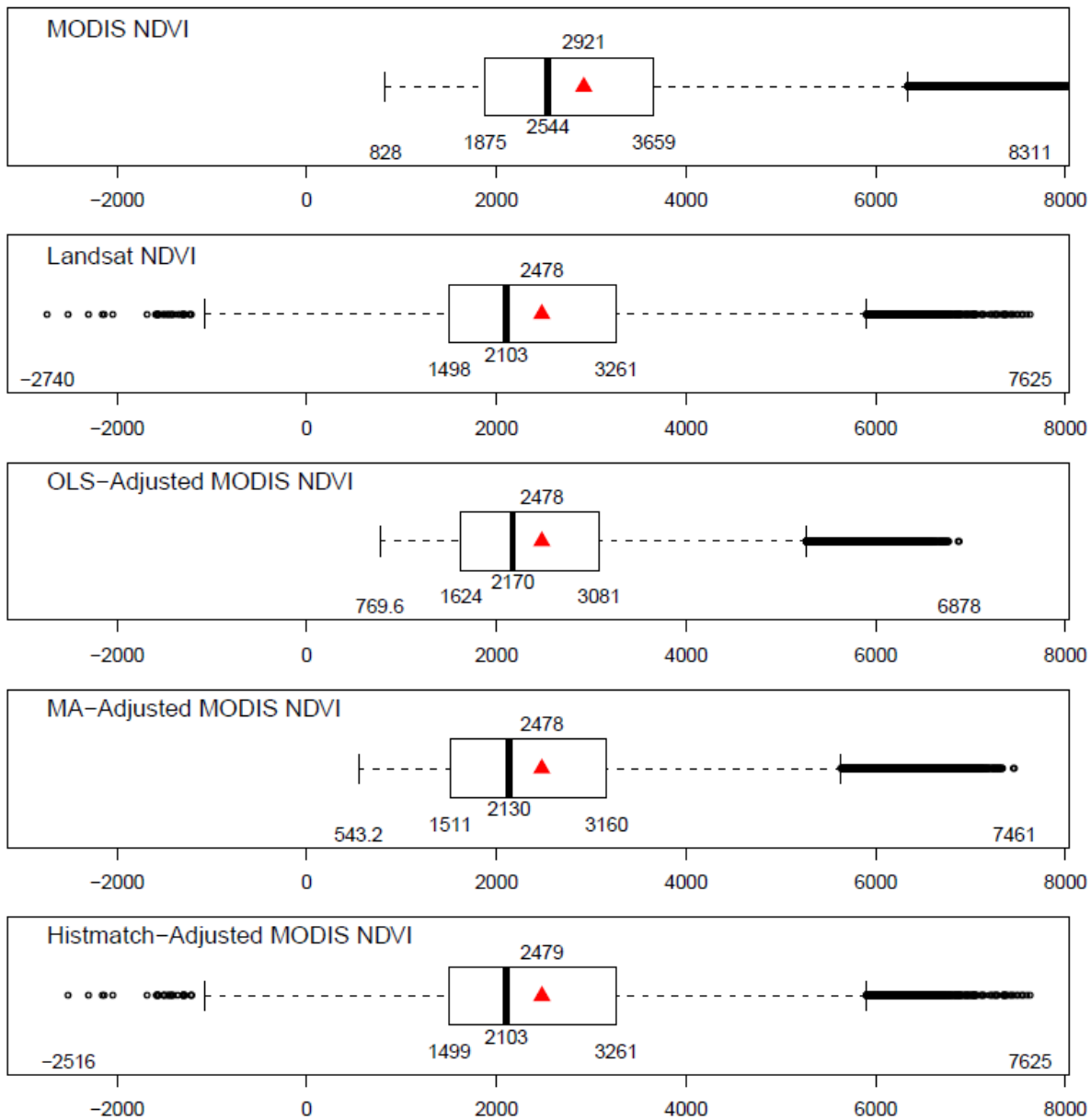


Figure D.10—Comparison of the distribution of values in the original 2011 MODIS normalized difference vegetation index (NDVI), prefire Landsat NDVI, and three versions of adjusted MODIS NDVI rasters for region 9. The adjusted MODIS rasters were created using ordinary least squares (OLS) regression, major axis (MA) regression, and histogram matching (histmatch) methods. In each boxplot, the box represents the inner quartile range (25th–75th percentiles), the solid vertical bar is the median, and the red triangle is the mean.

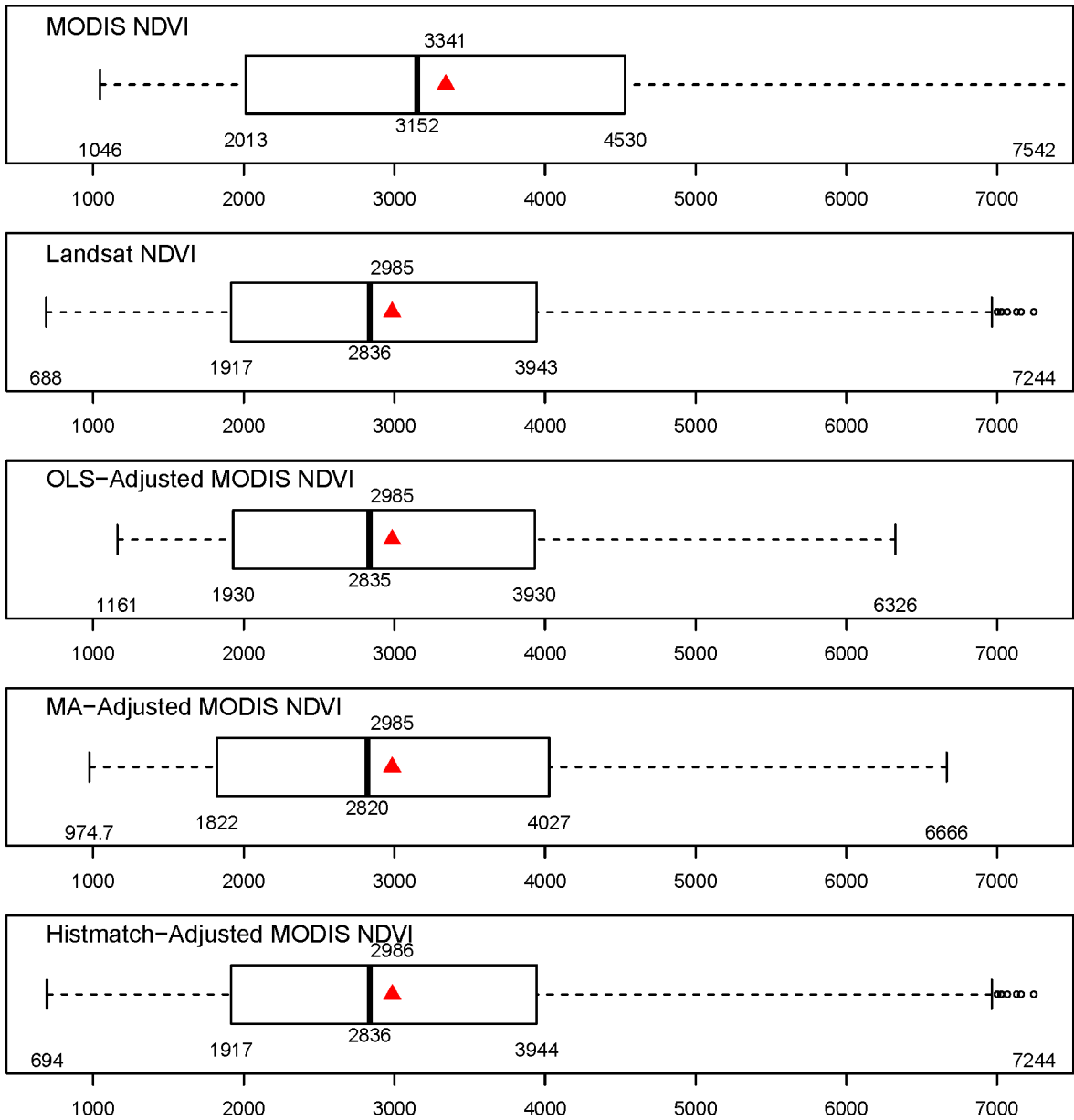


Figure D.11—Comparison of the distribution of values in the original 2011 MODIS normalized difference vegetation index (NDVI), prefire Landsat NDVI, and three versions of adjusted MODIS NDVI rasters for region 10. The adjusted MODIS rasters were created using ordinary least squares (OLS) regression, major axis (MA) regression, and histogram matching (histmatch) methods. In each boxplot, the box represents the inner quartile range (25th–75th percentiles), the solid vertical bar is the median, and the red triangle is the mean.

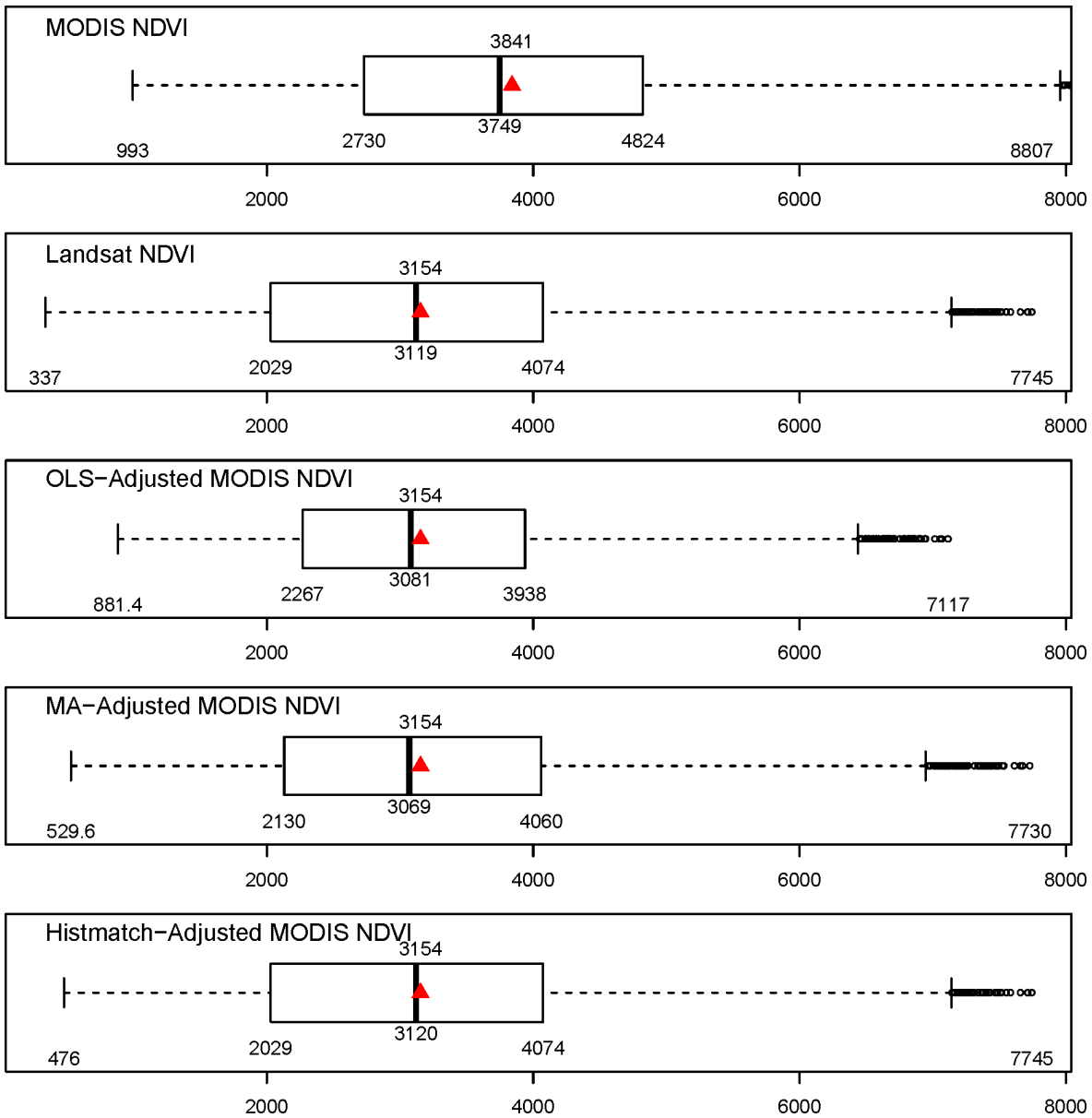


Figure D.12—Comparison of the distribution of values in the original 2011 MODIS normalized difference vegetation index (NDVI), prefire Landsat NDVI, and three versions of adjusted MODIS NDVI rasters for region 11. The adjusted MODIS rasters were created using ordinary least squares (OLS) regression, major axis (MA) regression, and histogram matching (histmatch) methods. In each boxplot, the box represents the inner quartile range (25th–75th percentiles), the solid vertical bar is the median, and the red triangle is the mean.

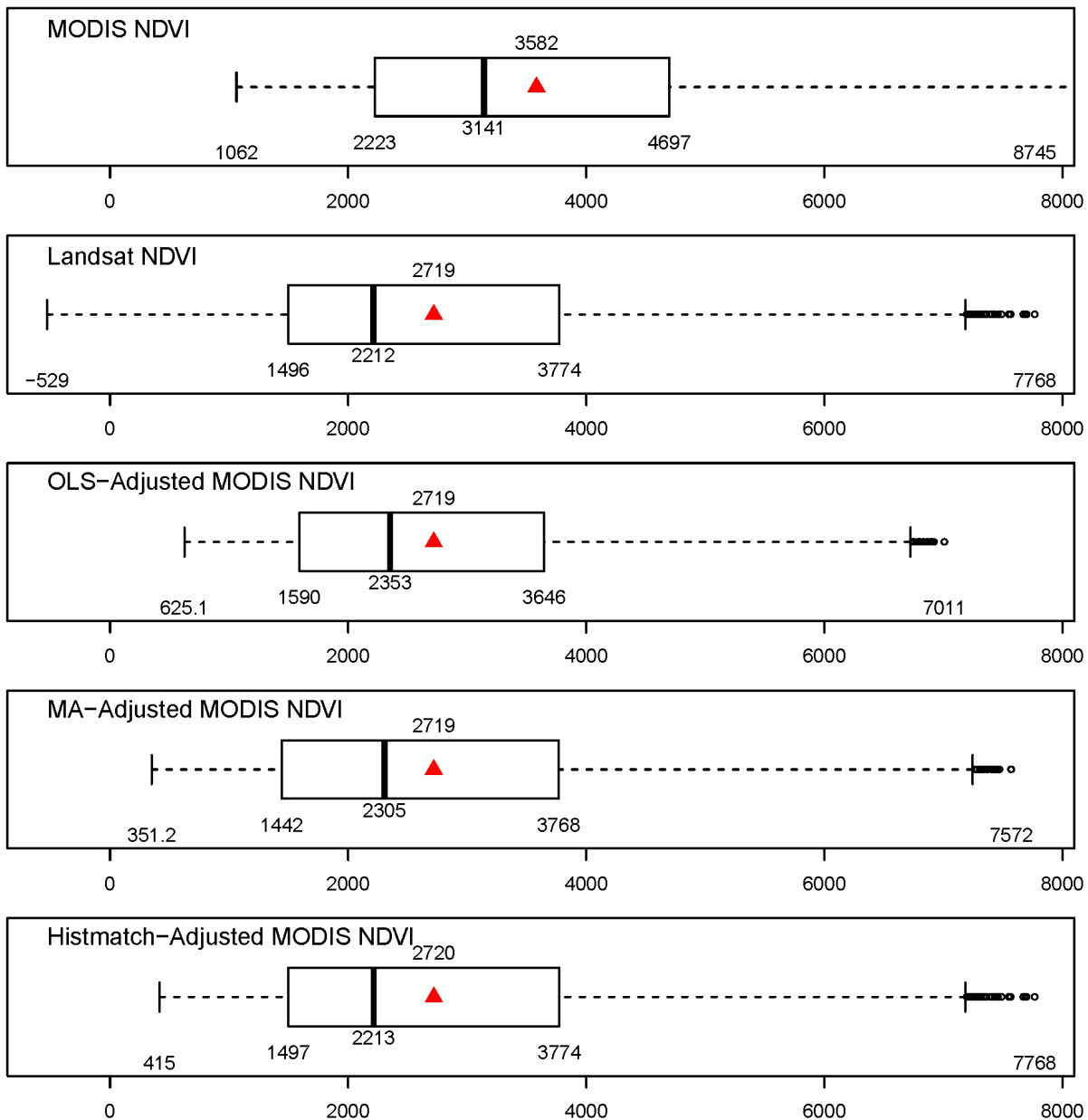


Figure D.13—Comparison of the distribution of values in the original 2011 MODIS normalized difference vegetation index (NDVI), prefire Landsat NDVI, and three versions of adjusted MODIS NDVI rasters for region 12. The adjusted MODIS rasters were created using ordinary least squares (OLS) regression, major axis (MA) regression, and histogram matching (histmatch) methods. In each boxplot, the box represents the inner quartile range (25th–75th percentiles), the solid vertical bar is the median, and the red triangle is the mean.

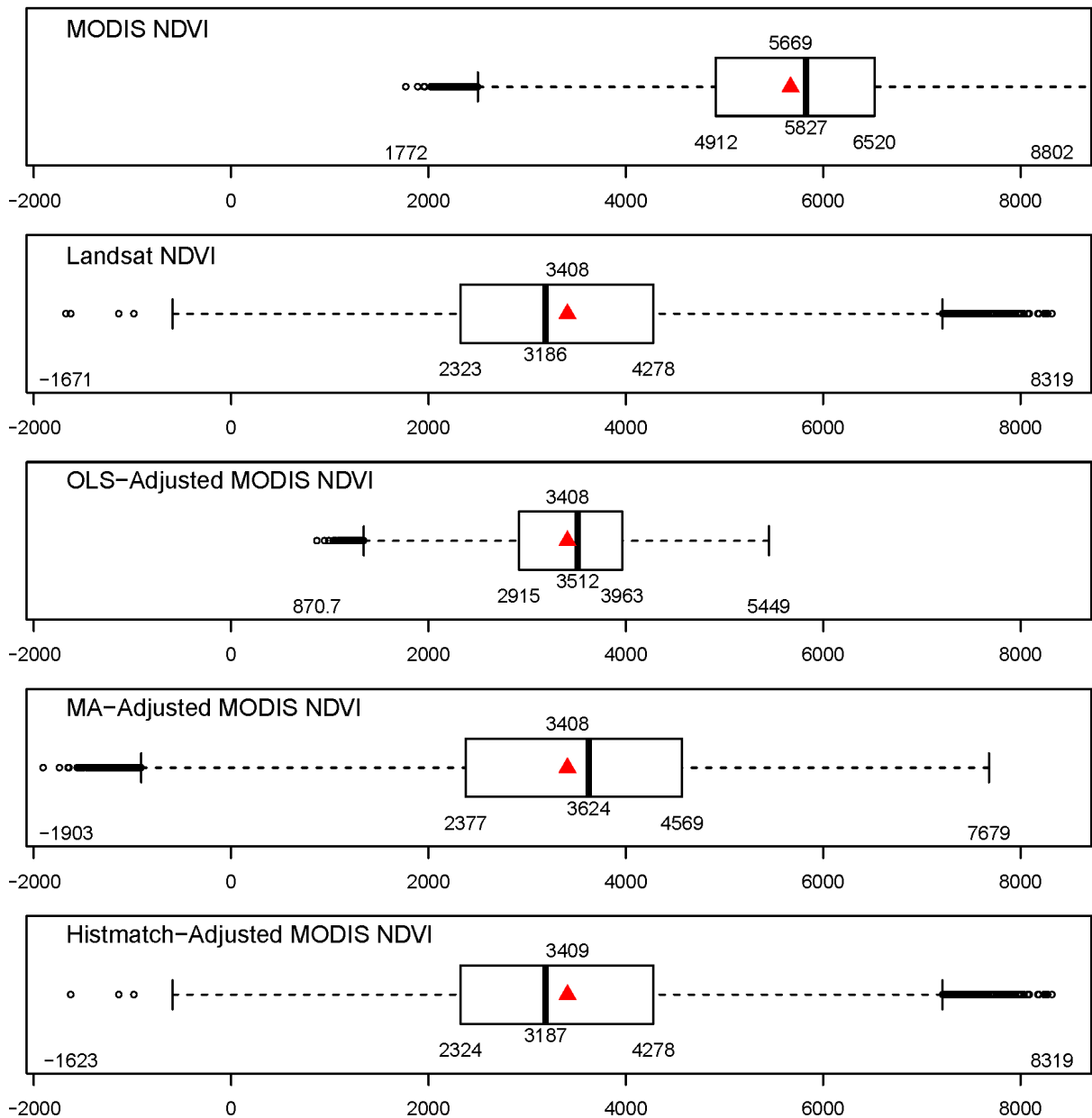


Figure D.14—Comparison of the distribution of values in the original 2011 MODIS normalized difference vegetation index (NDVI), prefire Landsat NDVI, and three versions of adjusted MODIS NDVI rasters for region 13. The adjusted MODIS rasters were created using ordinary least squares (OLS) regression, major axis (MA) regression, and histogram matching (histmatch) methods. In each boxplot, the box represents the inner quartile range (25th–75th percentiles), the solid vertical bar is the median, and the red triangle is the mean.

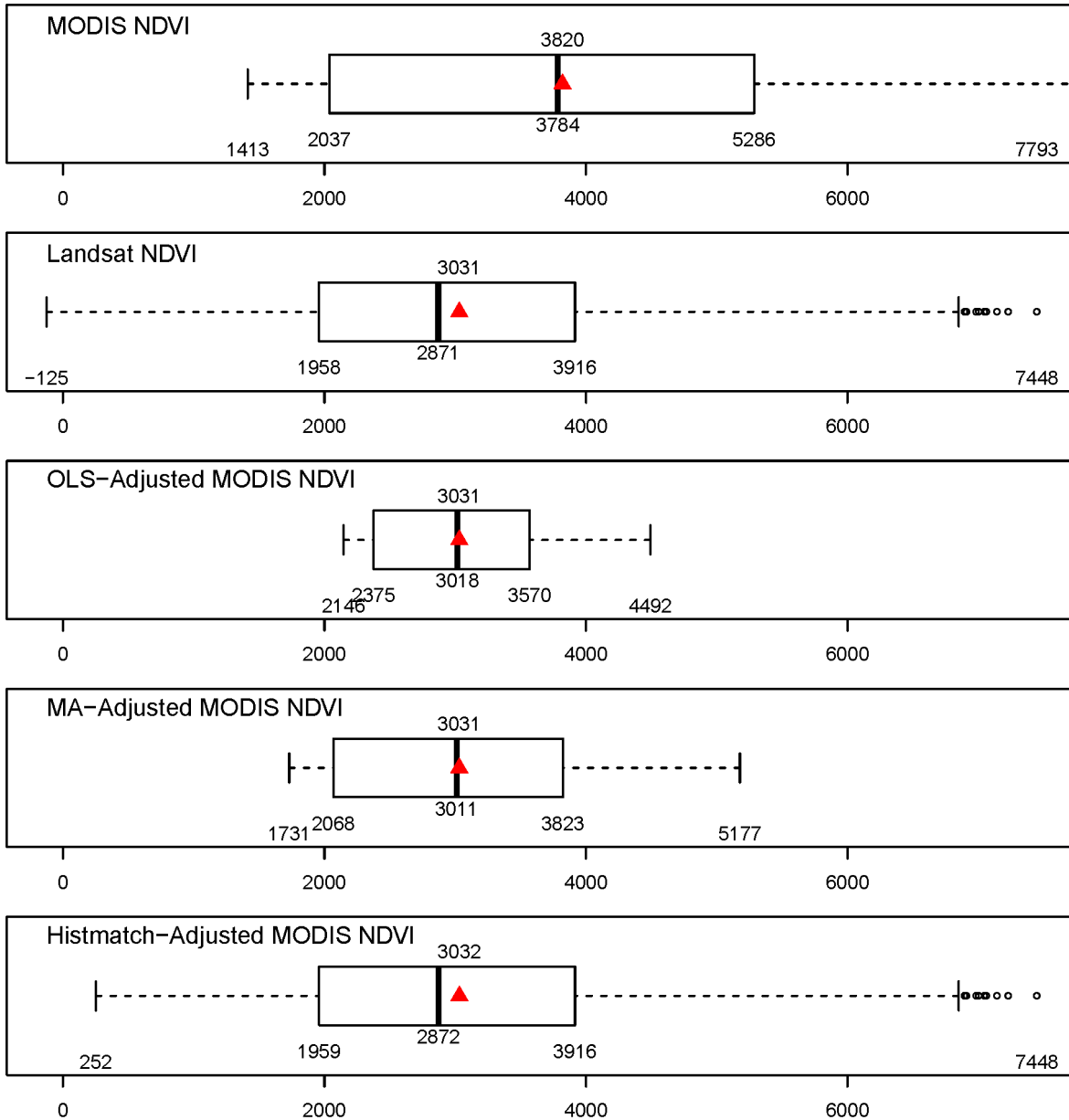


Figure D.15—Comparison of the distribution of values in the original 2011 MODIS normalized difference vegetation index (NDVI), prefire Landsat NDVI, and three versions of adjusted MODIS NDVI rasters for region 14. The adjusted MODIS rasters were created using ordinary least squares (OLS) regression, major axis (MA) regression, and histogram matching (histmatch) methods. In each boxplot, the box represents the inner quartile range (25th–75th percentiles), the solid vertical bar is the median, and the red triangle is the mean.

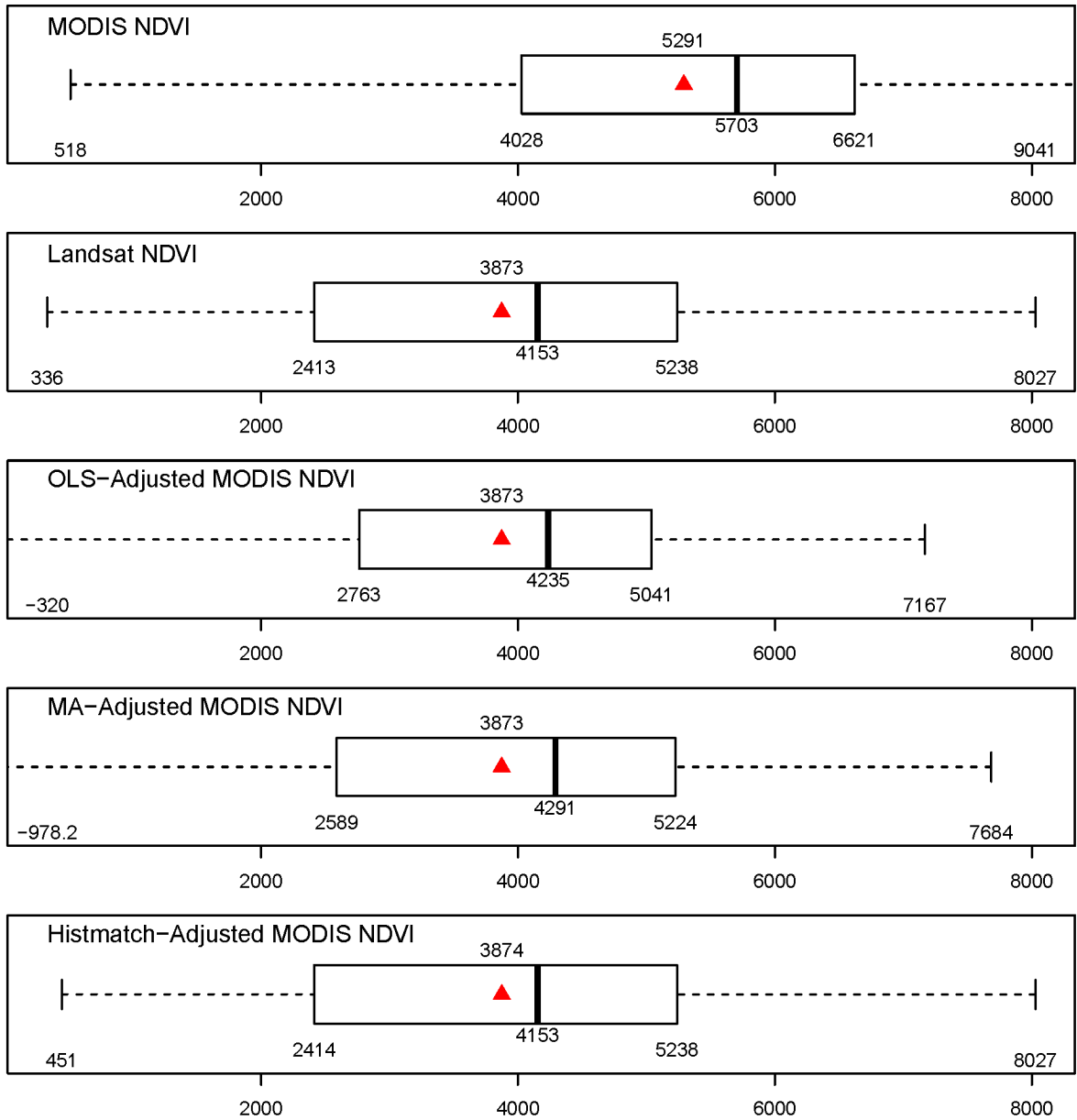


Figure D.16—Comparison of the distribution of values in the original 2011 MODIS normalized difference vegetation index (NDVI), prefire Landsat NDVI, and three versions of adjusted MODIS NDVI rasters for region 15. The adjusted MODIS rasters were created using ordinary least squares (OLS) regression, major axis (MA) regression, and histogram matching (histmatch) methods. In each boxplot, the box represents the inner quartile range (25th–75th percentiles), the solid vertical bar is the median, and the red triangle is the mean.

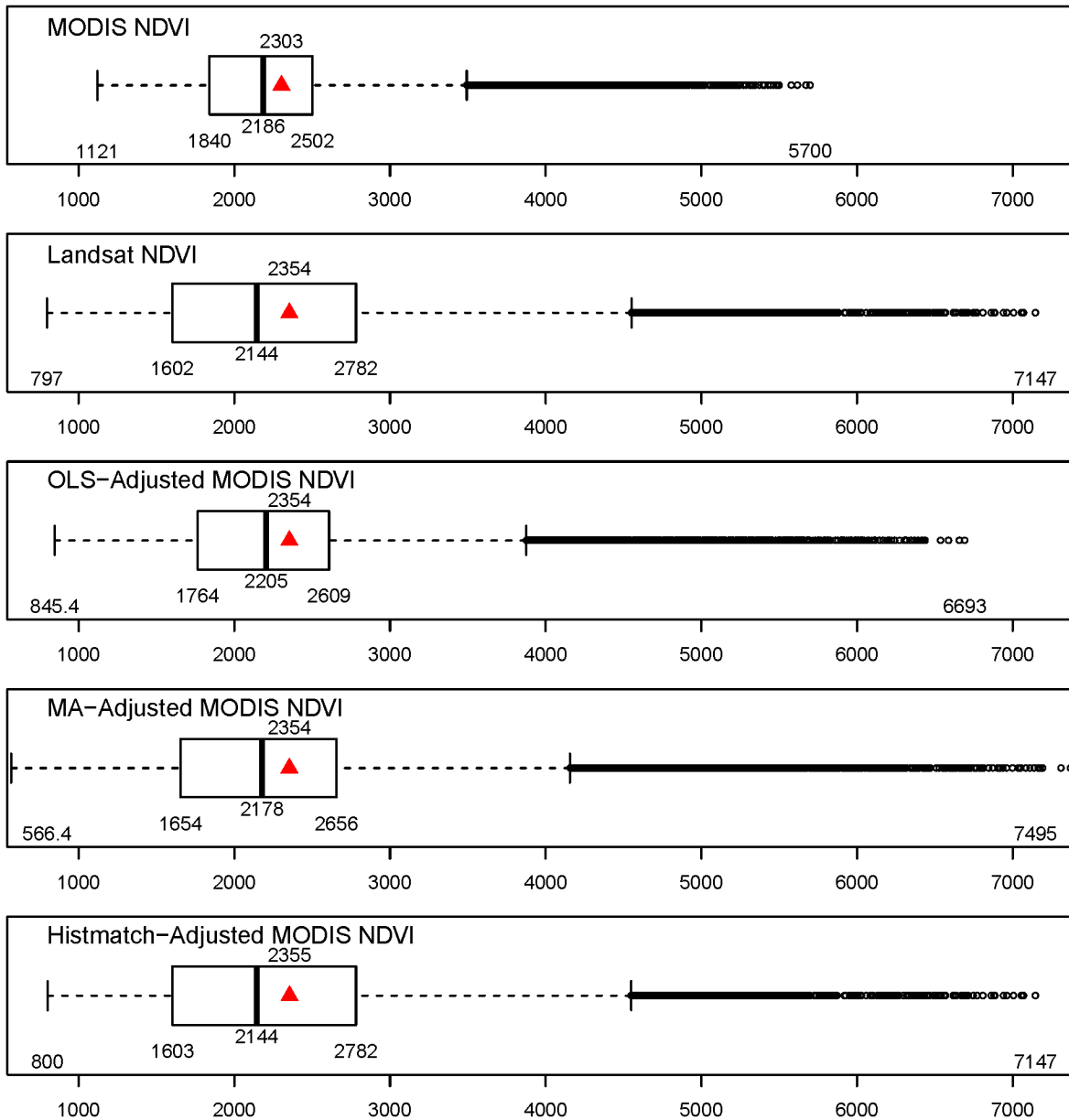


Figure D.17—Comparison of the distribution of values in the original 2011 MODIS normalized difference vegetation index (NDVI), prefire Landsat NDVI, and three versions of adjusted MODIS NDVI rasters for region 16. The adjusted MODIS rasters were created using ordinary least squares (OLS) regression, major axis (MA) regression, and histogram matching (histmatch) methods. In each boxplot, the box represents the inner quartile range (25th–75th percentiles), the solid vertical bar is the median, and the red triangle is the mean.

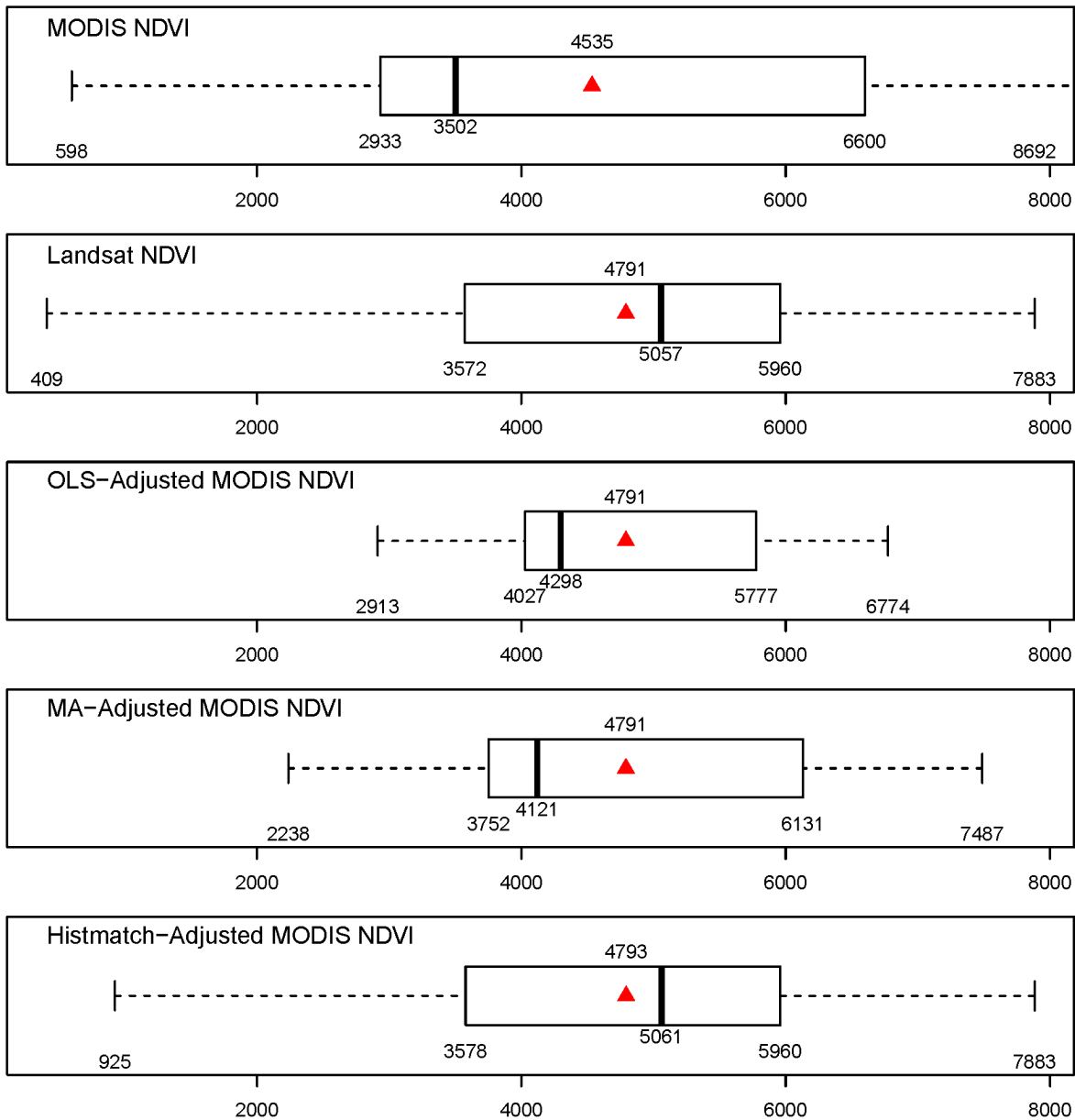


Figure D.18—Comparison of the distribution of values in the original 2011 MODIS normalized difference vegetation index (NDVI), prefire Landsat NDVI, and three versions of adjusted MODIS NDVI rasters for region 17. The adjusted MODIS rasters were created using ordinary least squares (OLS) regression, major axis (MA) regression, and histogram matching (histmatch) methods. In each boxplot, the box represents the inner quartile range (25th–75th percentiles), the solid vertical bar is the median, and the red triangle is the mean.

References

Goslee, Sarah C. 2011. Analyzing remote sensing data in R: The Landsat package. *Journal of Statistical Software*. 43(4): 1–25. doi: 10.18637/jss.v043.i04.

Legendre, Pierre. 2013. Model II regression user’s guide, R edition. The Comprehensive R Archive Network (CRAN). <https://cran.r-project.org/web/packages/lmodel2/vignettes/mod2user.pdf> [Accessed 28 March 2020].

Theobald, David; Stevens, Don; White, Denis; [et al.]. 2007. Using GIS to generate spatially balanced random survey designs for natural resource applications. *Environmental Management*. 40(1): 134–146. doi: 10.1007/s00267-005-0199-x.

In accordance with Federal civil rights law and U.S. Department of Agriculture (USDA) civil rights regulations and policies, the USDA, its Agencies, offices, and employees, and institutions participating in or administering USDA programs are prohibited from discriminating based on race, color, national origin, religion, sex, gender identity (including gender expression), sexual orientation, disability, age, marital status, family/parental status, income derived from a public assistance program, political beliefs, or reprisal or retaliation for prior civil rights activity, in any program or activity conducted or funded by USDA (not all bases apply to all programs). Remedies and complaint filing deadlines vary by program or incident.

Persons with disabilities who require alternative means of communication for program information (e.g., Braille, large print, audiotape, American Sign Language, etc.) should contact the responsible Agency or USDA's TARGET Center at (202) 720-2600 (voice and TTY) or contact USDA through the Federal Relay Service at (800) 877-8339. Additionally, program information may be made available in languages other than English.

To file a program discrimination complaint, complete the USDA Program Discrimination Complaint Form, AD-3027, found online at http://www.ascr.usda.gov/complaint_filing_cust.html and at any USDA office or write a letter addressed to USDA and provide in the letter all of the information requested in the form. To request a copy of the complaint form, call (866) 632-9992. Submit your completed form or letter to USDA by: (1) mail: U.S. Department of Agriculture, Office of the Assistant Secretary for Civil Rights, 1400 Independence Avenue, SW, Washington, D.C. 20250-9410; (2) fax: (202) 690-7442; or (3) email: program.intake@usda.gov.



To learn more about RMRS publications or search our online titles:
RMRS web site at: <https://www.fs.fed.us/rmrs/rmrs-publishing-services>